EVALUATION OF ELECTROMAGNETIC INTERFERENCE FRINGES FOR TWO-LAYER MEDIA

by

WENG CHO CHEW

S.B., Massachusetts Institute of Technology

(1976)

SUBMITTED IN PARTIAL FULFILLMENT OF THE REQUIREMENTS

FOR THE DEGREES OF

MASTER OF SCIENCE

and

ELECTRICAL ENGINEER

at the

MASSACHUSETTS INSTITUTE OF TECHNOLOGY

February, 1978

Signature redacted

Signature of Author .....
Department of Electrical Engineering and
Computer Science, January 20, 1978

Signature redacted

Certified by ... Thesis Supervisor

Signature redacted

Accepted by .....
Chairman, Departmental Committee on Graduate Students

EVALUATION OF ELECTROMAGNETIC INTERFERENCE FRINGES FOR TWO-LAYER MEDIA

by

WENG CHO CHEW

Submitted to the Department of Electrical Engineering and Computer Science on January 20, 1978 in partial fulfillment of the requirements for the Degrees of Master of Science and Electrical Engineer.

ABSTRACT

The asymptotic approximation of the electromagnetic interference fringes due to a time-harmonic dipole source on top of two-layer media is derived from integral representations of the solutions. An introduction on past analysis and its limitation is presented. The geometrical-optics approximation (GOA), where the reflections from the subsurface layer are approximated by a series of image-source contributions, is used throughout the analyses. Difficulties are encountered in obtaining asymptotic expansion of the integral representation of each term of the GOA series using ordinary saddle-point analysis due to the proximity of algebraic singularities to the saddle-point. For transverse electric (TE) waves, the singularity is a branch-point. This difficulty is surmounted by three different approaches: (1) numerical integration of each term in the GOA series, (2) modified saddle-point method where the singularity is factored out in the integrand to facilitate approximation of the integrand, and (3) multiple-saddle-point method where the singularity is removed by a transformation resulting in three saddle-points on the complex plane. The first approach is numerical whereas the latter two approaches are asymptotic-approximation analyses making use of parabolic cylinder functions. All three approaches give consistent results for TE waves. For transverse magnetic (TM) waves, in addition to a branch-point singularity, there is a Sommerfeld pole which can be near the saddle-point. The use of Generalized Weber's function results in a satisfactory asymptotic approximation of the TM waves. Multiple-saddle-point method, used in deriving an asymptotic expansion of an integral where an algebraic branch-point of any fractional order is in the neighborhood of a saddle-point, is also discussed.

Thesis Supervisor: Jin Au Kong

Title: Associate Professor of Electrical Engineering

ACKNOWLEDGEMENT

I would like to thank Professor J. A. Kong for his constant and careful guidance, advice and support without which this research would not be possible.

I am indebted to Dr. L. Tsang for his timely suggestions in our discussions which have helped me crystallize my ideas on several occassions in this research, and to Ms. Cindy Kopf for her excellent typing of this thesis.

A special word of thanks is due the Mathlab Group, MIT Laboratory for Computer Science, for the use of the Macsyma Consortium machine for some of my computations.

I also wish to express my gratitude to my family, especially my parents and Chew Chin, for their unflagging encouragement and moral support.

Finally, special mention must be made of my colleagues, in particular Howard Dyckman, for rendering help in unexpected quarters.

TABLE OF CONTENTS

LISTS OF FIGURES

CHAPTER 1. INTRODUCTION

1.1 Historical Perspective

In electromagnetic-interference-fringe method, a dipole antenna is placed over a stratified medium, possibly on top of the lunar surface, glacier, desert, etc. A receiver is placed at a distance from the source and the intensity of the electromagnetic field is measured as a function of distance from the source. An interference pattern of the electromagnetic field is obtained and this provides subsurface information about the area surveyed. This method was first used by El-Said[1] in the prospection of underground water in the desert. Its application to geophysical probing of lunar surface is described by Simmons et al[2] and by Rossiter et al.[3,4] Application to the study of terrestial glaciers is described by Strangway et al.[5] The main thrust of interest lies in the geophysical probing of high resistivity media.

Electromagnetic-interference field of a dipole antenna over a stratified medium has been studied for decades (Banos,[6] Brekhovskikh,[7] Ott,[8] and Sommerfeld[9]) and recently been pursued by severals authors (Wait,[10-12] Kong,[13-15] Tsang,[16-19] Sinha,[20] Annan,[21,22] etc). Propagation of electromagnetic waves along a half-space medium was first studied by Sommer-

feld as it would be important to the propagation of radio wave along the earth surface. He employed the Hertzian potential function and formulated the solution in terms of an integral representation. The complex nature of the solution is exemplified by a sign error committed by Sommerfeld in his original memoir (1909). His sign error resulted in an extra spurious term that caused the validity of his solution to be assailed for decades.[6] A number of writers[23-25] have attempted to disqualify the existence of Sommerfeld's electromagnetic surface wave. Other writers noted that Sommerfeld's solution was in error but failed to pin-point the exact reason for the occurrence of a spurious term. This celebrated controversy, having been assailed by numerous writers for more than half a century after it was published, was finally settled once and for all by Banos[6] (1966).

Past studies, as did Sommerfeld, have employed the Hertzian potential functions in the formulation of the solution. Kong (1972) abandoned the conventional use of the potential functions and expressed the field components directly in term of integral representations. This elegant approach simplifies the evaluation of the integral analytically and numerically. Tsang[16] did a numerical integration of the integral representation of the solution. Due to fast oscillation of the integrand, the integration consumes a lot of

computer time. However, numerical integration serves as the most convenient method of solving the integral. An analytical solution using both the normal-mode expansion and geometrical optic approximation was done by several authors.[15,17,20,21] The normal-mode approach and GOA method proved to be good for thin and thick stratified media respectively. Chan[26] applied analysis of Tsang[17] to a horizontal magnetic dipole and found sharp peaks in field intensity at the critical angle. We shall see that the peaks are not justified physically, but rather due to the inadequacy of the mathematical analysis.

1.2 Field Solution of a Horizontal Dipole

Horizontal dipoles are used more effectively in geophysical probing as more energy from the broadside radiation of the dipoles are coupled into the lower half-space as compared to vertical dipoles. Moreover, when a dipole is placed horizontally on the interface of a half-space, the radiation pattern shows high directivity in the direction of the critical angle for the two media. The integral representations of the field components of horizontal electric dipole and horizontal magnetic dipole will be presented here. (A dipole in this case refers to a Hertzian dipole. Physically, it is a dipole antenna whose effective length is much smaller than the wavelength of the operating frequency. A magnetic dipole can be represented by a small current loop.) The dipoles assume a position on the interface of the upper half-space and the first medium. It points in the positive $\hat{x}$-direction [Fig. 1.2.1].

(a) Horizontal Electric Dipole (HED)

$$E_z = \frac{iI\ell}{8\pi\omega\varepsilon} \int_{-\infty}^{\infty} dk_\rho \, k_\rho^2 (1 - R^{TM}) \, e^{ik_z z} \, H_1^{(1)}(k_\rho \rho) \cos\phi \qquad (1.2.1)$$

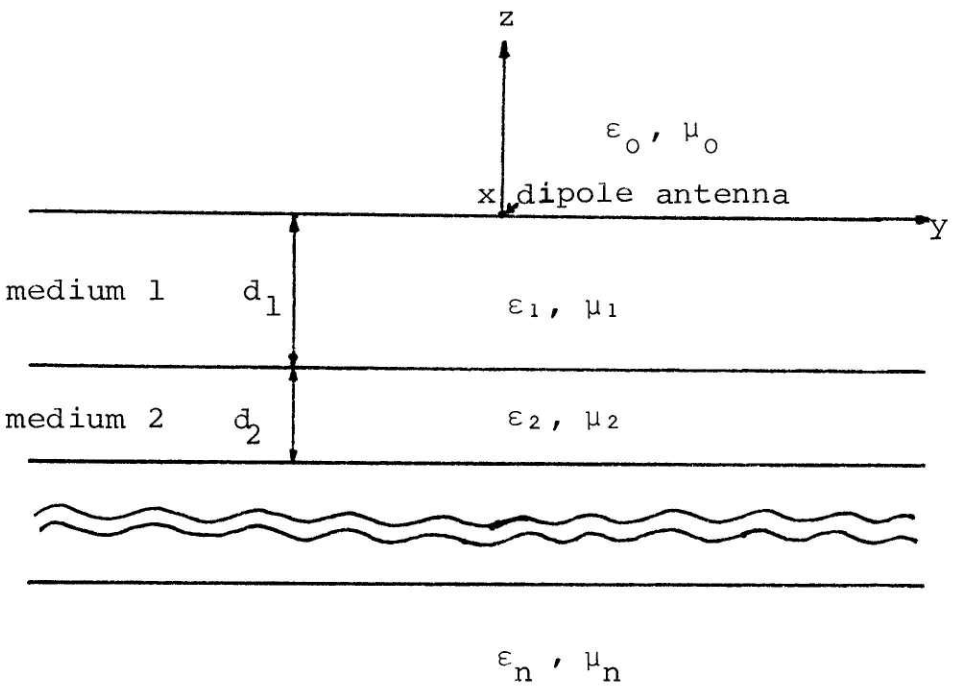

Fig. 1.2.1. A dipole antenna over stratified n-layer medium.

$$E_\rho = \frac{-I\ell}{8\pi\omega\varepsilon} \int_{-\infty}^{\infty} dk_\rho \, k_\rho k_z (1 - R^{TM}) \, e^{ik_z z} \, H_1^{(1)'}(k_\rho \rho) \cos\phi$$

$$+ \frac{-\omega\mu I\ell}{8\pi\rho} \int_{-\infty}^{\infty} dk_\rho \, \frac{1}{k_z} (1 + R^{TE}) \, e^{ik_z z} \, H_1^{(1)}(k_\rho \rho) \cos\phi \qquad (1.2.2)$$

$$E_\phi = \frac{I\ell}{8\pi\omega\varepsilon\rho} \int_{-\infty}^{\infty} dk_\rho k_z (1 - R^{TM}) \, H_1^{(1)}(k_\rho \rho) \sin\phi$$

$$+ \frac{\omega\mu I\ell}{8\pi} \int_{-\infty}^{\infty} dk_\rho \, \frac{k_\rho}{k_z} (1 + R^{TE}) \, H_1^{(1)'}(k_\rho \rho) \sin\phi \qquad (1.2.3)$$

$$H_z = \frac{iI\ell}{8\pi} \int_{-\infty}^{\infty} dk_\rho \, \frac{k_\rho^2}{k_z} (1 + R^{TE}) \, e^{ik_z z} \, H_1^{(1)}(k_\rho \rho) \sin\phi \qquad (1.2.4)$$

$$H_\rho = \frac{-I\ell}{8\pi\rho} \int_{-\infty}^{\infty} dk_\rho (1 - R^{TM}) \, e^{ik_z z} \, H_1^{(1)}(k_\rho \rho) \sin\phi$$

$$- \frac{I\ell}{8\pi} \int_{-\infty}^{\infty} dk_\rho k_\rho (1 + R^{TE}) \, H_1^{(1)'}(k_\rho \rho) \sin\phi \qquad (1.2.5)$$

$$H_\phi = \frac{-I\ell}{8\pi} \int_{-\infty}^{\infty} dk_\rho k_\rho (1 - R^{TM}) \, H_1^{(1)'}(k_\rho \rho) \cos\phi$$

$$- \frac{I\ell}{8\pi\rho} \int_{-\infty}^{\infty} dk_\rho (1 + R^{TE}) \, H_1^{(1)}(k_\rho \rho) \cos\phi \qquad (1.2.6)$$

(b) Horizontal Magnetic Dipole (HMD)

$$E_z = \frac{\omega\mu IA}{8\pi} \int_{-\infty}^{\infty} dk_\rho \frac{k_\rho^2}{k_z} (1 + R^{TM}) e^{ik_z z} H_1^{(1)}(k_\rho\rho) \sin\phi \quad (1.2.7)$$

$$E_\rho = \frac{i\omega\mu IA}{8\pi} \int_{-\infty}^{\infty} dk_\rho k_\rho (1 + R^{TM}) e^{ik_z z} H_1^{(1)'}(k_\rho\rho) \sin\phi$$

$$+ \frac{i\omega\mu IA}{8\pi\rho} \int_{-\infty}^{\infty} dk_\rho (1 - R^{TE}) e^{ik_z z} H_1^{(1)}(k_\rho\rho) \sin\phi \quad (1.2.8)$$

$$E_\phi = \frac{i\omega\mu IA}{8\pi\rho} \int_{-\infty}^{\infty} dk_\rho (1 + R^{TM}) e^{ik_z z} H_1^{(1)}(k_\rho\rho) \cos\phi$$

$$+ \frac{i\omega\mu IA}{8\pi} \int_{-\infty}^{\infty} dk_\rho k_\rho (1 - R^{TE}) e^{ik_z z} H_1^{(1)'}(k_\rho\rho) \cos\phi \quad (1.2.9)$$

$$H_z = \left(\frac{-IA}{8\pi}\right) \int_{-\infty}^{\infty} dk_\rho k_\rho^2 (1 - R^{TE}) e^{ik_z z} H_1^{(1)}(k_\rho\rho) \cos\phi \quad (1.2.10)$$

$$H_\rho = \frac{-iIAk^2}{8\pi\rho} \int_{-\infty}^{\infty} dk_\rho \frac{1}{k_z} (1 + R^{TM}) e^{ik_z z} H_1^{(1)}(k_\rho\rho) \cos\phi$$

$$+ \frac{-iIA}{8\pi} \int_{-\infty}^{\infty} dk_\rho k_\rho k_z (1 - R^{TE}) e^{ik_z z} H_1^{(1)'}(k_\rho\rho) \cos\phi$$

(1.2.11)

$$H_\phi = \frac{iIAk^2}{8\pi} \int_{-\infty}^{\infty} dk_\rho \frac{k_\rho}{k_z} (1 + R^{TM}) e^{ik_z z} H_1^{(1)'}(k_\rho \rho) \sin\phi$$

$$+ \frac{iIA}{8\pi\rho} \int_{-\infty}^{\infty} dk_\rho k_z (1 - R^{TE}) e^{ik_z z} H_1^{(1)}(k_\rho \rho) \sin\phi. \quad (1.2.12)$$

The above results are derived by Kong.[13] For a two-layer medium, the reflection coefficients are given by

$$1 \pm R = \frac{1 \pm R_{12} \exp(i2k_{1z}d)}{1 + R_{01}R_{12} \exp(i2k_{1z}d)} X_{01} \quad (1.2.13)$$

where R_{ij} and X_{ij} are reflection coefficient and transmission coefficient respectively between media i and j.

$$R_{ij} = \frac{k_{iz} - b_{ij}k_{jz}}{k_{iz} + b_{ij}k_{jz}}, \qquad X_{ij} = \frac{2k_{iz}}{k_{iz} + b_{ij}k_{jz}} \quad (1.2.14)$$

where

$$b_{ij} = \begin{cases} \mu_i/\mu_j & \text{for TE waves} \\ \varepsilon_i/\varepsilon_j & \text{for TM waves.} \end{cases} \quad (1.2.15)$$

$$k_{iz} = \sqrt{k_i^2 - k_\rho^2}, \quad (1.2.16)$$

(For k_{iz}, we omit the subscript i when $i = 0$.) and d is the thickness of medium 1.

In the normal-mode approach, the poles of $1 \pm R$ on the complex k_ρ-plane is found by solving for roots of $1 + R_{01}R_{12} \exp(i2k_{1z}d) = 0$. The original path of integration is deformed to the steepest-descent path passing through the saddle-point. The contribution of the original integral is the sum of the saddle-point contribution and the contribution from all the singularities enclosed in the course of deforming the path of integration. When d is large, $1 \pm R$ as can be seen from (1.2.13) is rapidly varying with respect to k_ρ. This makes the calculation of the saddle-point contribution difficult.[19] The geometrical-optics approximation serves as a complement of normal-mode approach for large d, a fact that we shall see later.

1.3 Geometrical-Optics Approximation (GOA)

In the geometrical-optics approximation, the reflection coefficient is expanded in a power series. It can be shown easily that

$$1 + R = X_{01}\left[1 + \sum_{m=1}^{\infty} X_{10}\, R_{10}^{m-1}\, R_{12}^{m} \exp(i2k_{1z}md)\right] \qquad (1.3.1a)$$

$$1 - R = X_{10}\left[1 - \sum_{m=1}^{\infty} X_{01}\, R_{10}^{m-1}\, R_{12}^{m} \exp(i2k_{1z}md)\right]. \qquad (1.3.1b)$$

For a typical integral

$$T = \int_{-\infty}^{\infty} \frac{k_\rho}{k_z} (1 + R)\, H_o^{(1)}(k_\rho \rho)\, e^{ik_z z}\, dk_\rho \qquad (1.3.2)$$

substitution of (1.3.1a) into T yields

$$T = \int_{-\infty}^{\infty} \frac{k_\rho}{k_z} X_{01}\, H_o^{(1)}(k_\rho \rho)\, e^{ik_z z}\, dk_\rho$$

$$+ \sum_{m=1}^{\infty} \int_{-\infty}^{\infty} \frac{k_\rho}{k_z} X_{01} X_{10}\, R_{10}^{m-1}\, R_{12}^{m}\, e^{ik_z z}$$

$$e^{ik_{1z}2md} H_o^{(1)}(k_\rho \rho)\, dk_\rho . \qquad (1.3.3)$$

The series in (1.3.1) converge for $|R_{10}R_{12}\, e^{ik_{1z}2md}| < 1$. This criterion is satisfied over the range of integration of k_ρ. Thus the interchanging of the summation and integral sign in (1.3.3) is valid. The series converges quickly for large d, as we shall see.

Physically, the first term of (1.3.3) corresponds to the half-space solution without the subsurface layer. The second term which is a summation of series corresponds to waves which have reached the surface through multiple reflections from the subsurface layer. It can also be thought of as field radiating from the image sources of the dipole source [Fig. 1.3.1].

The integration path in (1.3.3) is taken to be the Sommerfeld integration path, which is above the real axis when $k_\rho < 0$, passes above the origin and is below the real axis when $k_\rho > 0$. This avoids the branch-point singularities at $k_\rho = 0$, $\pm k$, $\pm k_1$ and $\pm k_2$, and the integral is well defined [Fig. 1.3.2].

(a) Half-Space Solution

To obtain the asymptotic expansion of the half-space solution, a transformation of $k_\rho = k \sin \beta$ is done to sim-

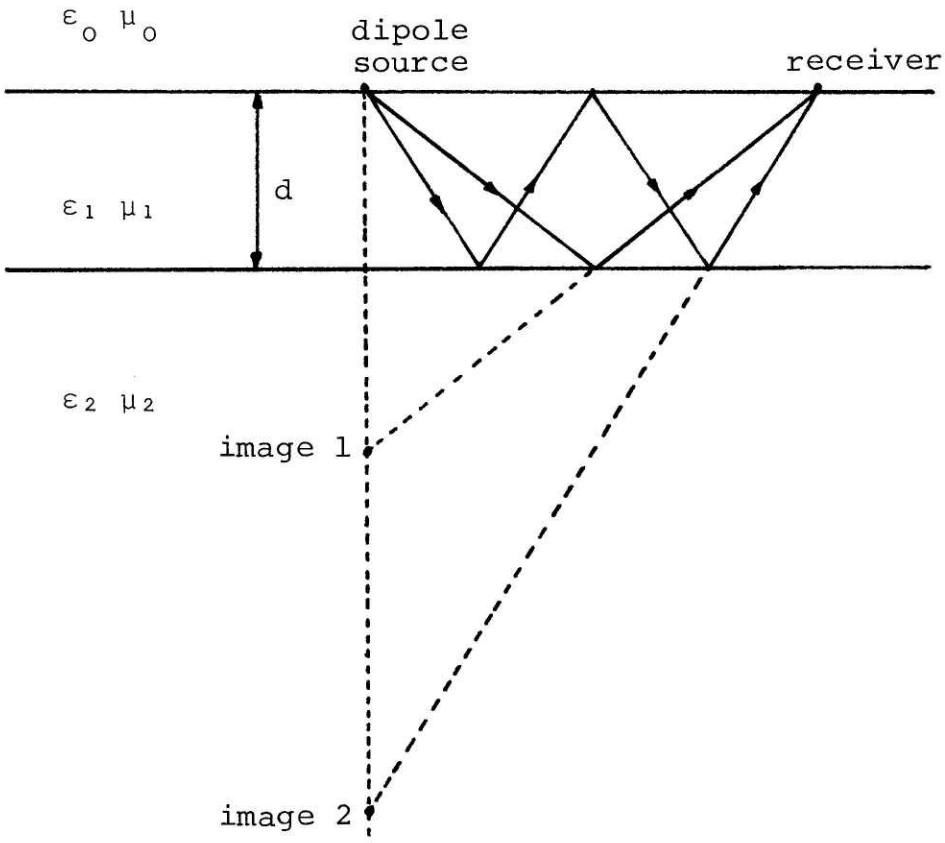

Fig. 1.3.1. Dipole source and its images for a two-layer medium.

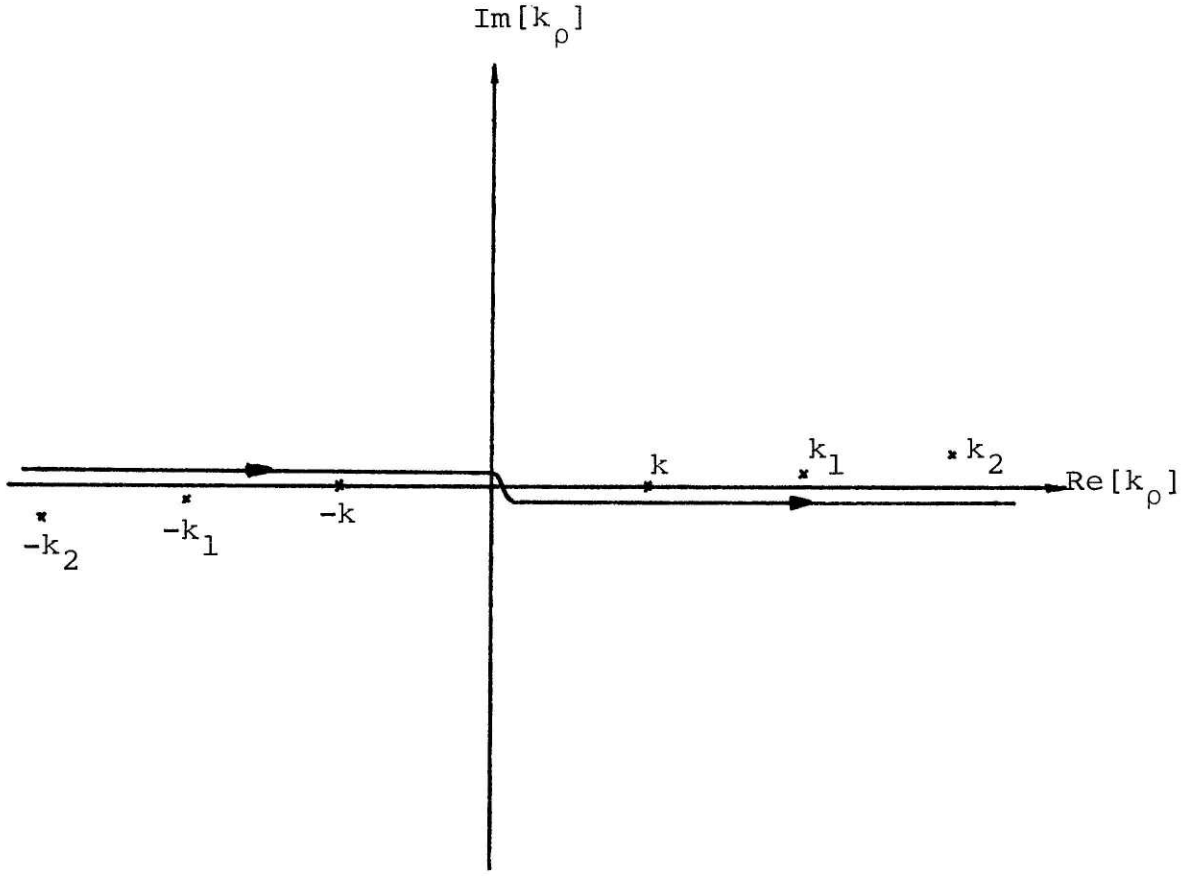

Fig.1.3.2. Sommerfeld path of integration.

plify the analysis. We replace $H_o^{(1)}(k_\rho \rho)$ by $\hat{H}_o^{(1)}(k_\rho \rho)\, e^{ik_\rho \rho}$ where $\hat{H}_o^{(1)}(k_\rho \rho) = H_o^{(1)}(k_\rho \rho)\, e^{-ik_\rho \rho}$. After the k_ρ-plane to β-plane transformation, the integral becomes

$$T_{HS} = \int_\Gamma k \sin\beta\, \hat{H}_o^{(1)}(k\rho \sin\beta)\, X_{01}(\beta)\, e^{ikR\cos(\beta - \alpha)}\, d\beta \qquad (1.3.4)$$

where

$$\alpha = \tan^{-1}\frac{\rho}{z}, \qquad R = (\rho^2 + z^2)^{1/2}.$$

The path of integration Γ on the β-plane is shown in Fig. 1.3.3. There is a saddle-point at $\beta = \alpha$, the angle of observation. The steepest-descent path passing through α is as shown. The path of integration can be deformed to the steepest-descent path and the saddle-point method[7,14] can be employed to approximate (1.3.4) if $k \sin\beta\, \hat{H}_o^{(1)}(k\rho \sin\beta)\, X_{01}(\beta)$ is slowly varying in the neighborhood of the saddle-point compared to $e^{ikR\cos(\beta - \alpha)}$ when $kR \to \infty$. This can be shown to be true if the argument of $\hat{H}_o^{(1)}(x)$ is large in the neighborhood of the saddle-point by using the asymptotic expansion of $\hat{H}_o^{(1)}(x)$ when $x \to \infty$.

Note that the branch-point at $k_\rho = k$ does not exist on the β-plane but the branch-point at $k_\rho = k_1$ is mapped to $\beta_1 = \sin^{-1} k_1/k$. As shown in Fig. 1.3.3, the branch-point

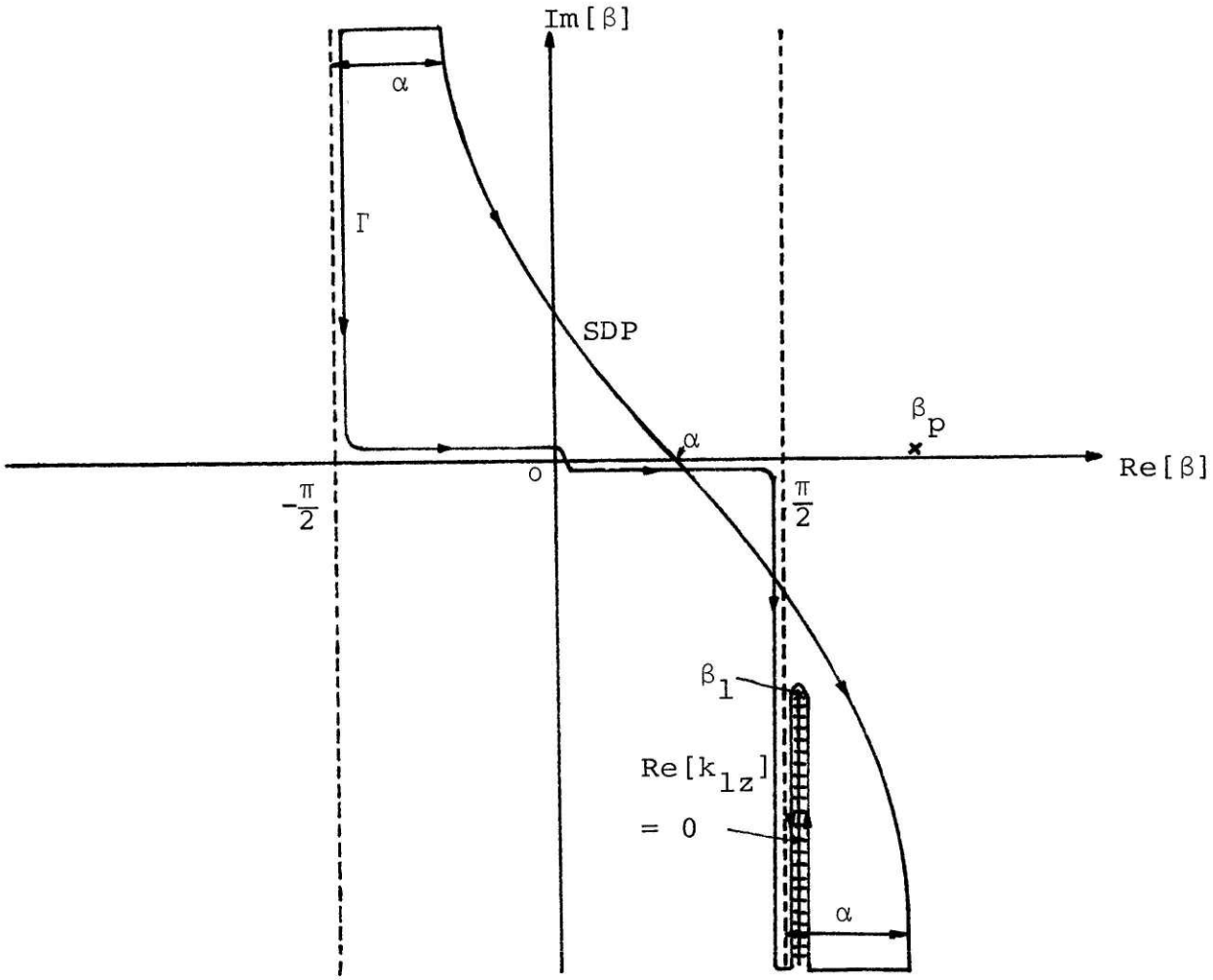

Fig. 1.3.3. β-plane showing Γ the original path of integration and SDP, the steepest-descent path passing through α.

contribution will have to be included if

$$\alpha > \theta_o = \sin^{-1} \frac{k}{k_1} .$$

In actual experiment, the receiver is placed near the surface. Thus, $\alpha \simeq \pi/2 > \theta_o$, and the branch-point contribution cannot be neglected. The asymptotic approximation of T_{HS}, including the branch-point contribution, and neglecting terms of $O(R^{-3})$ is[14,17]

$$T_{HS} \sim \frac{2}{i} \frac{e^{ikR}}{R} \left[X_{01}(\alpha) + \frac{1}{2ikR} \left[\cot \alpha \, X'_{01}(\alpha) + X''_{01}(\alpha) \right] \right]$$

$$- \frac{4k_1}{b\rho^2 a^2} \frac{e^{-az + ik_1\rho}}{\left(1 + i \frac{k_1 \cot \alpha}{a} \right)^{3/2}} , \quad kR \to \infty \tag{1.3.5a}$$

where

$$b = \begin{cases} \mu_1/\mu & \text{for TE waves} \\ \\ \varepsilon_1/\varepsilon & \text{for TM waves,} \end{cases} \tag{1.3.5b}$$

$$a = (k_1^2 - k^2)^{1/2}.$$

The first term is the saddle-point contribution and it

corresponds to the direct wave. The second term is the branch-point contribution and is identified as the lateral wave or inhomogeneous wave decaying away from the surface.

When $z = 0$, $X_{01}(\alpha) = 0$. Thus the direct wave becomes a term of $O(\rho^{-2})$ and propagates with a phase velocity of ω/k. The lateral wave, also of $O(\rho^{-2})$ propagates with a phase velocity of ω/k_1. The two waves give rise to a spatial beat frequency of $k_1 - k$ which can be used to determine the electrical properties of the lower half-space. When $b > 1$, there is a Sommerfeld pole of order 1 at

$$\beta_p = \sin^{-1}\left[\frac{(k_1/k)^2 - b^2}{1 - b^2}\right]^{1/2},$$

but it is not enclosed when the path of integration is deformed to the steepest-descent path.

(b) Reflected-Wave Contribution

Since when $z = 0$, the half-space solution is of $O(\rho^{-2})$ when $\rho \to \infty$, the reflected-wave contribution becomes important. As in the case of half-space solution, the analysis of the reflected-wave contribution is done by performing a transformation. If we let $k_\rho = k_1 \sin\theta$, the expression for reflected waves is

$$T_R = \sum_{m=1}^{\infty} \int_{\Gamma} k_1 \sin\theta \, \hat{H}_o^{(1)}(k_1 \rho \sin\theta) \, X_{01}(\theta) \, X_{10}(\theta) \, R_{10}^{m-1}(\theta)$$

$$R_{12}^{m}(\theta) \, e^{ik_z(\theta) z} \, e^{ik_1 R_m \cos(\theta - \alpha_m)} \, d\theta \qquad (1.3.6)$$

where

$$\alpha_m = \tan^{-1} \frac{\rho}{2md}, \qquad R_m = [\rho^2 + (2md)^2]^{1/2}.$$

There is a saddle-point at $\theta = \alpha_m$ due to $\exp[ik_1 R_m \cos(\theta - \alpha_m)]$. Thus, we can use the saddle-point analysis if the coefficient function of $\exp[ik_1 R_m \cos(\theta - \alpha_m)]$ is slowly varying in the neighborhood of the saddle-point when $k_1 R_m$ is large. This is true if the argument of $\hat{H}_o^{(1)}(x)$ is large in the neighborhood of the saddle-point, and $z \ll \lambda$, the free space wavelength.

The transformation from k_ρ-plane to θ-plane removes the branch-point at $k_\rho = k_1$. The branch-point at $k_\rho = k$ maps into $\theta_o = \sin^{-1} k/k_1$ while the branch-point at $k_\rho = k_2$ maps into $\theta_2 = \sin^{-1} k_2/k_1$. There is a Sommerfeld pole of order $m + 1$ at

$$\theta_p = \sin^{-1} \left[\frac{1 - (k/k_1 \, b)^2}{1 - b^2} \right]^{1/2}$$

where b is defined in (1.3.5b).

When the path of integration is deformed from Γ to the steepest-descent path through the saddle-point α_m, contributions from singularities enclosed have to be included. When $k_2 > k_1$, the branch-point at θ_2 gives rise to a lateral wave which decays exponentially away from the boundary between media 1 and 2. So if the thickness of medium 1 is large, it can be safely neglected. When $\alpha_m < \theta_o$, the branch-point at θ_o is not enclosed (see Fig. 1.3.4). The Sommerfeld pole is not enclosed too since it is on the upper Riemann sheet which is different from that on which the steepest-descent path passes through. When $\alpha_m > \theta_o$, as can be seen from Fig. 1.3.5, we have to include the branch-point contribution. To understand why the Sommerfeld pole does not contribute, we draw the steepest-descent path around the branch-point on the two different Riemann sheets of k_z. Since the asymptotic approximation to the branch-point contribution is derived by performing the integration along this path, we can deform the original path Γ to the path around the branch-point along the steepest-descent path and then to the steepest-descent path through the saddle-point. We see that the Sommerfeld pole, which is on the upper Riemann sheet, is not enclosed.

Using the ordinary saddle-point analysis, it can be shown that the m-th term of T_R for $\alpha_m < \theta_o$ and for large R_m is

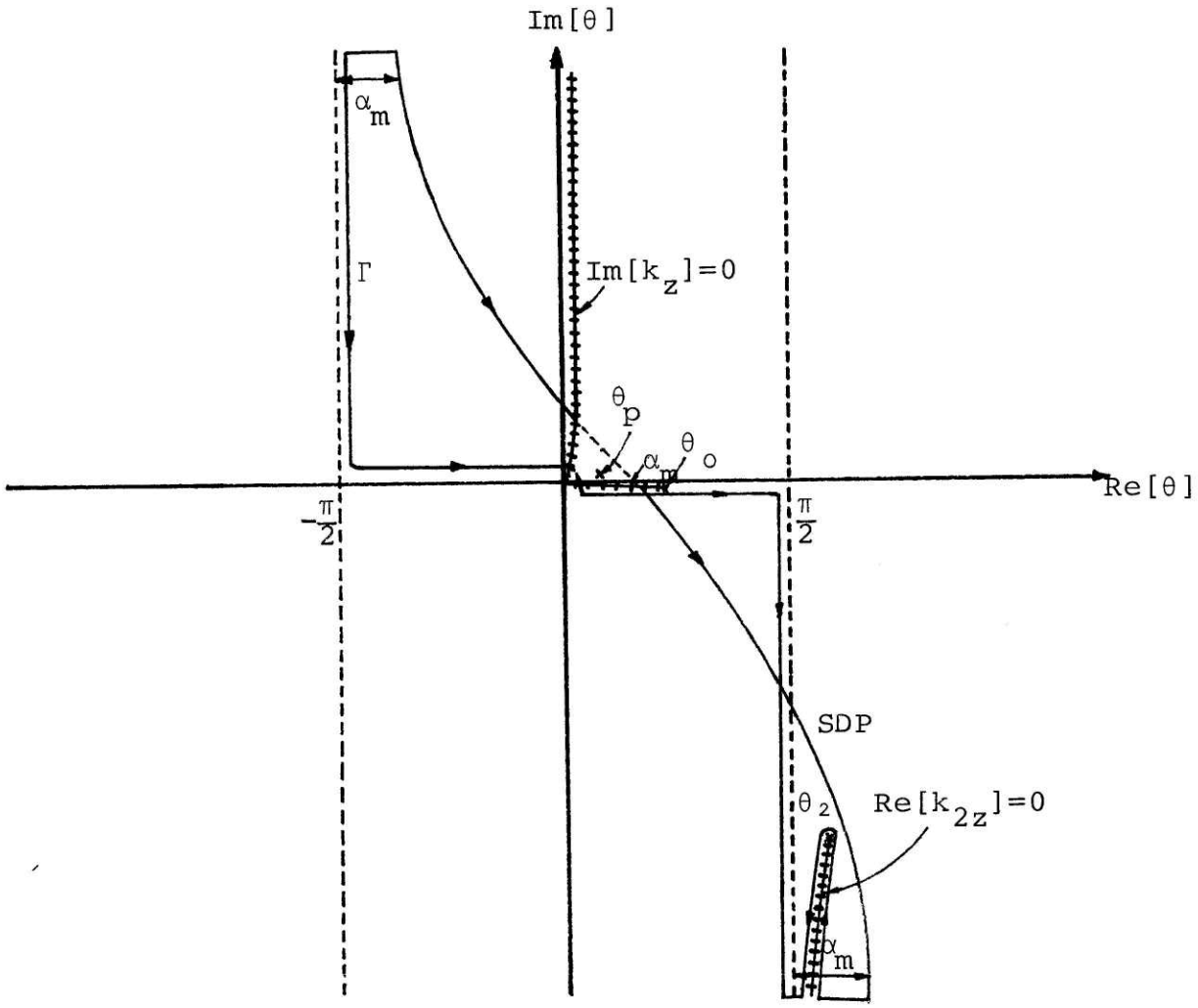

Fig. 1.3.4. θ-plane showing branch-points and steepest-descent path when $\alpha_m < \theta_o$.

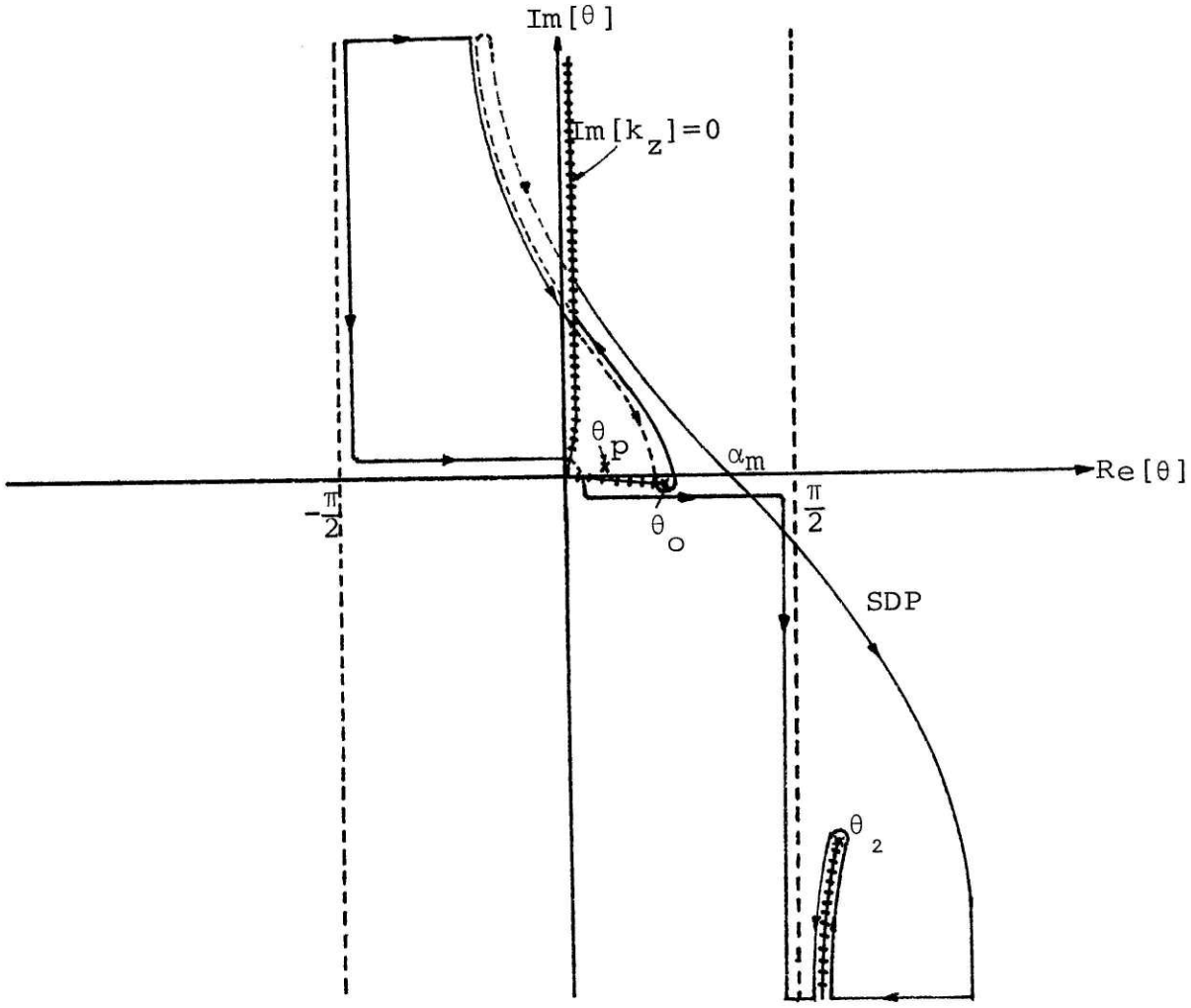

Fig. 1.3.5. θ-plane showing branch-points and steepest-descent paths when $\alpha_m > \theta_o$.

$$T_R^m \sim \frac{2}{i} \frac{e^{ik_1 R_m}}{R_m} \left[A_m(\alpha_m) + \frac{1}{2ik_1 R_m} \left(A_m''(\alpha_m) + \cot \alpha_m \, A_m'(\alpha_m) \right) \right] \tag{1.3.7a}$$

where

$$A_m(\alpha_m) = X_{01}(\alpha_m) \, X_{10}(\alpha_m) \, R_{10}^{m-1}(\alpha_m) \, R_{12}^m(\alpha_m).$$

When $\alpha_m > \theta_o$, the branch-point contribution has to be included. It is

$$-16 \frac{e^{ik_1 R_m \cos(\alpha_m - \theta_o)}}{\sqrt{\pi \rho}} \frac{k}{a} b \, R_{12}^m(\theta_o) \left(iz - \frac{2mb}{a} \right) \frac{\Gamma(3/2)}{R_m^{3/2}}$$

$$\frac{\cos^{3/2} \theta_o}{[\sin(\alpha_m - \theta_o)]^{3/2}} . \tag{1.3.7b}$$

In arriving at the above, terms of $O(R_m^{-3})$ has been neglected. The large-argument approximation to $\hat{H}_o^{(1)}(x)$ is used. The saddle-point contribution in this case corresponds to spherical waves which have been reflected off from the subsurface medium through multiple reflections. The branch-point contribution is a lateral wave in medium 1 leaving the first

boundary and is reflected back to the upper half-space due to the presence of subsurface medium. Note that the lateral wave has a conical wave-front. Also, the waves have a propagation constant of k_1 and R_m is the distance travelled by the waves in medium 1. Thus, if k_1 is lossy, and R_m is large (which is true for thick layer and large m), the wave reaching the surface is vanishing small. Thus the first few terms of T_R form a good approximation to it if d is large and k_1 is lossy.

1.4 Conclusions

We saw, in the previous sections, the analysis of the half-space solution and the reflected waves as it existed in the past literatures. In the analysis of the reflected waves, usually, only the term of $O(R_m^{-1})$ is considered.[17]

The half-space solution is of $O(\rho^{-2})$ when $z=0$. Since there is no singularities in the neighborhood of the saddle-point unless $b >> 1$, the requirement that the coefficient function be slowly varying is satisfied. Thus (1.3.5) is a good approximation to the half-space solution for large ρ and small b.

For slightly lossy media, the dominant field comes from the reflected wave. However, the reflected-wave approximation as given by (1.3.7) has several inadequacies. When α_m is near θ_o, the coefficient function becomes rapidly varying and thus the saddle-point analysis breaks down. The steepest-descent method used in obtaining the branch-point contribution also breaks down. In fact, the branch-point contribution is infinitely large when $\theta_o = \alpha_m$. Furthermore, when b is large, $\theta_p \simeq \theta_o$. The proximity of the Sommerfeld pole of order $m + 1$ for the m-th image to the branch-point cannot be ignored. We will see in subsequent chapters how these difficulties can be overcome.

CHAPTER 2. GOA BY NUMERICAL METHOD

2.1 Introduction

Numerical integration of the integral representations of the field components of a dipole antenna over stratified media was carried out by Tsang.[16] The integration was achieved without replacing the reflection coefficient with its geometrical-optics series. Using the Hankel transformation formulation, the range of integration is halved; that is from zero to infinity. For example, in the broadside direction, the H_z component of an HED has as its integral representation

$$H_z = \frac{iI\ell}{8\pi} \int_{-\infty}^{\infty} \frac{k_\rho^2}{k_z} (1 + R^{TE}) H_1^{(1)}(k_\rho \rho) e^{ik_z z} dk_\rho . \qquad (2.1.1)$$

By noting that $H_1^{(1)}(e^{i\pi} x) = H_1^{(2)}(x)$, this can be reduced to

$$H_z = \frac{iI\ell}{4\pi} \int_{0}^{\infty} \frac{k_\rho^2}{k_z} (1 + R^{TE}) J_1(k_\rho \rho) e^{ik_z z} dk_\rho . \qquad (2.1.2)$$

The fast oscillating Bessel function when ρ is large, coupled with the presence of k_z in the denominator which

results in a singularity of order $-1/2$ at $k_\rho = k$, makes the numerical integration of this integral difficult.[28] Moreover, z has to be greater than zero for the integral to converge near the real axis. Thus when $z = 0$, the solution of this integral cannot be obtained by numerical integration along the real axis.

However, for a two-layer stratified medium, when the thickness of the first layer is large, the field solution is dominated by the first few terms of the geometrical-optics series. Physically, it means that the first few images contribute to the field solution in the upper half-space. Moreover, when (2.1.1) is expressed in terms of the geometrical-optics series, each term has a distinct stationary point. This is advantageous since the integrand is varying slowly in the neighborhood of a stationary point.

2.2 GOA

The substitution of the geometrical optics series (1.8.1) into (2.1.2) yields

$$H_z = \frac{iI\ell}{4\pi}\left[\int_0^\infty \frac{k_\rho^2}{k_z} X_{01}\, J_1(k_\rho\rho)\, e^{ik_z z}\, dk_\rho + \sum_{m=1}^{\infty} \int_0^\infty \frac{k_\rho^2}{k_z} X_{01}X_{10}\, R_{10}^{m-1}\, R_{12}^{m}\, e^{ik_{1z}2md}\, e^{ik_z z}\, J_1(k_\rho\rho)dk_\rho\right] \tag{2.2.1}$$

(a) Half-Space Solution

The first term, which is the half-space solution, can be approximated sufficiently well by its asymptotic approximation when the Sommerfeld pole is far from the saddle-point (see Section 1.3(a)).

$$H_{zHS} \sim -\frac{I\ell}{4\pi}\frac{e^{ikR}}{R}\left[\sin\alpha\left(ik - \frac{1}{R}\right) X_{01}(\alpha) + \frac{3}{2R}\cos\alpha\, X'_{01}(\alpha) + \frac{\sin\alpha}{2R} X''_{01}(\alpha)\right] - \frac{I\ell}{4\pi}\frac{2k_1^2}{b\rho^2 a^2}\frac{e^{-az + ik_1\rho}}{\left(1 + i\frac{k_1}{a}\cot\alpha\right)^{3/2}}. \tag{2.2.2}$$

This can be derived from (1.3.5a) by noting that

$$H_z = - \frac{iI\ell}{8\pi} \frac{\partial}{\partial \rho} T.$$

When $z = 0$, this reduces to terms of $O(\rho^{-2})$ for large ρ.

$$H_{zHS} \sim \frac{I\ell}{2\pi} \frac{b^2}{\rho^2 a^2} \left[k^2 e^{ik\rho} - \frac{k_1^2}{b^3} e^{ik_1\rho} \right] \qquad (2.2.3)$$

When $b \to \infty$, this approximation of H_{zHS} becomes infinitely large. This is because that the Sommerfeld pole coalesces with the saddle-point when $b = \infty$ (see Section 1.3(a)). Thus the effect of the Sommerfeld pole cannot be neglected when b is large.[27] However, for our application, $b = \mu_1/\mu_o = 1$ for TE waves propagating in non-magnetic materials. For TM waves, $b = \varepsilon_1/\varepsilon_o \simeq 3$ for glacial ice. The Sommerfeld pole, which is of order 1, is at $\beta = \infty$ and $\beta \simeq 150°$ respectively for the two cases. It can be shown by numerical integration that (2.2.3) is a good approximation to the half-space solution for $z = 0$. The half-space solution for H_z is given by

$$H_{zHS} = \frac{iI\ell}{8\pi} \int_{-\infty}^{\infty} \frac{k_\rho^2}{k_z} X_{01} H_1^{(1)}(k_\rho \rho) e^{ik_z z} dk_\rho. \qquad (2.2.4)$$

When $z = 0$, the above integral does not converge near the real axis but its solution can be obtained by deforming the path of integration to $+ i\infty$. The contribution comes solely from the two branch points at $k_\rho = k$ and k_1 (see Fig. 2.2.1). The first branch point gives rise to the first term of (2.2.3).[14] The Sommerfeld pole is at

$$k_{\rho_p} = k_1 \left[\frac{1 - (kb/k_1)^2}{1 - b^2} \right]^{1/2}$$

and on the region of a Riemann sheet where $\mathrm{Re}[k_{1z}] > 0$ and $\mathrm{Re}[k_z] < 0$. Thus, it can only be near the first branch-point when $b \to \infty$. This means that the second term but not the first term of (2.2.3) is a good approximation to the contribution of branch point k_1 for all $1 < b < \infty$. The locus of the Somerfeld pole when b increases from 1 to ∞ is shown in Fig. 2.2.1.

By using the asymptotic approximation of $H_1^{(1)}(k_\rho \rho)$ for large argument, and noting that k_z assumes opposite signs on different sides of the branch-cut, the integration around the branch-point k can be reduced to

$$H_{zHS}^{k} \sim \frac{e^{-i\frac{\pi}{4}} I\ell}{\pi^{3/2}} \frac{1}{\sqrt{2\rho}} b^2 \int_k^{k + i\infty} \frac{k_\rho^{3/2} k_z}{k_{1z}^2 - b^2 k_z^2} e^{ik_\rho \rho} \, dk_\rho \qquad (2.2.5)$$

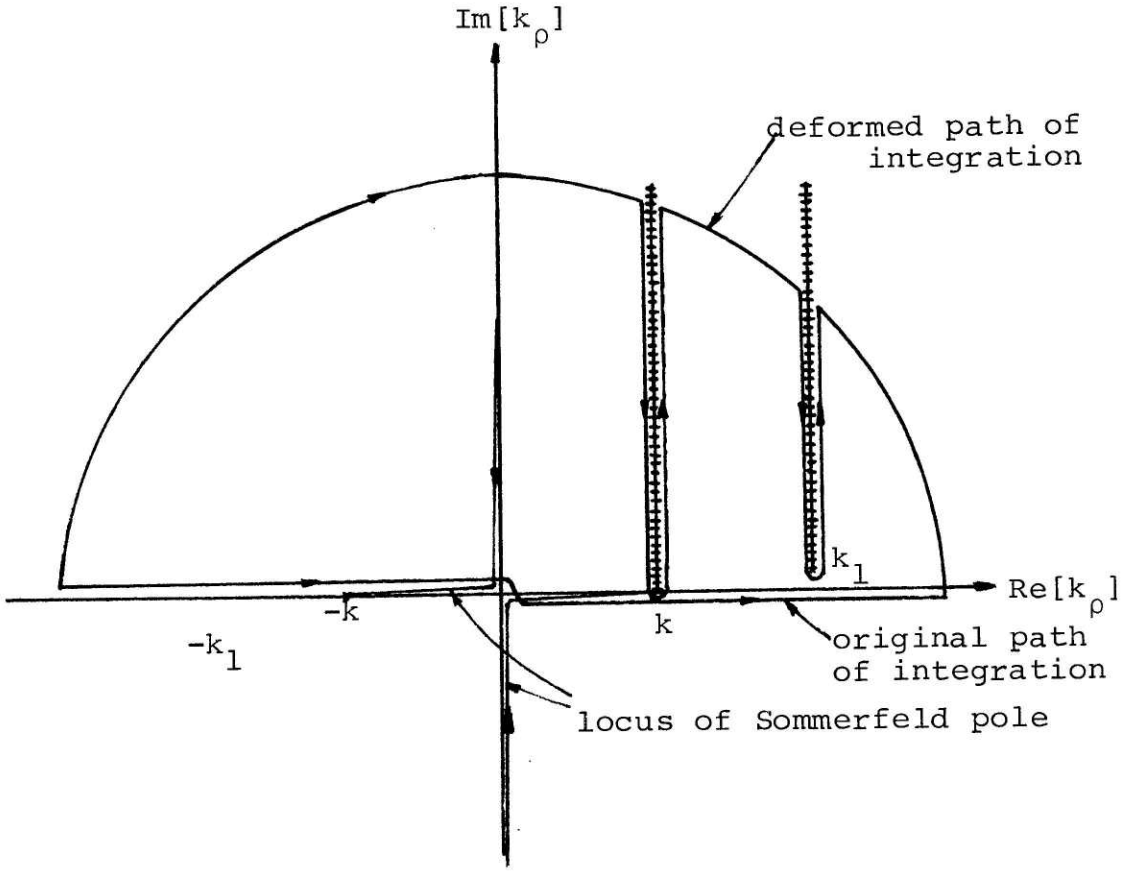

Fig. 2.2.1. The deformed path of integration and the Sommerfeld pole's locus when b increases from 1 to ∞.

where $\mathrm{Re}[k_z] > 0$ and $k_\rho^{1/2}$ assumes its priciple value along this path of integration. The integrand varies slowly along this path of integration and thus numerical integration can be readily performed. The result is shown in Fig. 2.2.2. Note that for Fig. 2.2.2(b), the vertical scale is exaggerated and thus the error is relatively small, considering the fact that most of the field intensity would come from the reflected wave for our applications.

(b) The Reflected-Wave Contribution

The dominant field of a dipole antenna over a stratified medium comes from the reflected wave when the medium is slightly lossy, e.g. glacial ice. For large d and lossy k_1, the first few terms of the series in (2.2.1) will be sufficient to approximate H_z. Note that k_z in the denominator of the integrand now cancels with the k_z in the numerator of X_{01}. The convergence of the integral now depends on $\exp(ik_{1z}\ 2md)$ rather than $\exp(ik_z z)$. Thus when $z = 0$, the solution can be obtained by numerical integration of the reflected-wave terms near the real axis.

To study the oscillatory behavior of the Bessel function, we replace it by its asymptotic form for large argument

$$J_1(k_\rho\rho) \sim -\sqrt{1/2\pi k_\rho\rho}\left(e^{ik_\rho\rho}\, e^{i\frac{\pi}{4}} + e^{-ik_\rho\rho}\, e^{-i\frac{\pi}{4}}\right). \quad (2.2.6)$$

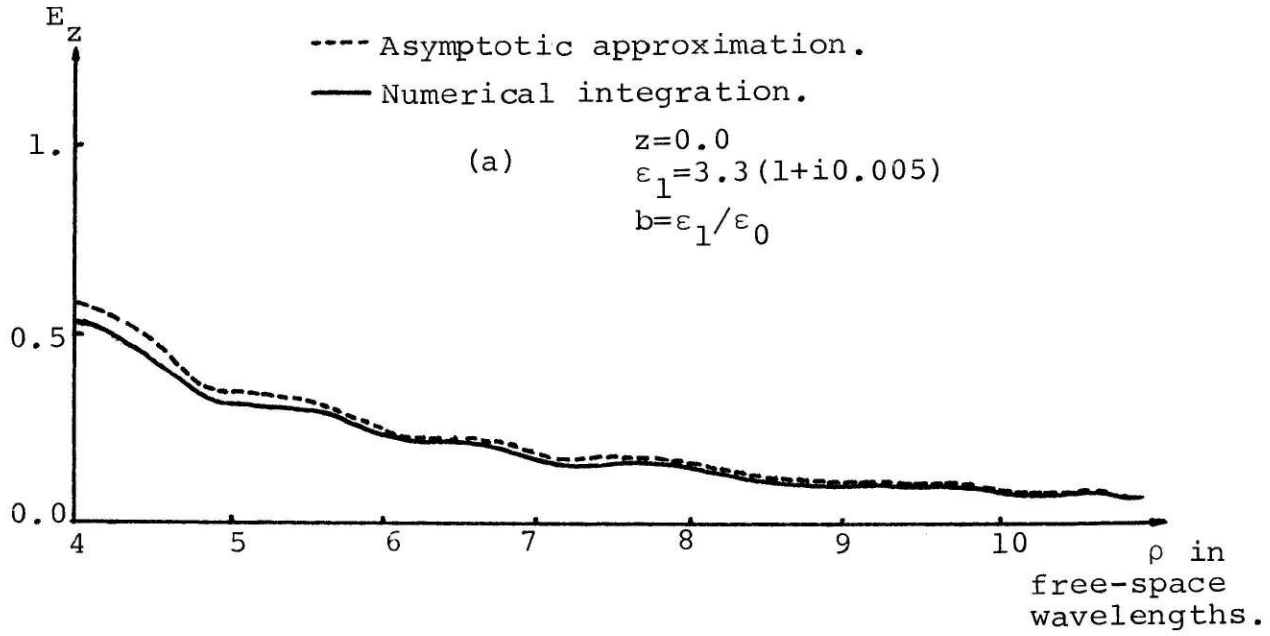

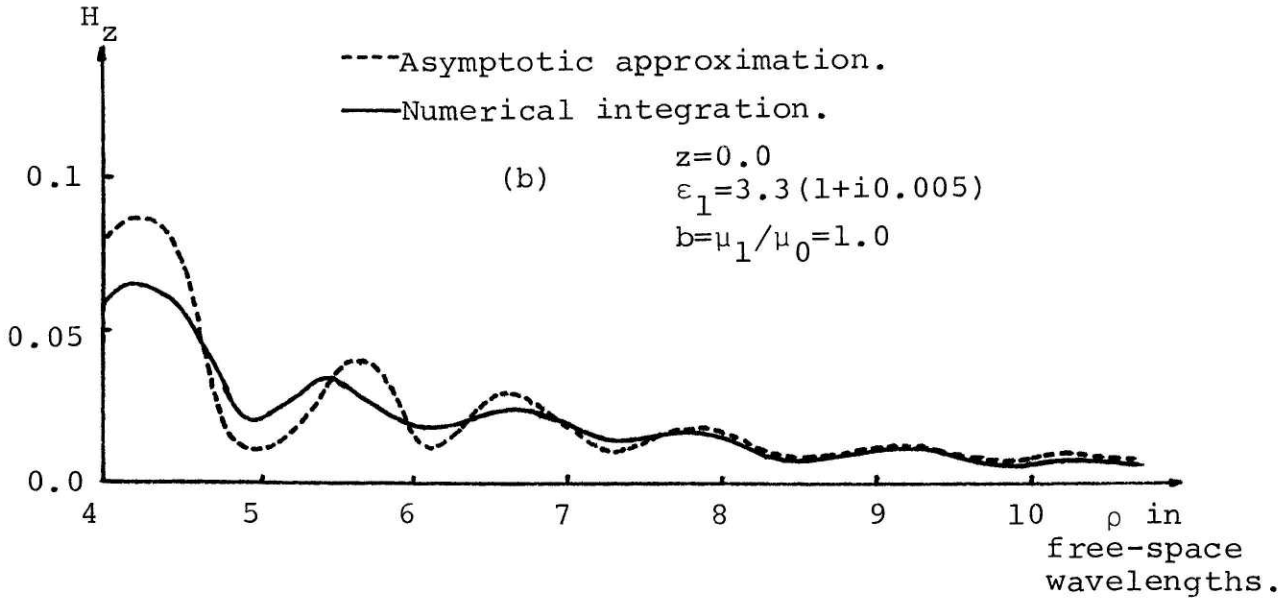

Fig. 2.2.2. (a) Half-space solution of the E_z component of an HMD. (b) Half-space solution of the H_z component of an HED.

The product of the first term with $e^{ik_{1z}2md}$ in the integrand results in a stationary point (or saddle point) at $k_\rho = k_1 \sin \alpha_m$ where $\alpha_m = \tan^{-1}(\rho/2md)$. The product of $e^{ik_{1z}2md}$ with the second term in (2.2.4) does not give rise to a stationary point within the range of integration. Therefore, the second term causes the integrand to oscillate rapidly for large ρ while the product of the first term and the rest of the integrand have a region of slow variation in the neighborhood of the stationary point. Thus if the path of integration is deformed to one such that the second term in (2.2.6) is much smaller than the first term, computation time can be reduced. The deformed path of integration is shown in Fig. 2.2.3.

Along such a path, the ratio of the magnitude of the first term to that of the second term is $e^{2\rho\Delta} >> 1$ for $\Delta >> 1/2\rho$. As such, the rapid variation of the integrand is reduced. The deformed integration path has an added advantage in that it is far from k, k_1 and k_2. Though these are mild singularities, they are still points where the derivatives of the integrand vary rapidly. Also Δ should not be chosen too large lest the first term of (2.2.6) becomes exponentially large which is undesirable in numerical integration. The constant-phase curves of $e^{i(k_{1z}2md + k_\rho\rho)}$ is shown in Fig. 2.2.4.

Fig. 2.2.5(a) shows the integrand as a function of $\mathrm{Re}[k_\rho]/k$

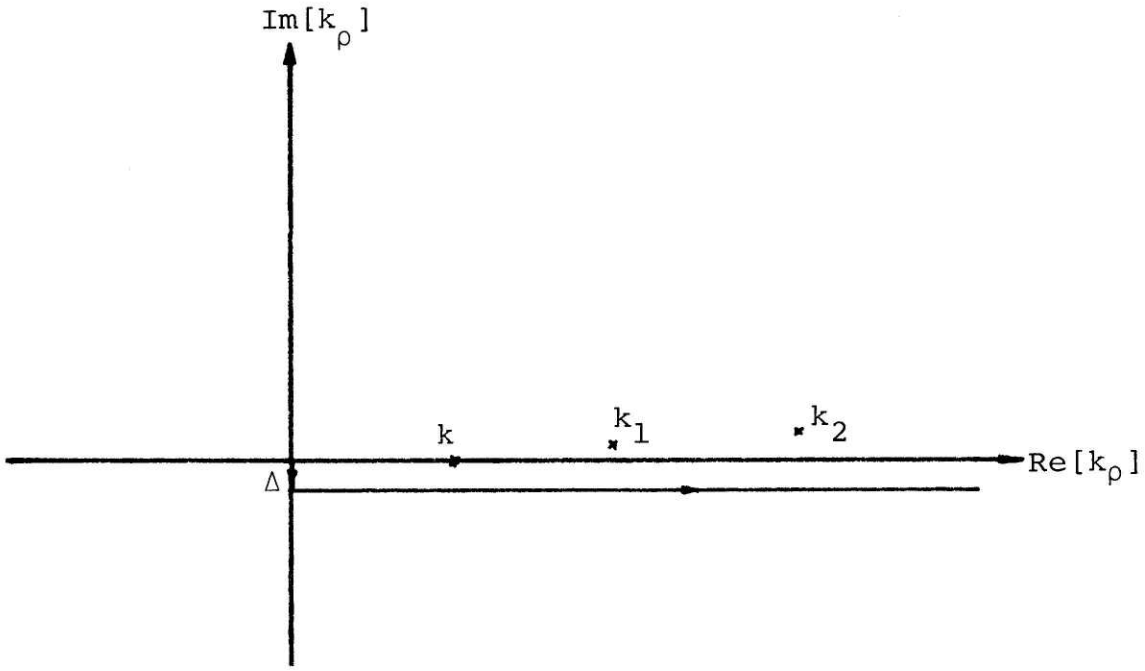

Fig. 2.2.3. Path for numerical integration.

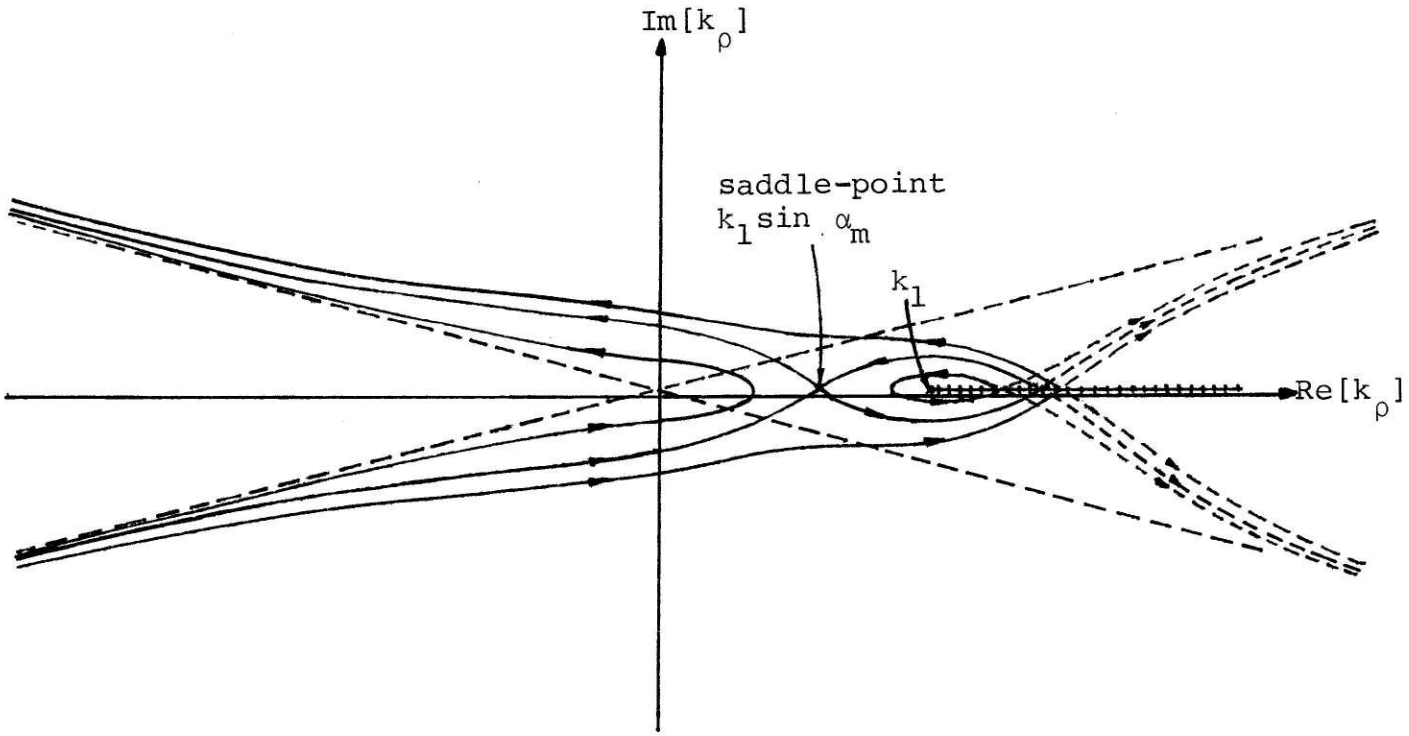

Fig.2.2.4. Constant-phase paths showing steepest-descent path on the k_ρ-plane. The arrows show directions of steepest descent.

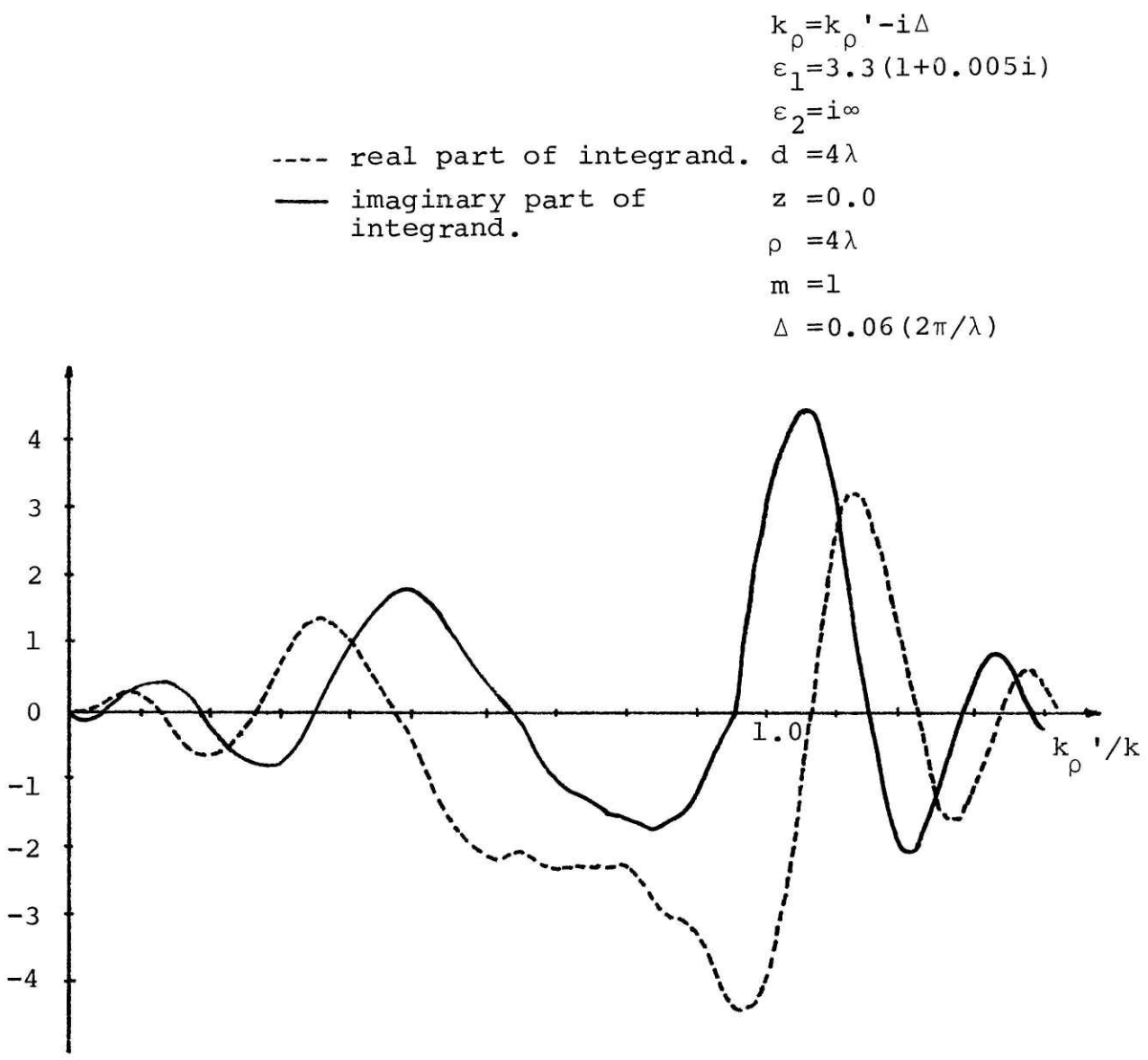

Fig. 2.2.5(a). Integrand of (2.1.2) as a function of k_ρ'/k when $\Delta = 0.06(2\pi/\lambda)$.

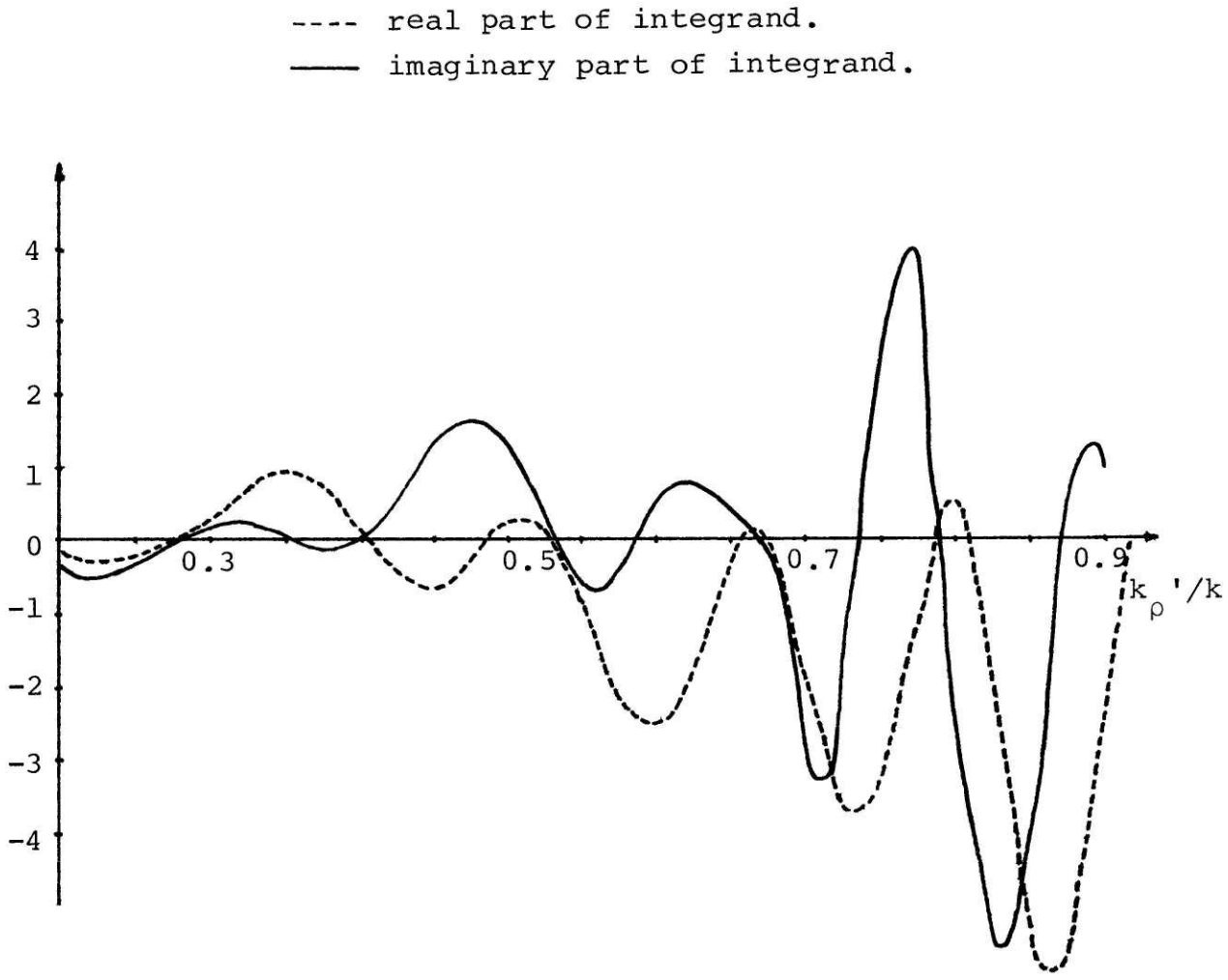

Fig. 2.2.5(b). Integrand of (2.1.2) as a function of k_ρ'/k for $\Delta = 0.001(2\pi/\lambda)$. The other parameters remains the same as (a). Note that the horizontal scale has been expanded c.f. (a).

for $\Delta = 0.06k$. Note that the integrand varies slowly around the stationary point, and that the period of oscillation is much bigger than that of $e^{ik_\rho \rho}$ (which has a period of $\underline{k}_\rho = 0.25k$). Fig. 2.2.5(b) shows the rapid variation of the integrand as a function of $\mathrm{Re}[k_\rho]/k$ for $\Delta = 0.001k$. Note that the horizontal scale has been expanded. Thus a judicious choice of Δ is $3/2\rho$, which is the value chosen in Fig. 2.2.5(a).

2.3 Integration Program

It was shown earlier that computation time can be saved by deforming the path of integration. The value of each reflected-wave term in (2.2.1) can be obtained by first integrating from $k_\rho = 0$ to $-i\Delta$ and then from $k_\rho = -i\Delta$ to $-i\Delta + \infty$. The second range of integration need not be to $-i\Delta + \infty$ as the integrand diminishes quickly after k_ρ' passes the branch point k_1. This is because of the presence of $e^{ik_{1z}2md}$ factor in the integrand (see 2.2.1).

As the integrand is still oscillating, it is advisable to section the range of integration to subsections of length $2\pi/\rho$. This length is chosen because the period of oscillation is always greater than $2\pi/\rho$, the period of oscillation of the Bessel function. Within each subsection, the function is slow varying, but there are occassional "wiggles" as can be seen from Fig. 2.2.5(a). As the occurrence of the wiggles is a local phenomenon, we want to design a program that can intelligently detect such wiggles, and apply a more accurate routine, e.g. by sectioning the subsection into smaller sections. This can be achieved with a recursive program written in a high level programming language. For example, by using Simpson's rule,[29] it is

```
INTEGRATE (F(x) FROM x = a to x = b): =

     A = SIMPSON (F(x) FROM x = a to x = b),
     B = SIMPSON (F(x) FROM x = a to x = (a+b)/2)
       + SIMPSON (F(x) FROM x = (a+b)/2 to x = b),

IF |A - B| < TOLERANCE THEN B
ELSE INTEGRATE (F(x) FROM x = a to x = (a+b)/2)
       + INTEGRATE (F(x) FROM x = (a+b)/2 to x = b).
```

The above program is written in a comprehensive form and can be translated to high level programming languages easily. It says that when integrating a function from a to b, Simpson's rule can be applied to the interval (a, b) to obtain A and to the halved intervals (a, (a+b)/2) and ((a+b)/2, b) to obtain B respectively. If the difference of A and B is less than the tolerance, it indicates that B is a good approximation to the integration of F(x) from x = a to x = b, or else, the INTEGRATE function can be applied recursively to the halved intervals again until a good approximation is obtained.

Simpson's rule is used here because the number of functional evaulation needed for subsequent sectioning of the range of integration does not increase as fast as say if Gaussian integration formula[30] is used. The use of recursion here is

is important as it enables the numerical integrator to intelligently section ranges of rapid variation into smaller subsections. Another kind of recursive method commonly used is the Romberg's method.[29] Romberg's method has the disadvantage that it indiscriminately sections the range of integration by half even if some part of the integration range varies slowly, thus causing unnecessary functional evaluations. However, the concept of Richardson's extrapolation used in Romberg's method can be applied here. The first iteration of Romberg's method gives rise to Simpson's rule. The second iteration of Romberg's method, which is equivalent to the use of Richardson's extrapolation on Simpson's rule gives rise to a value of integration which is exact for a polynomial of degree five. This more accurate result is given by

$$B' = B + (B - A)/15. \qquad (2.3.1)$$

This value of B' should replace B of the fifth line of the program. So the fifth line should be

IF |A - B| < TOLERANCE THEN B + (B - A)/15.

2.4 Conclusions

The integration program presented in the previous section was written in MACSYMA (Project MAC's Symbolic Manipulation System).[31] It was used to derive the numerical field solutions of a dipole antenna over two-layer media. The results are shown in Fig. 2.4.1 and in the next chapters alongside with the analytical approach. They agree well for the values of parameters within which the analysis is correct. However, numerical integration provides only an unsophisticated approach in deriving the field solutions. It does not improve our understanding of behaviors of the spherical wave generated by the dipole antenna over stratified media. Its merit is that it provides a counter-check for the correctness of an analytical solution. We shall see in the next chapters the derivations of the analytical solutions using various approaches.

It is to be noted that the numerical method presented here is by no means the best. Though the use of recursion has made the numerical integrator foolproof, it still consumes much computer time. For computers with large storage, the Fast Fourier Transform (FFT) method used by Tsang[19] and Kong et al[27] is far superior in speed. In the FFT method, the ingenious use of the Laplace transform of the Bessel function removes the rapid variation of the integrand due to the Bessel

function. It also removes the ρ dependence of the Discrete Fourier Transform (DFT) of the integrand. However, the rapid variation of the integrand due to $\exp[ik_{1z}2md]$ for large m and d causes the number of sampling points for the DFT to increase resulting in proportionately large storage requirement.

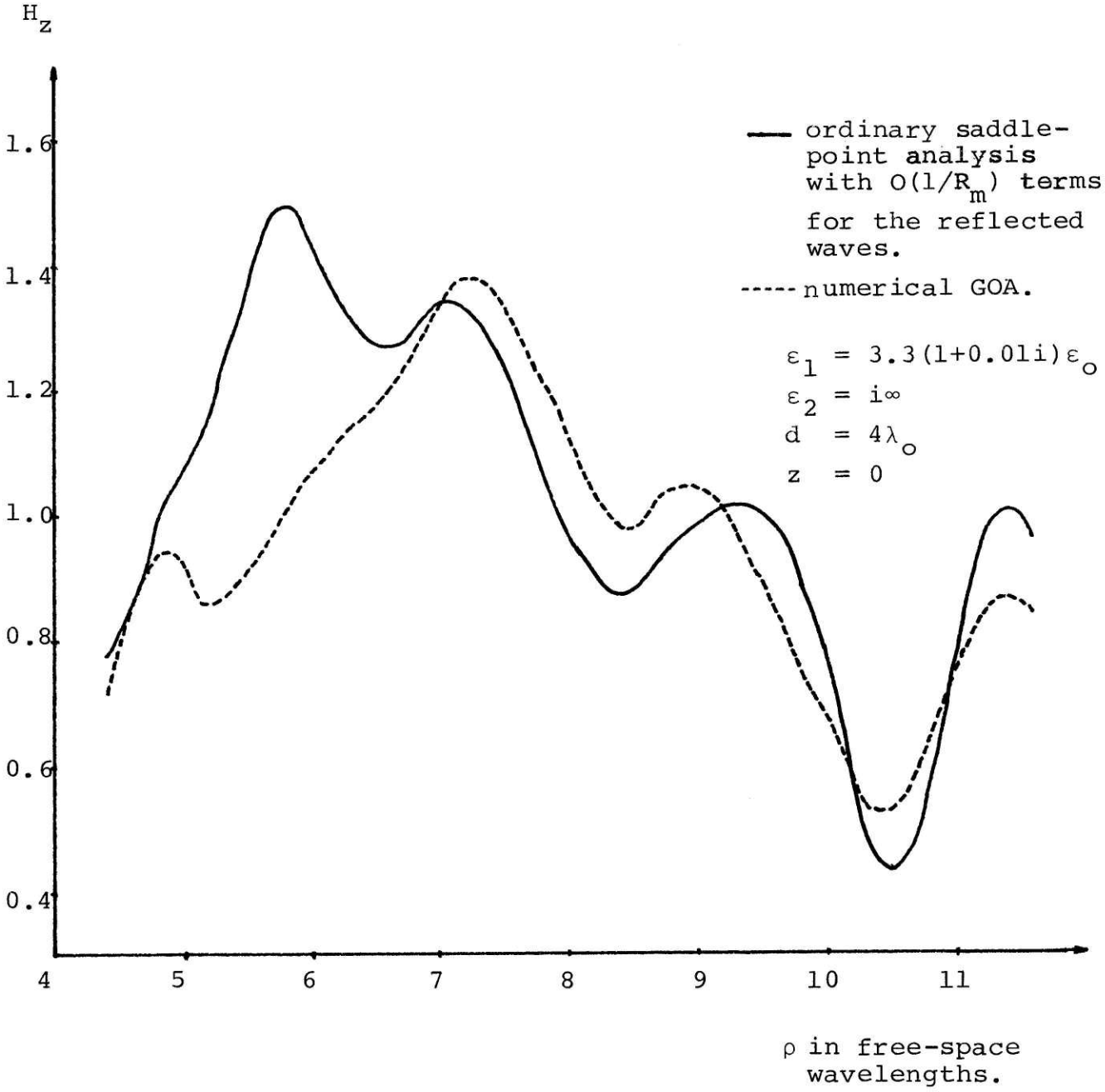

Fig. 2.4.1(a). H_z component in the broadside direction of an HED, normalized with respect to $I\ell/4\pi\lambda^2$. The discrepancies between the two results are high when $\alpha_m \simeq \theta_o$.

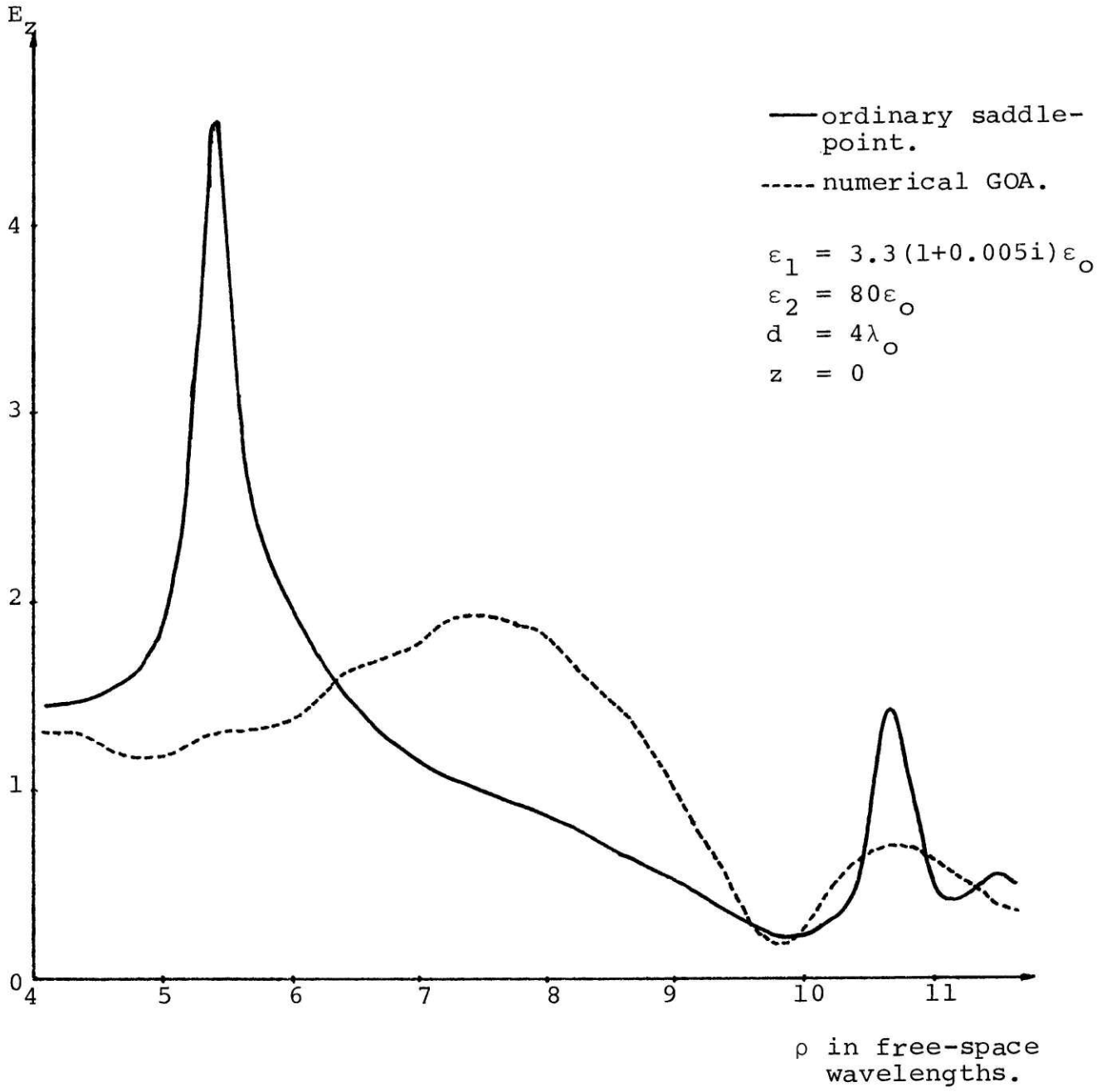

Fig. 2.4.1(b). E_z component in the broadside direction of an HMD normalized with respect to $I\ell /4\pi\omega\varepsilon\lambda^2$. The proximity of the branch-point and Sommerfeld pole to the saddle-point causes the solution to be invalid.

Chapter 3. MODIFIED SADDLE-POINT METHOD

3.1 Introduction

We have seen the use of the ordinary saddle-point method in the asymptotic expansions of integrals in Chapter 1. Its use in deriving the asymptotic expansions of the integral representations of the field solution becomes invalid when there is a singularity in the coefficient function which is in the neighborhood of the saddle-point, therefore a modified saddle-point method has to be used for such cases. For singularities which are poles[6,7], they can be subtracted from the integrand and ordinary saddle-point analysis can be performed on the integral whose integrand is pole-free. The contributions of the poles can then be expressed in terms of known functions. But when the algebraic singularities are of fractional order, the above method does not apply. The discussion here involves a modified saddle-point analysis that is valid for an algebraic singularity of finite, arbitrary order in the vicinity of the saddle-point. This is important in the study of anomalous wave behaviors in electromagnetic field problems.

3.2 Asymptotic Expansions of Integrals

The asymptotic expansion of an integral with an exponential factor $e^{-\lambda f(t)}$ as a part of the integrand, and whose path of integration lies on the complex plane is best facilitated by the saddle-point method. In such method, the original path of integration is deformed to the steepest-descent path passing through the saddle-point. The contribution from the saddle-point together with the contributions from singularities enclosed in the course of deformation is equal to the original integral. For integrals with finite end-points, the end-point contributions have to be considered. There are two advantages in deforming the path of integration; firstly, the asymptotic approximation of the contributions from the critical points (i.e. saddle-points and singularities) can be obtained, and secondly, physical interpretation can often be associated with their contributions. A discussion of the asymptotic expansions of the critical-point contributions when an algebraic singularity which can be arbitrarily close to the saddle-point is given here.

(a) Saddle-Point Contribution

A typical integral where an algebraic singularity is in the neighborhood of a saddle-point can be expressed as

$$I = \int_C (t - t_b)^r \, g(t) \, e^{-\lambda f(t)} \, dt \qquad (3.2.1)$$

where r can be fractional as well as negative integers and λ is a big parameter. We shall consider the case where C, the integration path, extends to infinity. Without loss of generality, the saddle-point is assumed to be at the origin, i.e. $f'(0) = 0$. Thus t_b measures the distance of the singularity from the saddle-point.

To find the saddle-point contribution, the path of integration C is deformed to the steepest-descent path that passes through the saddle-point. Contributions from singularities enclosed have to be included according to Cauchy's theorem. With the following transformation;

$$f(t) = f(0) - s^2, \qquad (3.2.2)$$

the steepest-descent path that passes through the saddle-point on the t-plane is mapped into the real axis on the s-plane. Thus, the saddle-point contribution of (3.2.1) is given by

$$I_s = e^{-\lambda f(0)} \int_{-\infty}^{\infty} (s - s_b)^r \, G(s) \, e^{-\lambda s} \, ds \qquad (3.2.3)$$

where

$$G(s) = \left\{\frac{t - t_b}{s - s_b}\right\}^r g(t) \, \frac{dt}{ds}.$$

$G(s)$ is analytic in the neighborhood of the saddle-point since $t = t_b$ when $s = s_b$; i.e. the singularity at $t = t_s$ is mapped onto the singularity at $s = s_b$. Therefore, from (3.2.2)

$$s_b = \pm \sqrt{f(t_b) - f(0)} \ . \tag{3.2.4}$$

The branch of square-root of (3.2.4) can be determined as follows. Since the mapping from the t-plane to the s-plane is conformal, the angle between two lines is preserved. For a straight line that joins the saddle point at $t = 0$ to the branch point at $t = t_b$, the angle it makes with the steepest-descent path passing through $t = 0$ is preserved on the s-plane. When t_b and s_b are small, this angle corresponds to the argument of s_b. Hence, we can decide the branch of square-root of s_b.

Note that as $\lambda \to \infty$, the dominant contribution of I_s comes from around $s = 0$; consequently, $G(s)$ is Taylor-series expanded around $s = 0$ to approximate I_s. We let

$$\hat{I} = e^{-\lambda f(0)} \int_{-\infty}^{\infty} (s - s_b)^r \sum_{n=0}^{\infty} \frac{G^{(n)}(0)}{n!} s^n e^{-\lambda s^2} \, ds. \tag{3.2.5}$$

Strictly speaking, $\hat{I} \neq I_s$ since $G(s)$ is replaced by a power series, which is valid over a finite region in general, while the range of integration extends to infinity. The series $\hat{I}$ does not necessarily converge, but we will show that the series $\hat{I}$ is asymptotic to I_s in generalized Poincare's sense.[32]

With the change of variable to $u = \sqrt{2\lambda}\ (s - s_b)$ the n-th term of $\hat{I}$ is

$$\hat{I}_n = \frac{e^{-\lambda[f(0) + s_b^2]}}{(2\lambda)^{\frac{n+1+r}{2}}} \frac{G^{(n)}(0)}{n!} \int_{-\infty}^{\infty} (u + \sqrt{2\lambda}\ s_b)^n\ u^r\ e^{-\left(\frac{u^2}{2} + \sqrt{2\lambda}\ s_b u\right)}\ du. \qquad (3.2.6)$$

$(u + \sqrt{2\lambda}\ s_b)^n$ can be expanded binomially, and $\hat{I}_n$ can be expressed as

$$\hat{I}_n = \frac{e^{-\lambda[f(0) + s_b^2]}}{(2\lambda)^{\frac{n+1+r}{2}}} \frac{G^{(n)}(0)}{n!} \sum_{\ell=0}^{n} {}_n C_\ell\, (\sqrt{2\lambda}\ s_b)^\ell\ W_{n-\ell+r}\ (\sqrt{2\lambda}\ s_b) \qquad (3.2.7)$$

where

$$W_k(\sqrt{2\lambda}\, s_b) = \int_{-\infty}^{\infty} u^k\, e^{-\left(\frac{u^2}{2} + \sqrt{2\lambda}\, s_b u\right)}\, du. \qquad (3.2.8)$$

In (3.2.8), the path of integration is above the singularity at the origin when the saddle-point is above the real axis, and it is below the singularity at the origin when the saddle-point is below the real axis. The location of the saddle-point on the u-plane is at $u = -\sqrt{2\lambda}\, s_b$. By taking the principle value of u^r when u is on the positive real axis, and using the linear relation of parabolic cylinder function[33,34]

$$W_k(\sqrt{2\lambda}\, s_b) = \begin{cases} \sqrt{2\pi}\, e^{\frac{\pi}{2} ri}\, e^{\lambda \frac{s_b^2}{2}}\, D_k(i\sqrt{2\lambda}\, s_b), & Im[s_b] < 0 \\ \sqrt{2\pi}\, e^{-\frac{\pi}{2} ri}\, e^{\lambda \frac{s_b^2}{2}}\, D_k(-i\sqrt{2\lambda}\, s_b) & Im[s_b] > 0. \end{cases}$$

(3.2.9)

Using the small argument approximation of $D_k(x)$, it is seen that $\hat{I}_n \sim O(\hat{I}_{n-2}/\lambda)$ when $\sqrt{2\lambda}\,|s_b| << 1$ and λ large. Using the large argument approximation of $D_k(x)$, it is also noted that $\hat{I}_n \sim O(\hat{I}_{n-2}/\lambda)$ when $\sqrt{2\lambda}|s_b| >> 1$ and λ large. Since $D_k(x)$ is of finite order when its argument

is moderately large, therefore $\hat{I}_n \sim O(\hat{I}_{n-2}/\lambda)$ when $\lambda \to \infty$ is always true. Thus if we let $s_m = \hat{I}_{2m} + \hat{I}_{2m+1}$, then $s_m \sim O(s_{m-1}/\lambda)$ when $\lambda \to \infty$. As a consequence, I_s of (3.2.2) is asymptotic to the series $\sum_{m=0}^{\infty} s_m$, or

$$I_s \sim \sum_{m=0}^{\infty} (\hat{I}_{2m} + \hat{I}_{2m+1}) \qquad \lambda \to \infty \tag{3.2.10}$$

in the generalized Poincare's sense for all values of s_b.

$\hat{I}_n$ can also be evaluated by repeated integration by parts, resulting in

$$\hat{I}_n = \frac{e^{-\lambda[f(0) + s_b^2]}}{(2\lambda)^{\frac{1+r+n}{2}}} \frac{G^{(n)}(0)}{n!} A(n, r) \tag{3.2.11}$$

where $A(n, r)$ satisfies the recursion relation

$$A(n, r) = (n-1)\, A(n-2, r) + r\, A(n-1, r-1)$$

$$A(0, r) = W_r(\sqrt{2\lambda}\, s_b). \tag{3.2.12}$$

Using the above, we obtain

$$\hat{I}_o = \frac{e^{-\lambda [f(0) + s_b^2]}}{(2\lambda)^{\frac{1+r}{2}}} G(0)\ W_r(\sqrt{2\lambda}\ s_b) \qquad (3.2.13)$$

$$\hat{I}_1 = \frac{e^{-\lambda [f(0) + s_b^2]}}{(2\lambda)^{\frac{2+r}{2}}} G'(0)\ W_{r-1}(\sqrt{2\lambda}\ s_b). \qquad (3.2.14)$$

From (3.2.3) and using

$$\left.\frac{dt}{ds}\right|_{s=0} = \sqrt{2/f''(0)},$$

$$\frac{d^2t}{ds^2} = -\frac{2}{3}\frac{f'''(0)}{[f''(0)]^2},$$

which are obtained from power series inversion,[7,14]

$$G(0) = (t_b/s_b)^r\ g(0)\ \sqrt{2/f''(0)} \qquad (3.2.15)$$

$$G'(0) = (t_b/s_b)^r \left[\frac{r}{t_b}\ g(0) \left(\frac{t_b}{s_b} - \sqrt{2/f''(0)}\right) \sqrt{2/f''(0)}\right.$$

$$+ g'(0) \frac{2}{f''(0)} - g(0) \frac{2f'''(0)}{3[f''(0)]^2} \Bigg] . \qquad (3.2.16)$$

In the above expressions, the choice of the branch of square-root for dt/ds is such that its argument gives the correct rotation under the conformal mapping of a point on the t-plane to the s-plane. This is because that $\arg(dt/ds)$ measures the angle of rotation of the mapping.

(b) Contribution from Algebraic Singularities

In (a), we have shown the approach to approximate the saddle-point contribution with an asymptotic expansion. When the original path of integration is deformed to the steepest-descent path passing through the saddle-point, contributions from singularities enclosed have to be included. For algebraic singularities which are poles, their residue contributions are included. For branch-points, the branch-cut integrals are included. One can always choose a branch-cut so that it can be deformed to the steepest-descent path passing through it. As such, the asymptotic expansion of the branch-cut integral can be obtained by the method of steepest descent. We will include here a derivation of the asymptotic expansion of the branch-cut integral which is uniformly valid when it is in the neighborhood of a saddle-point.

The general form of a branch-cut integral is

$$I_b = \int_C t^r \, h(t) \, e^{-\lambda \phi(t)} \, dt. \tag{3.2.17}$$

Without loss of generality, the branch-point is assumed to be at the origin. C is the path of integration from zero to complex infinity such that (3.2.17) converges. C can also be deformed to the steepest-descent path passing through the branch-point, $\phi'(\alpha) = 0$ so that there is a simple saddle-point at $t = \alpha$ where $|\alpha|$ can be arbitrarily small. With the following transformation,

$$\phi(t) - \phi(0) = \frac{s^2}{2} + \gamma s. \tag{3.2.18}$$

(3.2.17) becomes

$$I_b = e^{-\lambda \phi(0)} \int_0^\infty s^r \, H(s) \, e^{-\lambda \left[\frac{s^2}{2} + \gamma s \right]} \, ds \tag{3.2.19}$$

where

$$H(s) = (t/s)^r \, h(t) \, \frac{dt}{ds} \tag{3.2.20}$$

$$\frac{dt}{ds} = \frac{s + \gamma}{\phi'(t)} .$$

The saddle-point is at $s = -\gamma$. Thus from (3.2.18), the relation between α and γ is

$$\gamma = \pm \sqrt{2[\phi(0) + \phi(\alpha)]} . \qquad (3.2.21)$$

The branch of square-root for (3.2.21) is decided as follows. On the s-plane, the constant-phase path passing through the origin is given by

$$\mathrm{Im}\left[\frac{s^2}{2} + \gamma s\right] = 0. \qquad (3.2.22)$$

Solving this, we obtain

$$\frac{\mathrm{Re}[\gamma]}{\mathrm{Re}[s]} + \frac{\mathrm{Im}[\gamma]}{\mathrm{Im}[s]} = -1 \qquad (3.2.23)$$

The branch-cut integral is from 0 to ∞ on the s-plane. For this path of integration to be deformable to the steepest-descent path passing through the origin, $|\arg[\gamma]| < \pi/2$. This provides the criterion for choosing the branch of square-root in (3.2.21).

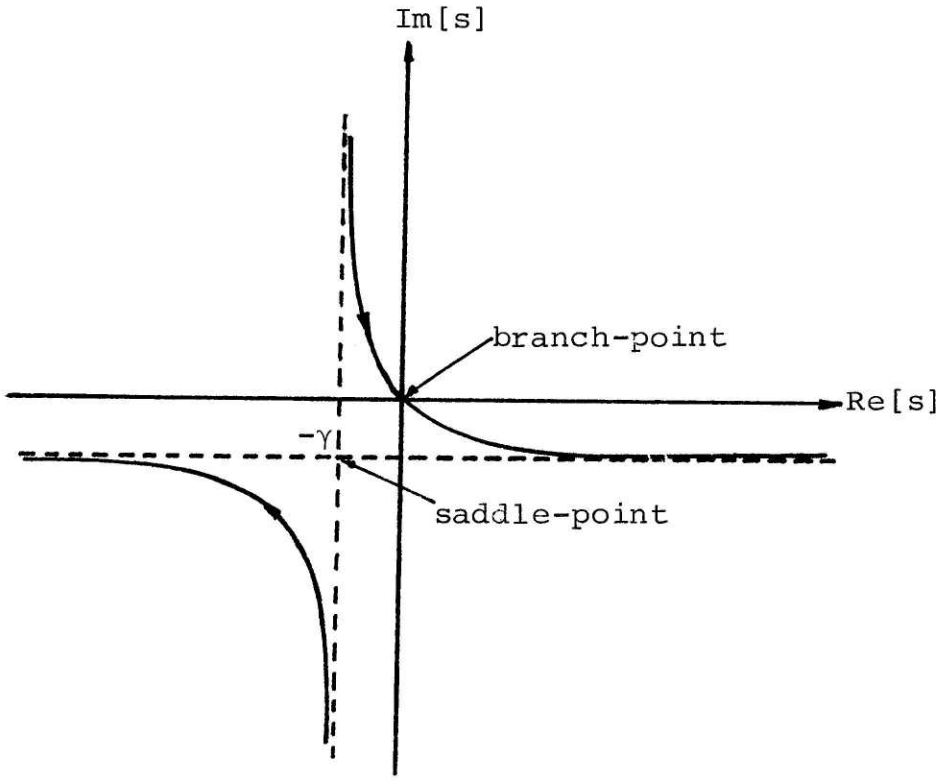

Fig. 3.2.1. The constant-phase path that passes through the branch-point when $|\arg[\gamma]| < \pi/2$.

Since the path of integration is along the steepest-descent path on the x-plane (which is the same as integrating from 0 to ∞), most of the contribution to the integral comes from around $s = 0$ when $\lambda \to \infty$. Thus if $H(s)$ in (3.2.19) is Taylor-series expanded around $s = 0$, and the integration is carried out for each term, we obtain a series which does not necessarily converge but is asymptotic to I_b.

$$I_b \sim e^{-\lambda\phi(0)} \sum_{n=0}^{\infty} \frac{H^{(n)}(0)}{n!} \int_0^{\infty} s^{n+r} e^{-\lambda\left[\frac{s^2}{2} + \gamma s\right]} ds. \quad (3.2.24)$$

Noting that the above integral is the integral representation of parabolic cylinder function,

$$I_b \sim e^{-\lambda\left[\phi(0) - \frac{\gamma^2}{4}\right]} \sum_{n=0}^{\infty} \frac{H^{(n)}(0)}{n!} \frac{\Gamma(n+r+1)}{\lambda^{(n+r+1)/2}}$$

$$D_{-(n+r+1)}(\sqrt{\lambda}\,\gamma). \quad (3.2.25)$$

Using the large-argument approximation of parabolic cylinder function, the n-th term of I_b, we note that $I_{bn} \sim O(\lambda^{-(n+r+1)})$ when $\sqrt{\lambda}\,\gamma >> 1$ and $|\arg[\gamma]| < \pi/2$. Using

the small-argument approximation,

$$I_{bn} \sim O\left(\lambda^{-\frac{(n + r + 1)}{2}}\right)$$

when $\sqrt{\lambda}\ \gamma << 1$. Since the parabolic cylinder function is of finite order when its argument is moderately large, $I_{bn} \sim o(I_{bn - 1})$ for all γ when $\lambda \to \infty$. Thus, the series in (3.2.27) is asymptotic to I_b in generalized Poincare's sense.

The following formula is useful for evaluating the first two terms of the expansion:

$$H(0) = \left[\frac{\gamma}{\phi'(0)}\right]^{r + 1} h(0) \qquad (3.2.26)$$

$$H'(0) = h(0)\left(\frac{r}{2} + 1\right)\left[\frac{\gamma}{\phi'(0)}\right]^{r}\left[\frac{1}{\phi'(0)} - \frac{\gamma^2\ \phi''(0)}{[\phi'(0)]^3}\right]$$

$$+ h'(0)\left[\frac{\gamma}{\phi'(0)}\right]^{r + 2} . \qquad (3.2.27)$$

3.3 An Example of the Asymptotic Expansions of Integrals

A commonly encountered example of a saddle-point analysis in the field evaluation of a dipole antenna over stratified media is

$$I = \int_{-\infty}^{\infty} k_z \, A(k_\rho) \, e^{iR(k_\rho \sin \alpha_o + k_{1z} \cos \alpha_o)} \, dk_\rho \qquad (3.3.1)$$

where $k_{iz} = (k_i^2 - k_\rho^2)^{1/2}$ and $A(k_\rho)$ is an analytic function of k_ρ.

There is a saddle-point at $k_{\rho s} = k_1 \sin \alpha_o$. The branch-point at $k_\rho = k$ can be arbitrarily close to the saddle-point for differing values of α_o (see Fig. 3.3.1). Branch-cuts of $Im[k_z] = 0$ and $Im[k_{1z}] = 0$ are chosen for the double-valued function k_z and k_{1z} respectively. The original path of integration is on the Riemann sheet where $Im[k_z] > 0$ and $Im[k_{1z}] > 0$. The path of integration can be deformed to the steepest-descent path passing through the saddle-point as shown.

When

$$\alpha_o > \sin^{-1} \frac{k}{k_1} ,$$

the branch-cut contribution, as shown in Fig. 3.3.2 has to be

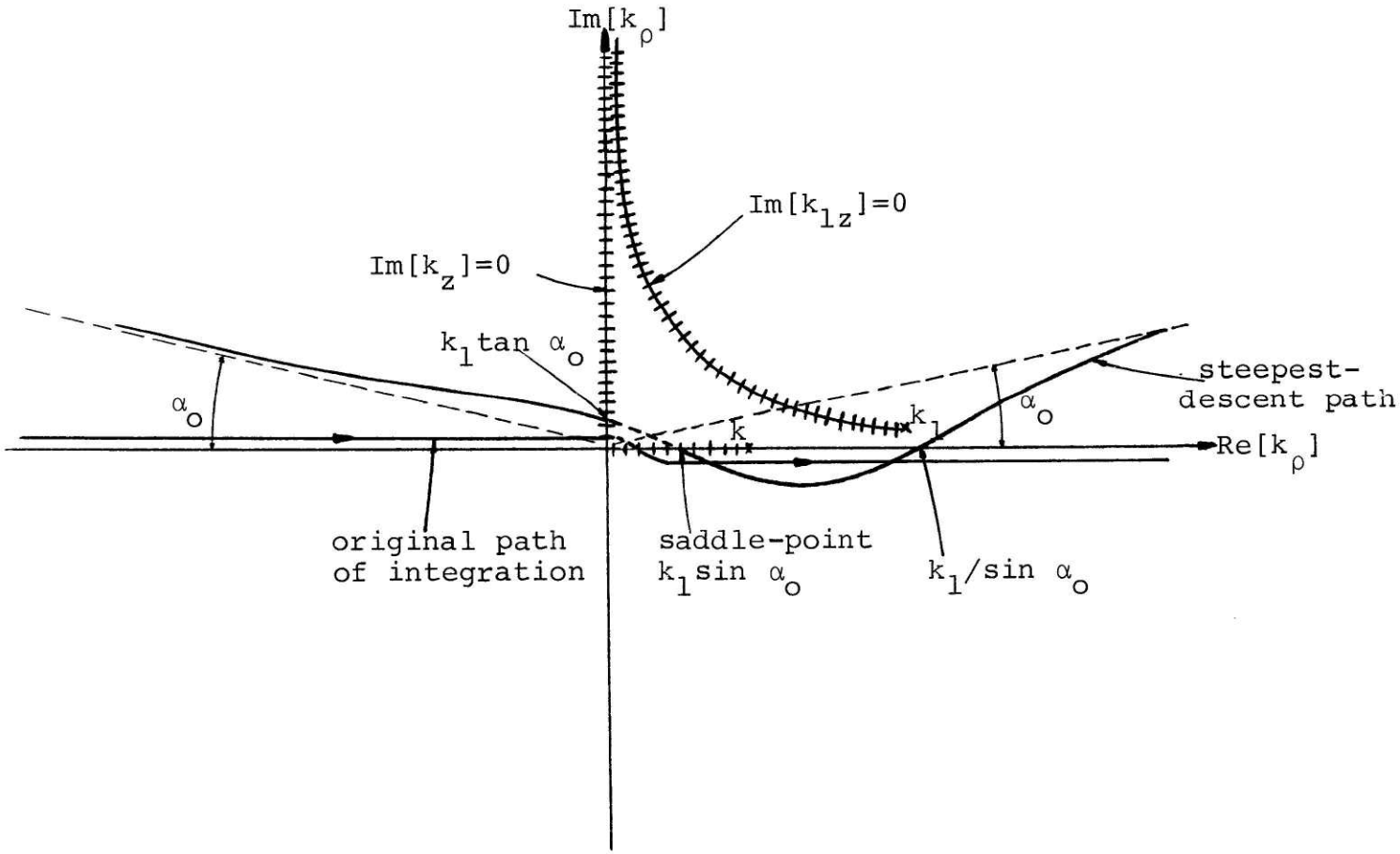

Fig. 3.3.1. The original path of integration, steepest-descent path and branch-cuts for integral I.

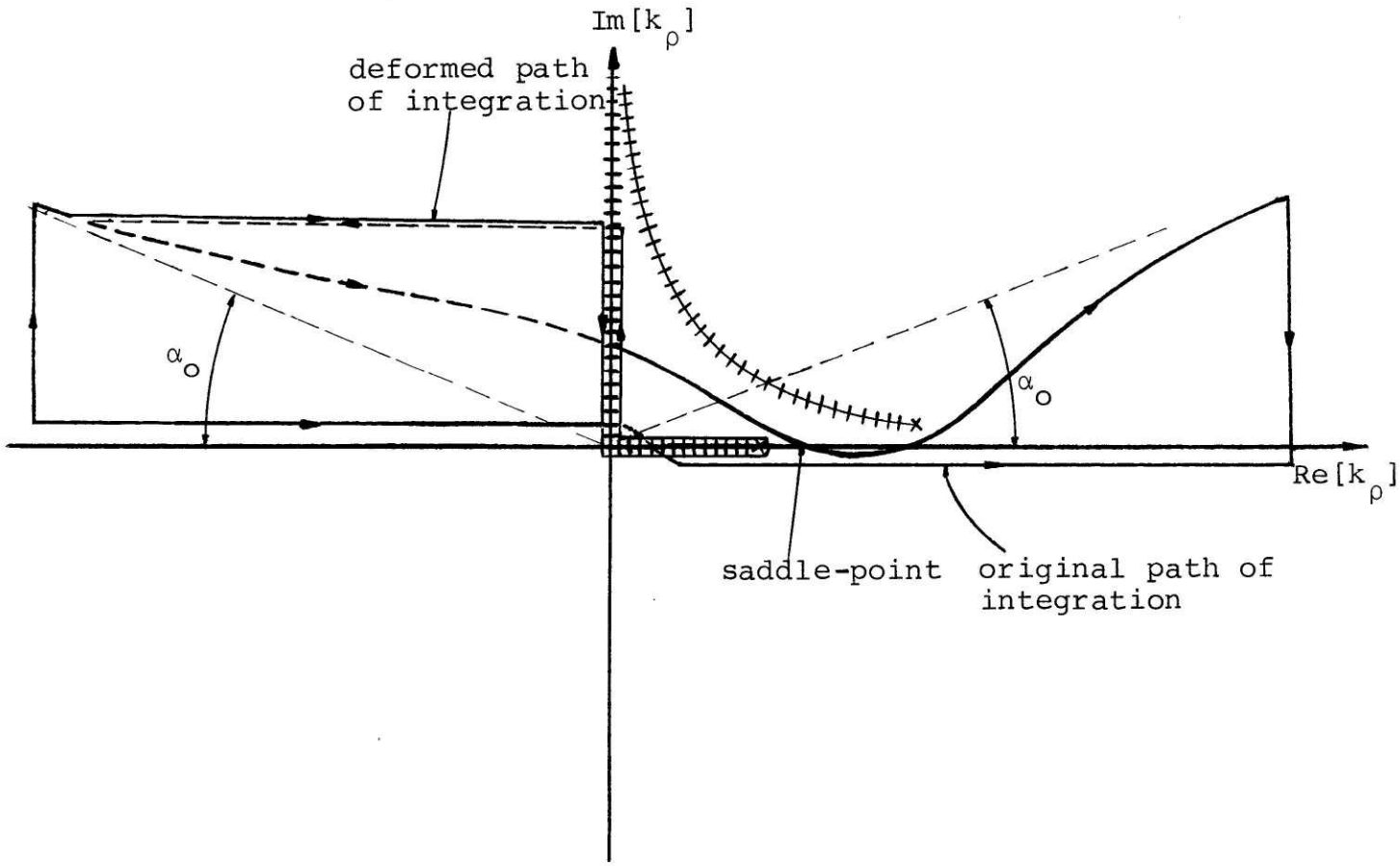

Fig. 3.3.2. The branch-cut contribution and saddle-point contribution when $\alpha_o > \sin^{-1} k/k_1$.

included. The branch-point k_1 does not contribute to the integral as it is never enclosed.

(a) Saddle-Point Contribution

We will first calculate the saddle-point contribution to the integral I. Letting

$$\lambda = R, \qquad t = k_\rho - k_1 \sin \alpha_o, \qquad t_b = k - k_1 \sin \alpha_o \tag{3.3.2}$$

$$f(t) = - i[\sin \alpha_o \, k_\rho + (k_1^2 - k_\rho^2)^{1/2} \cos \alpha_o] \tag{3.3.3}$$

$$g(t) = e^{i\frac{\pi}{2}} (k + k_\rho)^{1/2} A(k_\rho). \tag{3.3.4}$$

(3.3.1) becomes the form of (3.2.1). Hence, we can apply the asymptotic analysis described in the previous section to the integral (3.3.1). On the s-plane,

$$S_b = \pm e^{-i\frac{\pi}{4}} [k \sin \alpha_o + (k_1^2 - k^2)^{1/2} \cos \alpha_o - k_1]^{1/2} \tag{3.3.5}$$

where S_b is the location of branch-point. Letting

$$\theta_o = \sin^{-1} \frac{k}{k_1} ,$$

and with proper choice of signs, (3.3.5) becomes

$$S_b = e^{i\frac{\pi}{4}} \sqrt{2k_1} \sin\left[\frac{\theta_o - \alpha_o}{2}\right] . \tag{3.3.6}$$

To find the asymptotic expansion to the integral (3.3.1), we make use of (3.2.13) and (3.2.14) with $r = 1/2$. In (3.2.13)

$$W_{1/2}(\sqrt{2\lambda}\, S_b) = e^{\lambda \frac{S_b^2}{2}} \sqrt{2\pi} \left[e^{\mp \frac{\pi}{4} i} D_{1/2}(\mp i\sqrt{2\lambda}\, S_b) \right] \begin{matrix} \alpha_o < \theta_o \\ \\ \alpha_o > \theta_o \end{matrix}$$

(3.3.7)

where the notation means that the upper sign is chosen when $\alpha_o < \theta_o$ and the lower sign is chosen when $\alpha_o > \theta_o$. Thus

$$\hat{I}_o = \frac{e^{ik_1 R}}{[k_1 R]^{3/4}} e^{i\frac{\pi}{8}} \frac{(k^2 - k_1^2 \sin^2\alpha_o)^{1/2}}{\sqrt{2}\, \sin^{1/2}\left(\frac{\theta_o - \alpha_o}{2}\right)} k_1 \cos\alpha_o\, A(k_1 \sin\alpha_o)$$

$$e^{-ik_1 R \sin^2\left(\frac{\alpha_o - \theta_o}{2}\right)} \sqrt{2\pi} \left\{ e^{\mp\frac{\pi}{4}i} \right.$$

$$\left. D_{1/2}\left[\mp e^{i3\frac{\pi}{4}} 2\sqrt{k_1 R} \sin\left(\frac{\theta_o - \alpha_o}{2}\right)\right]\right\} \quad \begin{matrix} \alpha_o < \theta_o \\ \alpha_o > \theta_o \end{matrix} \qquad (3.3.8)$$

In (3.2.14),

$$W_{-1/2}(\sqrt{2\lambda}\, S_b) = e^{\lambda \frac{S_b^2}{2}} \sqrt{2\pi} \left[e^{\pm \frac{\pi}{4} i} D_{-1/2}(\mp i\sqrt{2\lambda}\, S_b) \right] \quad \begin{matrix} \alpha_o < \theta_o \\ \alpha_o > \theta_o \end{matrix}$$

(3.3.9)

and from (3.2.16)

$$G'(0) = \left[\frac{k - k_1 \sin\alpha_o}{\sin\left(\frac{\theta_o - \alpha_o}{2}\right)}\right]^{1/2} \frac{e^{-i\frac{5\pi}{8}}}{(2k_1)^{1/4}} \left\{ \frac{g(0)}{\sqrt{2}} \frac{\sqrt{k_1}\cos\alpha_o}{k - k_1 \sin\alpha_o} \right.$$

$$\left[\frac{k - k_1 \sin\alpha_o}{\sqrt{2k_1}\sin\left(\frac{\theta_o - \alpha_o}{2}\right)} - \sqrt{2k_1}\cos\alpha_o\right] + g'(0)\, 2k_1 \cos^2\alpha_o$$

$$\left. - 2g(0)\sin\alpha_o \right\} \qquad (3.3.10)$$

where

$$g(0) = e^{i\frac{\pi}{2}} (k + k_1 \sin \alpha_o)^{1/2} A(k_1 \sin \alpha_o) \qquad (3.3.11)$$

$$g'(0) = e^{i\frac{\pi}{2}} \left[\frac{1}{2} \frac{A(k_1 \sin \alpha_o)}{(k + k_1 \sin \alpha_o)^{1/2}} + (k + k_1 \sin \alpha_o)\, A'(k_1 \sin \alpha_o) \right] \qquad (3.3.12)$$

Therefore

$$\hat{I}_1 = \frac{e^{ik_1 R}}{(2R)^{5/4}} e^{-ik_1 R \sin^2 \left(\frac{\alpha_o - \theta_o}{2} \right)} G'(0) \sqrt{\pi/2}$$

$$\begin{cases} e^{\pm \frac{\pi}{4} i} D_{-1/2}\left[\mp i2 \sqrt{k_1 R} \sin \left(\frac{\theta_o - \alpha_o}{2} \right) \right] & \alpha_o < \theta_o \\ & \alpha_o > \theta_o \end{cases} \qquad (3.3.13)$$

The above expression for the saddle-point contribution is uniformly valid for the saddle-point arbitrarily close to the branch-point.

(b) Branch-Point Contribution

When

$$\alpha_o > \sin^{-1} \frac{k}{k_1} ,$$

the branch-point contribution has to be included (see Fig. 3.3.2). The branch-cut integral is given by

$$I_b = \int_{BC} (k_z^- - k_z^+) A(k_\rho) e^{iR(k_\rho \sin \alpha_o + k_{1z} \cos \alpha_o)} dk_\rho \qquad (3.3.14)$$

where BC is a path of integration which starts from $k_\rho = k$, and follows along the branch-cut to ∞. k_z^- means that k_z is evaluated to the left to the branch-cut and thus $Re[k_z] < 0$. k_z^+ implies the converse. On the branch-cut, $k_z^+ = - k_z^-$, which means that (3.3.14) can be written as

$$I_b = - \int_{BC} 2k_z^+ A(k_\rho) e^{iR(k_\rho \sin \alpha_o + k_{1z} \cos \alpha_o)} dk_\rho . \qquad (3.3.15)$$

The path of integration BC can be deformed to the steepest-

descent path that passes through the branch-point at $k_\rho = k$. With the following transformation,

$$\lambda = R, \quad t = k_\rho - k, \quad \alpha = k_1 \sin \alpha_o - k \tag{3.3.16}$$

$$\phi(t) = - i[\sin \alpha_o \, k_\rho + (k_1^2 - k_\rho^2)^{1/2} \cos \alpha_o] \tag{3.3.17}$$

$$h(t) = 2 e^{i \frac{\pi}{2}} (k + k_\rho)^{1/2} A(k_\rho). \tag{3.3.18}$$

(3.3.15) is cast into the form of (3.2.17). On the s-plane,

$$\gamma = 2 e^{i \frac{\pi}{4}} \sqrt{k_1} \sin \left(\frac{\alpha_o - \theta_o}{2} \right) . \tag{3.3.19}$$

Therefore, the leading term of the asymptotic expansion to I_b is

(3.3.20)

$$I_{bo} = e^{ik_1 R \cos(\alpha_o - \theta_o)} \, e^{ik_1 R \sin^2 \left(\frac{\alpha_o - \theta_o}{2} \right)} \left[\frac{\cos \theta_o}{\cos \left(\frac{\alpha_o - \theta_o}{2} \right)} \right]^{3/2}$$

$$e^{-i \frac{3\pi}{8}} (k_1/R)^{3/4} \sqrt{2k\pi} \, A(k) \quad D_{-3/2} \left[2 e^{i \frac{\pi}{4}} \sqrt{k_1 R} \sin \left(\frac{\alpha_o - \theta_o}{2} \right) \right]$$

The first correction term to the above, with $H'(0)$ given by (3.2.27) where $r = 1/2$, is given by

$$I_{b1} = e^{ik_1 R \cos(\alpha_o - \theta_o)} \, e^{ik_1 R \sin^2\left(\frac{\alpha_o - \theta_o}{2}\right)} \, \frac{H'(0)}{R^{5/4}} \, \frac{3}{4} \sqrt{\pi}$$

$$D_{-5/2}\left[2 \, e^{i\frac{\pi}{4}} \sqrt{k_1 R} \sin\left(\frac{\alpha_o - \theta_o}{2}\right)\right] . \qquad (3.3.21)$$

3.4 Interference Fringes of a Dipole Antenna Over Two-Layer Media

The evaluation of the field components of a dipole antenna over two-layer media can be reduced to the evaluation of a typical integral

$$T = \int_{-\infty}^{\infty} \frac{k_\rho}{k_z} (1 + R) H_o^{(1)}(k_\rho \rho) e^{ik_z z} dk_\rho . \qquad (3.4.1)$$

In geometical-optics approximation, $(1 + R)$ is expanded in terms of a series (see Section 1.3). Therefore

$$T = \int_{-\infty}^{\infty} \frac{k_\rho}{k_z} X_{01} H_o^{(1)}(k_\rho \rho) e^{ik_z z} dk_\rho + \sum_{m=1}^{\infty} \int_{-\infty}^{\infty} \frac{k_\rho}{k_{1z}} A_m(k_\rho)$$

$$e^{ik_{1z}\, 2md} H_o^{(1)}(k_\rho \rho) dk_\rho \qquad (3.4.2)$$

where

$$A_m(k_\rho) = \frac{k_{1z}}{k_z} X_{01} X_{10} R_{10}^{m-1} R_{12}^{m} e^{ik_z z} . \qquad (3.4.3)$$

As discussed previously (Section 1.3), the saddle-point in the second integral, i.e. the reflected-wave term, can be

arbitrarily close to branch-point. After replacing $H_o^{(1)}(k_\rho \rho)$ by $\hat{H}_o^{(1)}(k_\rho \rho)\, e^{ik_\rho \rho}$, the exponential factor of the second integrand is of the form (3.3.1). To cast it into the form of (3.3.1), we have to factor out the k_z-dependence in $A_m(k_\rho)$, since the branch-point at $k_z = 0$ is in the vicinity of the saddle-point. To do this, we expand $A_m(k_\rho)$ in a power series in k_z. First we obtain, after some algebraic manipulation,

$$A_m = b\, X_{10}^2\, R_{10}^{m-1}\, R_{12}^m\, e^{ik_z z} \tag{3.4.4}$$

where b equals μ_1/μ_o for TE wave and $\varepsilon_1/\varepsilon_o$ for TM wave. By multiplying the denominators of X_{10} and R_{10} by $k_{1z} - b\, k_z$, k_z in the denominator is not a double-valued function anymore. Expanding the numerator using binomial expansion and the identity

$$e^x = \sum_{n=0}^{\infty} \frac{x^n}{n!},$$

$A_m(k_\rho)$ can be written as

$$A_m(k_\rho) = \frac{4b\, R_{12}^m}{\left[1 - \left(b\, \frac{k_z}{k_{1z}}\right)^2\right]^{m+1}} \left[\sum_{r=0}^{2m} {}_{2m}C_r \left(\frac{-b}{k_{1z}}\right)^r k_z{}^r\right]$$

$$\left[\sum_{s=0}^{\infty} \frac{(iz)^s}{s!} k_z^s \right] \tag{3.4.5}$$

for $k_z z << 1$. Multiplying out the series, and separating terms with even and odd powers of k_z, we obtain

$$A_{m\text{-even}} = \frac{4b\, R_{12}^m}{\left[1 - \left(\frac{bk_z}{k_{1z}}\right)^2\right]^{m+1}} \sum_{n=0}^{\infty} k_z^{2n} \sum_{r=0}^{\min(2n,\, 2m)} {}_{2m}C_r \left(\frac{-b}{k_{1z}}\right)^r \frac{(iz)^{2n-r}}{(2n-r)!} \tag{3.4.6}$$

$$A_{m\text{-odd}} = \frac{4b\, R_{12}^m}{\left[1 - \left(\frac{bk_z}{k_{1z}}\right)^2\right]^{m+1}} k_z \sum_{n=0}^{\infty} k_z^{2n} \sum_{r=0}^{\min(2n+1,\, 2m)} {}_{2m}C_r \left(\frac{-b}{k_{1z}}\right)^r \frac{(iz)^{2n+1-r}}{(2n+1-r)!} . \tag{3.4.7}$$

Thus it can be seen that only $A_{m\text{-odd}}$ has a branch-point at $k_z = 0$. Therefore ordinary saddle-point analysis can be applied to $A_{m\text{-even}}$ term. For the $A_{m\text{-odd}}$ term, we rewrite it as

$$A_{m\text{-odd}} = k_z A_{mo} \tag{3.4.8}$$

where A_{mo} is branch-point free at $k_z = 0$. Therefore, the odd term can be cast into the form of (3.3.1). Consequently the m-th reflected-wave term due to odd powers at k_z is

$$T^m_{R\text{-odd}} = \int_{-\infty}^{\infty} k_z A_{mo} \frac{k_\rho}{k_{1z}} \hat{H}_o^{(1)}(k_\rho \rho)\, e^{i(k_\rho \rho + 2md\, k_{1z})}\, dk_\rho . \tag{3.4.9}$$

Letting $R_m = [\rho^2 + (2md)^2]^{1/2}$, $\alpha_m = \tan^{-1}(\rho/2md)$, $T^m_{R\text{-odd}}$ becomes

$$T^m_{R\text{-odd}} = \int_{-\infty}^{\infty} k_z A_{mo} \frac{k_\rho}{k_{1z}} \hat{H}_o^{(1)}(k_\rho \rho)\, e^{iR(k_\rho \sin \alpha_m + k_{1z} \cos \alpha_m)}\, dk_\rho \tag{3.4.10}$$

which is of the form (3.3.1). From (3.3.8), the leading term of the saddle-point contribution is

$$T^{m(0)}_{R\text{-odd}} = \sqrt{2/\pi\rho}\; e^{-i\frac{\pi}{8}} \frac{e^{ik_1 R_m}}{(k_1 R_m)^{3/4}} \frac{(k - k_1 \sin \alpha_m)^{1/2}}{\left[2 \sin\left(\frac{\theta_o - \alpha_m}{2}\right)\right]^{1/2}} F(k_1 \sin \alpha_m)$$

$$k_1 \cos \alpha_m \, e^{-ik_1 R_m \sin^2\left(\frac{\alpha_m - \theta_o}{2}\right)} \sqrt{2\pi}$$

$$\begin{cases} e^{\mp i \frac{\pi}{4}} D_{1/2}\left[\mp e^{i\frac{3\pi}{4}} 2\sqrt{k_1 R_m} \sin\left(\frac{\theta_o - \alpha_m}{2}\right)\right] & \alpha_m < \theta_o \\ & \alpha_m > \theta_o \end{cases}$$

(3.4.11)

where

$$F(k_\rho) = \frac{\sqrt{k_\rho (k + k_\rho)}}{k_{1z}} A_{mo}.$$

The first correction to the above is given by (3.3.13). Hence

$$T^{m(1)}_{R\text{-odd}} = \sqrt{2/\pi\rho}\, e^{i\frac{\pi}{4}} \frac{e^{ik_1 R_m}}{(R_m)^{5/4}} \frac{e^{-ik_1 R_m \sin^2\left(\frac{\alpha_m - \theta_o}{2}\right)}}{2^{1/4}} G'(0) \sqrt{2\pi}$$

$$\begin{cases} e^{\pm i \frac{\pi}{4}} D_{-1/2}\left[\mp e^{i\frac{3\pi}{4}} 2\sqrt{k_1 R_m} \sin\left(\frac{\theta_o - \alpha_m}{2}\right)\right] & \alpha_m < \theta_o \\ & \alpha_m > \theta_o \end{cases}$$

(3.4.12)

where

$$G'(0) = \left[\frac{k - k_1 \sin \alpha_m}{\sin\left(\frac{\theta_o - \alpha_m}{2}\right)}\right]^{1/2} \frac{e^{-i\frac{5\pi}{8}}}{(2k_1)^{1/4}} \left\{\left[\frac{\cos \alpha_m}{\sin \theta_o - \sin \alpha_m}\right.\right.$$

$$\left.\left[\frac{\sin \theta_o - \sin \alpha_m}{\sin\left(\frac{\theta_o - \alpha_m}{2}\right)} - \cos \alpha_m\right] - 2 \sin \alpha_m\right] F(k_1 \sin \alpha_m)$$

$$\left. + F'(k_1 \sin \alpha_m)\, 2k_1 \cos^2 \alpha_m\right\} . \qquad (3.4.13)$$

When ordinary saddle-point analysis is applied to the $A_{m\text{-even}}$ term in the reflected-wave term, it gives rise to leading terms of $O(R_m^{-1})$ and $O(R_m^{-2})$ (see Section 1.3). The modified saddle-point analysis when applied to $A_{m\text{-odd}}$ term gives rise to leading terms of $O(R_m^{-5/4})$ and $O(R_m^{-7/4})$ for the branch point in the vicinity of the saddle-point. Consequently, the first two leading terms to the reflected-wave term are of $O(R_m^{-1})$ and $O(R_m^{-5/4})$. In general, for the computation of the field components of a dipole antenna, the terms of $O(R_m^{-1})$ and $O(R_m^{-5/4})$ sufficiently approximate the reflected wave component when the branch-point is close to the saddle-point. When

the branch-point is far away from the saddle-point, the above analysis is still correct but cumbersome, whereas the use of (1.3.7a) saves computation time.

Furthermore, (3.4.9) gives rise to a branch-point contribution when $\alpha_m > \theta_o$. In accordance with (3.3.20), the leading term of the branch-point contribution of the reflected-wave term is

$$T_{RB}^{m(0)} = -\sqrt{2/\rho}\, e^{i\frac{3\pi}{8}}\, e^{ik_1 R_m \cos(\alpha_m - \theta_o)}\, F(k)\,(k_1/R_m)^{3/4}$$

$$\left[\frac{\cos\theta_o}{\cos\left(\frac{\alpha_m - \theta_o}{2}\right)}\right]^{3/2} \times \exp\left[\frac{ik_1 R_m}{2}\sin^2\left(\frac{\alpha_m - \theta_o}{2}\right)\right] D_{-3/2}$$

$$\left[e^{i\frac{\pi}{4}}\, 2\sqrt{k_1 R_m}\, \sin\left(\frac{\alpha_m - \theta_o}{2}\right)\right] . \qquad (3.4.14)$$

The first correction to the branch-point contribution is

$$T_{RB}^{m(1)} = -2\sqrt{2/\pi\rho}\, e^{i\frac{\pi}{4}}\, e^{ik_1 R_m \cos(\alpha_m - \theta_o)}\, H'(0)\, \frac{\frac{3}{4}\sqrt{\pi}}{R_m^{5/4}}$$

$$e^{\frac{ik_1 R_m}{2} \sin^2\left(\frac{\alpha_m - \theta_o}{2}\right)} \quad D_{-5/2}\left[e^{i\frac{\pi}{4}} 2\sqrt{k_1 R_m} \sin\left(\frac{\alpha_m - \theta_o}{2}\right)\right] \tag{3.4.15}$$

where

$$H'(0) = e^{i\frac{7\pi}{8}} k_1^{1/4} \left[\frac{\sin\left(\frac{\alpha_m - \theta_o}{2}\right) \cos\theta_o}{\frac{1}{2}\sin(\alpha_m - \theta_o)}\right]^{1/2} \left\{F(k)\ \frac{5}{4}\right.$$

$$\left[\frac{-\cos\theta_o}{\sin(\alpha_m - \theta_o)} + \frac{4\sin^2\left(\frac{\theta_o - \alpha_m}{2}\right)}{\sin^3(\alpha_m - \theta_o)} \cos\alpha_m\right]$$

$$\left. + F'(k)\ \frac{4k_1 \sin^2\left(\frac{\alpha_m - \theta_o}{2}\right) \cos^2\theta_o}{\sin^2(\alpha_m - \theta_o)}\right\} . \tag{3.4.16}$$

In general, (3.4.14) sufficiently approximates the branch-point contribution. It is of $O(R_m^{-5/4})$ when $\alpha_m \simeq \theta_o$ and is of $O(R_m^{-2})$ when α_m is not close to θ_o.

The asymptotic approximation to the typical integral T can be used to evaluate various components of a dipole field

over two-layer media. For example, for an HED (see Section 1.2), its H_z-field component is given by

$$H_z = i \frac{I\ell}{8\pi} \int_{-\infty}^{\infty} \frac{k_\rho^2}{k_z} (1 + R^{TE}) e^{ik_z z} H_1^{(1)}(k_\rho \rho) \sin \phi \, dk_\rho . \tag{3.4.17}$$

It is related to the typical integral as follows:

$$H_z = - i \frac{I\ell}{8\pi} \frac{\partial}{\partial \rho} T \sin \phi . \tag{3.4.18}$$

Since we know that similar asymptotic approximation to H_z exists, we can obtain such approximation to H_z by differentiating the asymptotic approximation to T, and neglecting higher order terms. Fig. 3.4.1 shows the H_z component of an HED as compared with numerical integration and ordinary saddle-point analysis. Only terms of $O(R_m^{-1})$ and $O(R_m^{-5/4})$ is included in the reflected-wave terms. In the computation, (1.3.7a), is used when the saddle-point is far away from the branch-point at $k_z = 0$ in order to save computation time.

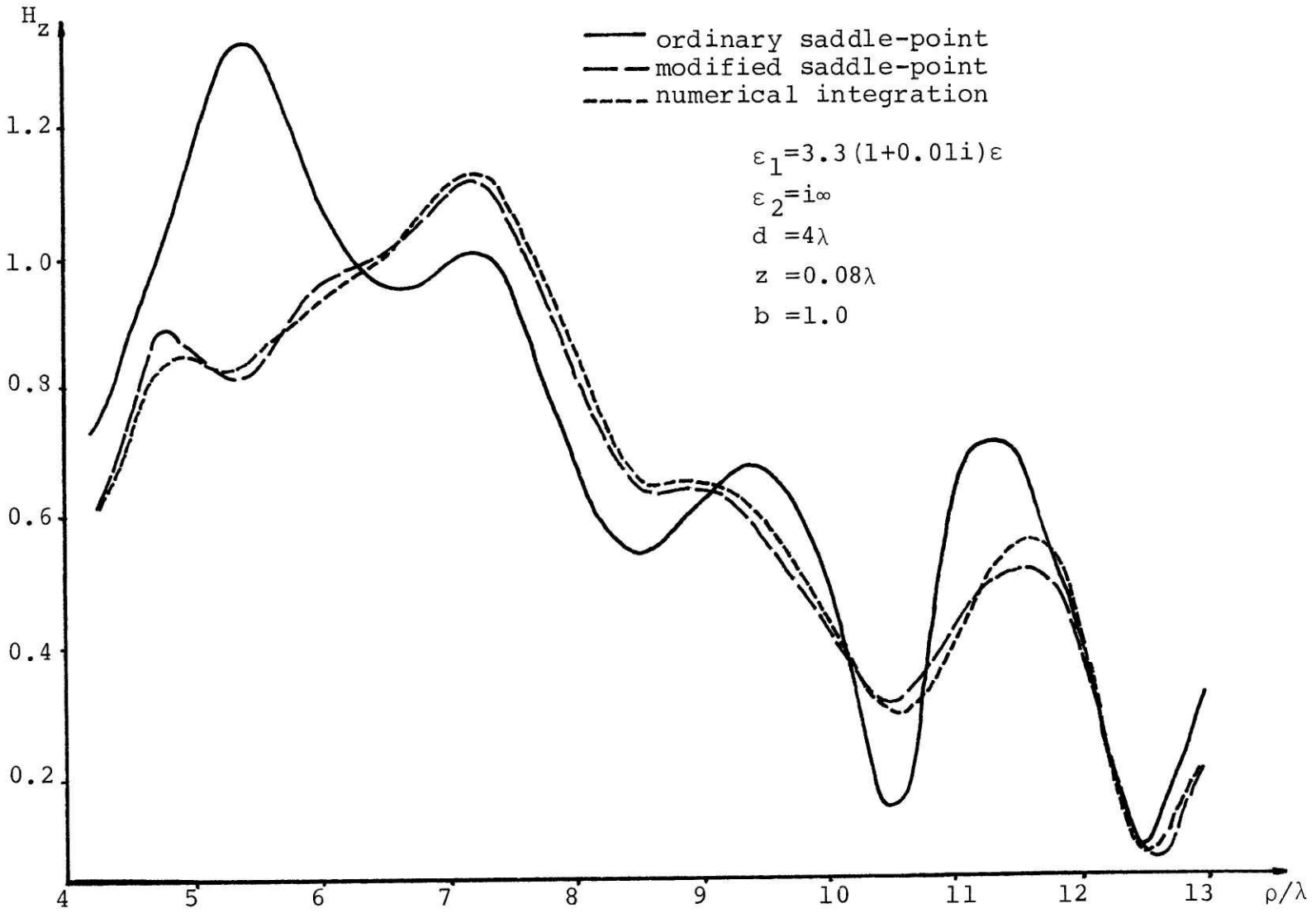

Fig. 3.4.1. Noemalized H_z component of an HED in its broadside direction computed from three different approaches (λ is the free-space wavelength).

3.5 Bleistein's Approach

For an integral of the form of (3.2.1)

$$I = \int_C (t - t_b)^r \, g(t) \, e^{-\lambda f(t)} \, dt \qquad (3.5.1)$$

without deforming the path of integration to the steepest-descent path, a transformation of (3.2.2) results in

$$I = e^{-\lambda f(0)} \int_{C'} (s - s_b)^r \, G(s) \, e^{-\lambda s^2} \, ds \qquad (3.5.2)$$

where

$$G(s) = \left(\frac{t - t_b}{s - s_b}\right)^r g(t) \, \frac{dt}{ds} \, .$$

C' is the image of the integration path C on the s-plane extending from $-\infty$ to $+\infty$.

For an asymptotic expansion of (3.5.2), Bleistein[35] suggests that the leading order approximation to (3.5.2) can be obtained by approximating G(s) by a first order polynomial that interpolates the critical points, i.e. the branch-point and the saddle-point. For instance, G(s) can be written as

$$G(s) = \gamma_o + \gamma_1(s - s_b) + s(s - s_b)\, G_1(s) \qquad (3.5.3)$$

where $G_1(s)$ is analytic in a region around the saddle-point. Solving for γ_o and γ_1 gives

$$\gamma_o = G(s_b) \qquad (3.5.4)$$

$$\gamma_1 = \frac{G(s_b) - G(0)}{s_b} . \qquad (3.5.5)$$

Consequently,

$$I = e^{-\lambda f(0)} \int_{C'} (s - s_b)^r [\gamma_o + \gamma_1(s - s_b)]\, e^{-\lambda s^2}\, ds$$

$$+ e^{-\lambda f(0)} \int_{C'} (s - s_b)^{r+1}\, s\, G_1(s)\, e^{-\lambda s^2}\, ds. \qquad (3.5.6)$$

The second integral can be shown to be of $O(1/\lambda)$ smaller than the original integral using integration by parts.

$$K = e^{-\lambda f(0)} \int_{C'} (s - s_b)^{r+1}\, s\, G_1(s)\, e^{-\lambda s^2}\, ds$$

$$= \frac{1}{2\lambda} \int_{C'} (s - s_b)^r [(s - s_b)\, G_1'(s) + (r + 1)\, G_1(s)]$$

$$e^{-\lambda s^2}\, ds. \qquad (3.5.7)$$

In arriving at the above, we make use of the fact that the integrand vanishes at the end-points of C', i.e. at $s = \pm\infty$.

When λ is large, (3.4.7) is of order $1/\lambda$ smaller than I. For this reason,

$$I \sim e^{-\lambda f(0)} \int_{C'} (s - s_b)^r [\gamma_o + \gamma_1 (s - s_b)]\, e^{-\lambda s^2}\, ds. \qquad (3.5.8)$$

With change of variable to $u = \sqrt{2\lambda}\ (s - s_b)$,

$$I \sim e^{-\lambda [f(0) + s_b^2]} \int_{-\infty}^{\infty} \left[\frac{\gamma_o\, u^r}{(2\lambda)^{r/2}} + \frac{\gamma_1\, u^{r+1}}{(2\lambda)^{(r+1)/2}} \right]$$

$$e^{-\left(\frac{u^2}{2} + \sqrt{2\lambda}\, s_b u \right)}\, du. \qquad (3.5.9)$$

In (3.5.9), the path of integration is above the singularity at the origin if the original path is above the singularity at

the origin, and it is below the singularity at the origin for the converse. Using (3.2.8),

$$I \sim e^{-\lambda[f(0) + s_b^2]} \left[\frac{\gamma_o}{(2\lambda)^{r/2}} W_r(\sqrt{2\lambda}\, s_b) + \frac{\gamma_1}{(2\lambda)^{(r+1)/2}} W_{r+1}(\sqrt{2\lambda}\, s_b) \right] \tag{3.5.10}$$

where

$$W_k(\sqrt{2\lambda}\, s_b) = \begin{cases} \sqrt{2\pi}\, e^{-\frac{\pi}{2} ri}\, e^{\lambda \frac{s_b^2}{2}} D_k(-i\sqrt{2\lambda}\, s_b) & \text{for integration path above the origin,} \\ \sqrt{2\pi}\, e^{+\frac{\pi}{2} ri}\, e^{\lambda \frac{s_b^2}{2}} D_k(+i\sqrt{2\lambda}\, s_b) & \text{for integration path below the origin.} \end{cases} \tag{3.5.11}$$

Note that distinct difference in definition between (3.5.11) and (3.2.9). In (3.5.11) the signs are decided by the original path of integration whereas in (3.2.9), they are decided by the location of the branch-point with respect to the saddle-point. Once the signs in (3.5.11) is confirmed, they remain the same for all possible values of s_b. In Bleistein's approach, there

is no distinction between the saddle-point and branch-point contributions as they are all inclusive in the expression (3.5.10). The correspondence to the singularity contribution in the author's earlier analysis is exhibited in the Stoke's phenomenon of the parabolic cylinder function for various arguments.[33,34] Bleistein's approach has the advantage that the leading order approximation to I does not involve the derivatives of G(s). This is particularly useful when G(s) is a complicated expression.

Applying Bleistein's approach to obtain the asymptotic approximation of (3.3.1) we obtain a solution which gives numerically equivalent answer when compared with the author's analysis as shown in Fig. 3.5.1.

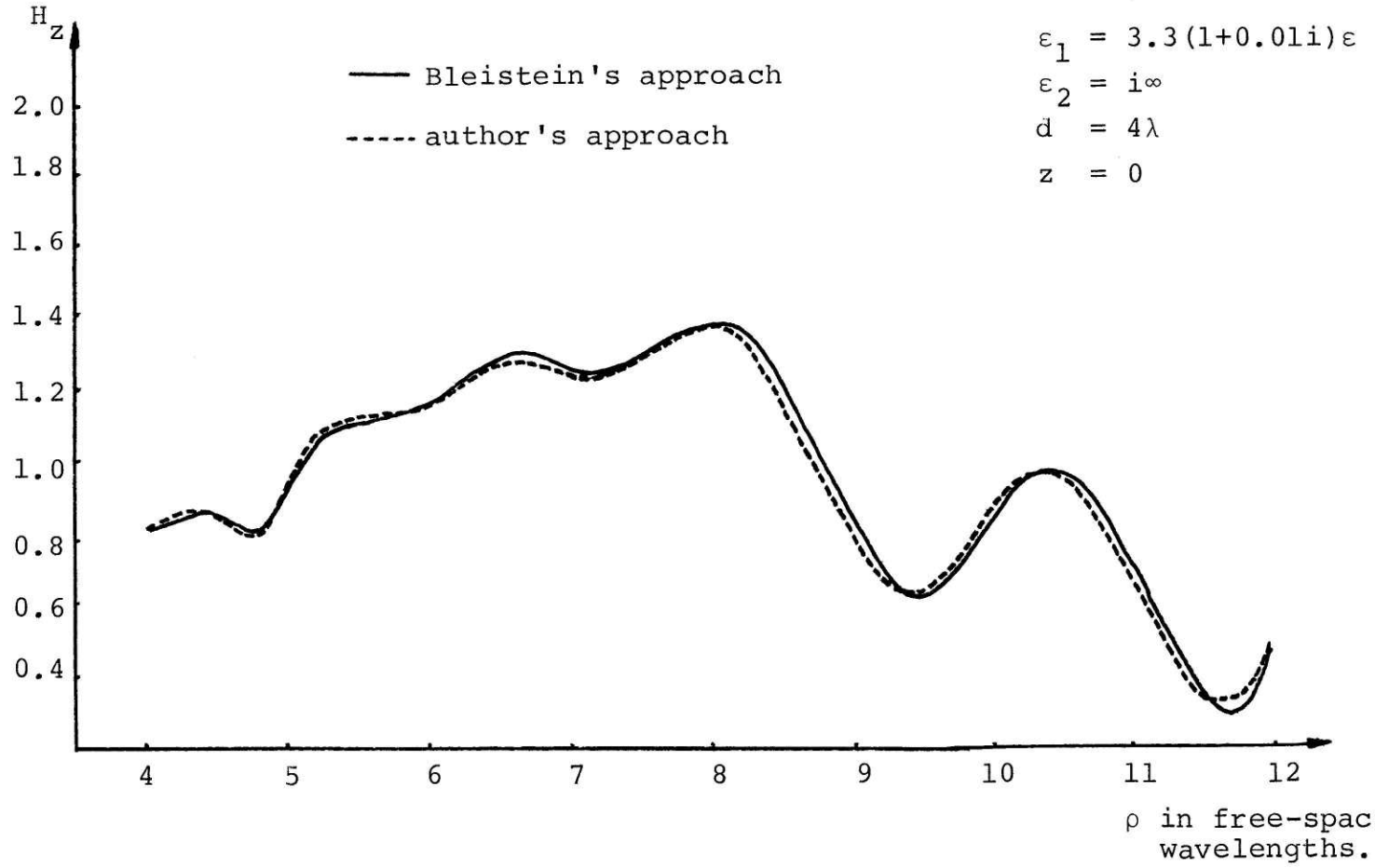

Fig. 3.5.1. Normalized H_z component of an HED using Bleistein's approach and the author's approach in the modified saddle-point analysis.

3.6 Conclusions

In Section 3.4, it is demonstrated that terms of $O(R_m^{-1})$ and $O(R_m^{-5/4})$ in the author's analysis sufficiently approximate the H_z-field component of an HED where $b = \mu_o/\mu_1 = 1$. The above analysis also shows that the wave that is associated with the saddle-point contribution has a spherical wavefront. Also when $\alpha_m > \theta_o$, an additional kind of wave is observed; namely, the lateral wave which has a conical wave-front. This is attributed to the branch-point contribution. These properties of the wave can be confirmed by using the small and large argument approximation of the parabolic cylinder functions. As for Bleistein's approach, these anomalous behavior of the wave is associated with the Stoke's phenomenon in parabolic cylinder function.

When the saddle-point is close to the branch-point, in other words, $\alpha_m \simeq \theta_o$, the spherical wave and lateral wave that is due to $A_{m\text{-odd}}$ becomes physically the same wave and is indistinguishable from each other when $\alpha_m = \theta_o$. Furthermore, this wave diminishes with a rate of $R_m^{-5/4}$ from the source. This forms an important correction to the spherical wave generated by the $A_{m\text{-even}}$ term which diminishes with a rate of R_m^{-1}.

This analysis sheds light on the behavior of the wave

when a spherical wave source is placed on top of a half-space. The transmitted wave behaves just like the reflected wave for the two-layer problem. A typical integral representation of the transmitted wave can be written as

$$T_t = \int_{-\infty}^{\infty} \frac{2b\, k_\rho}{k_{1z}^2 - bk_z^2} (k_{1z} - bk_z)\, H_o^{(1)}(k_\rho \rho)\, e^{ik_{1z}z}\, dk_\rho . \tag{3.6.1}$$

This resembles the reflected-wave expression since there is also a term even in k_z and one which is odd in k_z. The transmitted wave is shown in Fig. 3.6.1. The lateral wave is observed only when the angle of observation in the lower half-space is greater than θ_o the critical angle. The lateral wave is phase-matched to the spherical wave at the place where it merges with the spherical wave. At the boundary, the lateral wave is phase-matched to the spherical wave in the upper half-space. In the upper half-space, the inhomogeneous wave decays exponentially away from the boundary. In the analysis discussed in Chapter 1, it is, associated with the branch-point contribution. The fact that it is observed only when the angle of observation is greater than the critical angle is a requirement for phase matching as this inhomogeneous wave has a wavelength λ_1 propagating in the ρ-direction.

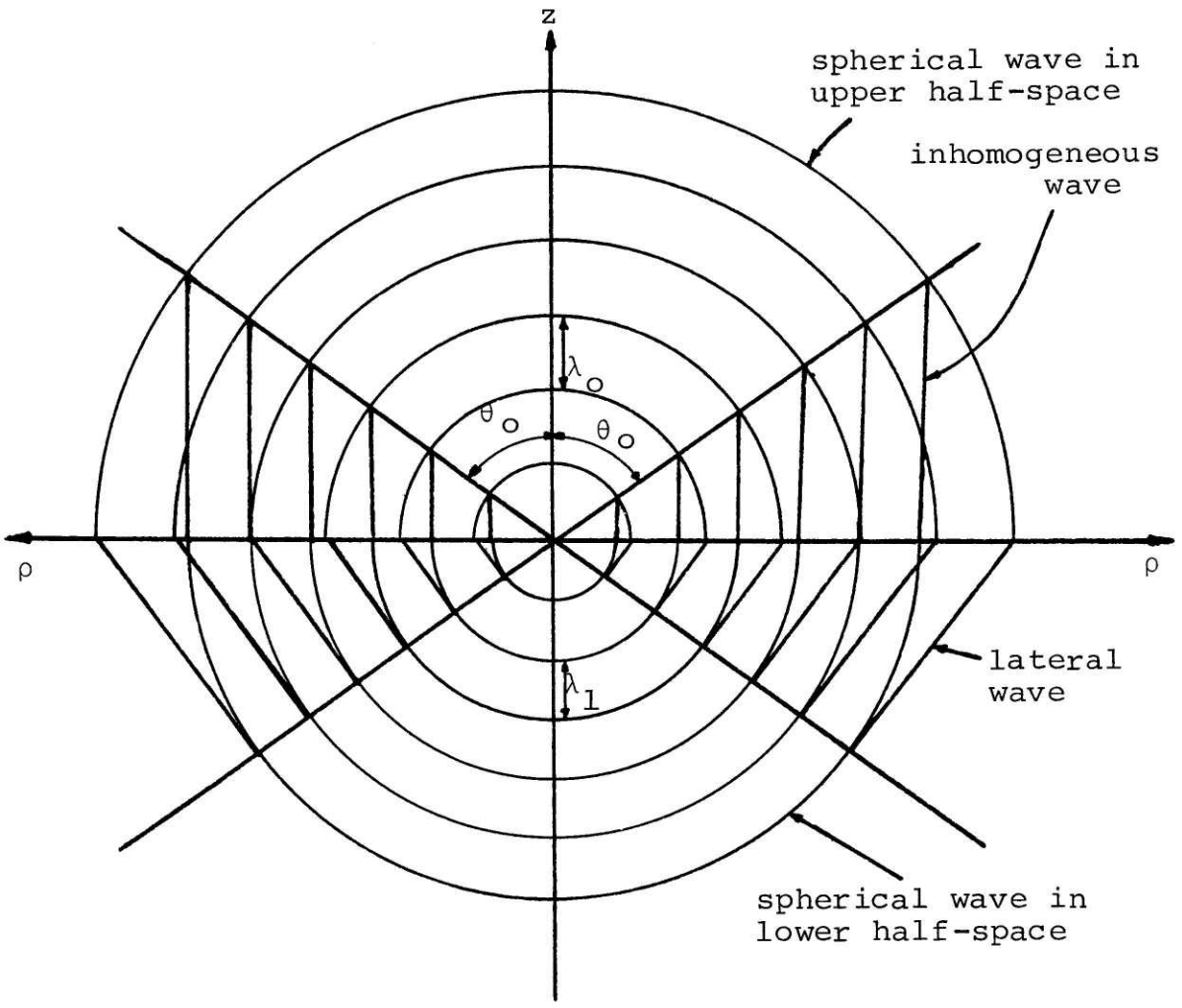

Fig. 3.6.1. The behavior of waves generated by a spherical-wave source placed on top of a half-space.

The analysis presented in this chapter nevertheless has its limitation. Having $A_m(k_\rho)$ in the form of (3.4.6) and (3.4.7) introduces a pole at

$$k_{\rho p} = k \left[\frac{(k_1/k)^2 - b^2}{1 - b^2} \right]^{1/2}$$

which occurs on both the Riemann sheets of k_z. When $b = 1$, $k_{\rho p} = \infty$, but for TM waves, $b = \varepsilon_1/\varepsilon_o > 1$ and b^2 can be large so that the pole, which is of order $m + 1$ for the m-th image, will be close to the saddle-point. As such, the above analysis cannot be applied to compute the field of TM waves. The locus of the pole is the same as that of the Sommerfeld poles shown in Fig. 2.2.1 except that now it is on both Riemann sheets. The failure of the modified saddle-point analysis is alluded to the proximity of two singularities in the vicinity of the saddle-point.

Chapter 4. MULTIPLE-SADDLE-POINT METHOD

4.1 Introduction

The modified saddle-point method discussed in Chapter 3 presupposes that the singularity of the integrand exists in the form of an algebraic factor which multiplies the rest of the integrand. For singularities which are poles, the integrand can always be expressed in such form. In the case of algebraic singularities of fractional order, though it is possible to put the integrand into the desired form, objectionable effects often ensued. For instance, in its application to field analysis of a dipole antenna over layered media, the introduction of a pole is undesirable when it can be arbitrarily near the saddle-point.

For an algebraic singularity of fractional order, the singularity can be removed by a transformation. Such transformation results in multiple saddle-points on the transformed plane. In this chapter, we shall discuss the case of an algebraic singularity of order 1/2. On the transformed plane, this corresponds to three colinear saddle-points. The case of an algebraic singularity of general fractional order shall be discussed in the appendix.

4.2 Asymptotic Expansion of Integrals with Three Colinear Saddle-Points

Ordinary saddle-point method only applies to the case of one simple saddle-point without singularities and other saddle-points in the vicinity of the saddle-point. For three colinear saddle-points which can be arbitrarily close together or can coalesce, the ordinary saddle-point method becomes invalid. Thus a new analysis has to be used to treat such a case.

An integral with three colinear saddle-points is of the form

$$I = \int_C g(t)\, e^{-\lambda f(t)}\, dt \qquad (4.2.1)$$

where $g(t)$ is analytic in a region around the origin, C is the contour of integration extending to infinity, and $f'(t)$ equals zero at $t = 0$, $-t_b$ and t_b. Without loss of generality, we have assumed one saddle-point to be at the origin. The saddle-points coalesce when $t_b = 0$ giving rise to a third-order saddle-point. To facilitate an asymptotic expansion of (4.2.1) which is uniformly valid for all t_b, the transformation,

$$f(t) - f(0) = \frac{s^4}{4} - \frac{(s_b s)^2}{2} \qquad (4.2.2)$$

simplifies the exponential factor in (4.2.1). As such,

$$I = e^{-\lambda f(0)} \int_{C'} G(s)\, e^{-\lambda\left[\frac{s^4}{4} - \frac{(s_b s)^2}{2}\right]}\, ds \qquad (4.2.3)$$

where

$$G(s) = g(t)\, \frac{dt}{ds}\,, \qquad (4.2.4)$$

and C' is the image of C on the s-plane. From (4.2.2), differentiating with respect to s, we obtain

$$\frac{dt}{ds} = \frac{s(s^2 - s_b^{\,2})}{f'(t)}\,. \qquad (4.2.5)$$

Since the saddle-points are mapped from the t-plane to the s-plane, it follows from (4.2.2) that

$$s_b = \sqrt{2}\, [f(0) - f(t_b)]^{1/4}. \qquad (4.2.6)$$

We can choose the branch of (4.2.6) so that s_b is in the fourth quadrant. The steepest-descent paths that pass

through the three saddle-points on the s-plane are shown in Fig. 4.2.1. The asymptotic approximation of (4.2.3) can be obtained in several ways. One way is to approximate $G(s)$ with a polynomial that interpolates the saddle-points.[36] Another approach is to approximate $G(s)$ with its Taylor series expansion about the saddle-points that contribute most. For instance, if the original path of integration C' extends from $s = -i\infty$ to to $s = \infty$ as shown in Fig. 4.2.1, C' can be deformed to the steepest-descent path that passes through s_b. Hence, the saddle-point at $s = s_b$ contributes most to the integral. An asymptotic approximation to I is obtained by approximating $G(s)$ by its Taylor-series expansion about s_b. Consequently, for large λ,

$$I \sim e^{-\lambda f(0)} \sum_{n=0}^{\infty} \frac{G^{(n)}(s_b)}{n!} \int_{-i\infty}^{\infty} (s - s_b)^n \, e^{-\lambda\left(\frac{s^4}{4} - s_b^2 \frac{s^2}{2}\right)} \, ds. \tag{4.2.7}$$

I is asymptotic to such a series only because the Taylor series representation of $G(s)$ is valid only within its radius of convergence while the range of integration extends to infinity. The integral in (4.2.7) can be expressed in terms of parabolic cylinder functions by making use of the following identity [see

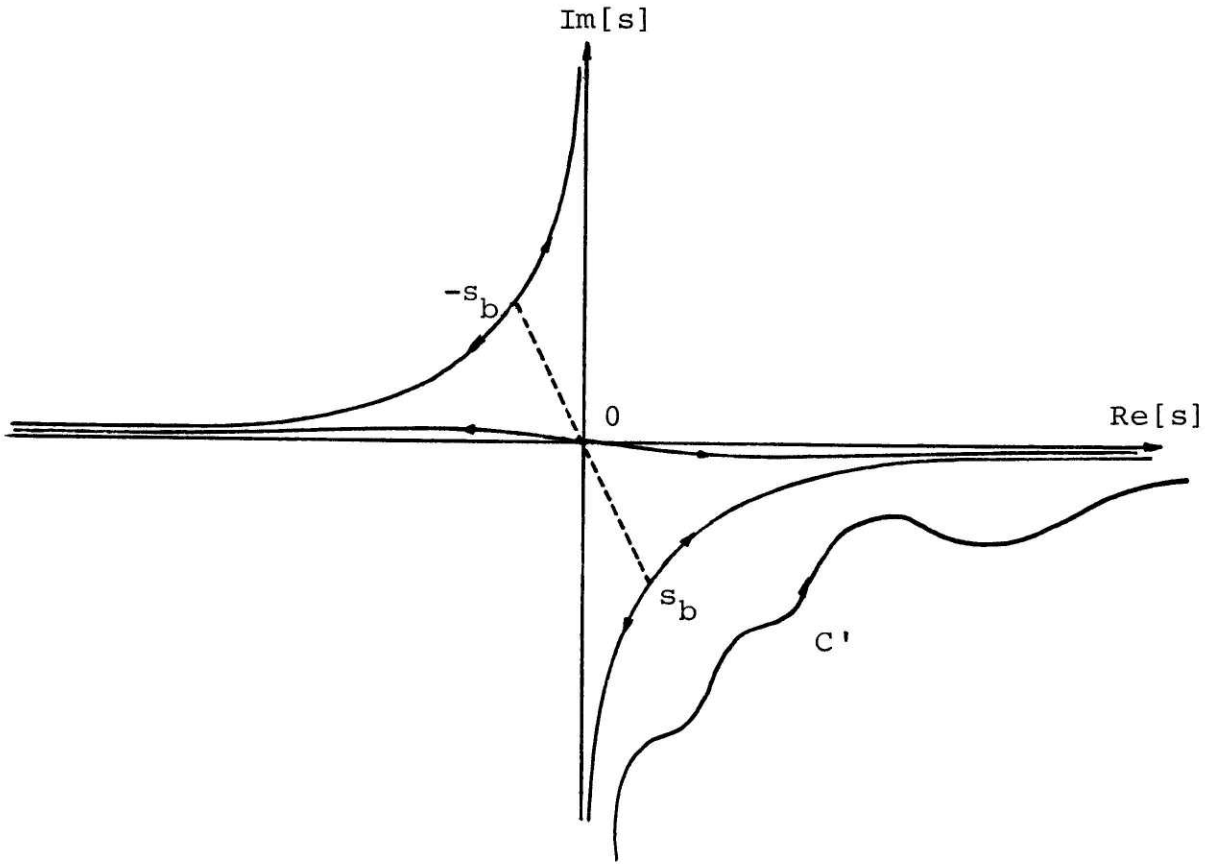

Fig. 4.2.1. Steepest-descent paths passing through the three saddle-points on the s-plane. The arrows show directions of descent. C' is the original path of integration.

Appendix, eq. (4A.1.19)];

$$\int_{-i\infty}^{\infty} s^n \, e^{-\lambda\left(\frac{s^4}{4} - s_b^2 \frac{s^2}{2}\right)} \, ds = 2^{\frac{n-1}{2}} (2\lambda)^{-\left(\frac{n+1}{4}\right)} e^{\lambda \frac{s_b^4}{8}} \sqrt{2\pi}$$

$$e^{-\frac{\pi}{4}(n-1)i} D_{(n-1)/2}(i\sqrt{\lambda/2}\, s_b^2). \qquad (4.2.8)$$

Therefore, the n-th term of the series in (4.2.7) is given by

$$\tilde{I}_n = e^{-\lambda f(0)} \frac{G^{(n)}(s_b)}{n!} \sum_{r=0}^{n} {}_nC_r \, s_b^{n-r} \, 2^{\frac{r-1}{2}} (2\lambda)^{-\left(\frac{r+1}{4}\right)}$$

$$e^{\lambda \frac{s_b^4}{8}} \sqrt{2\pi}\, e^{-\frac{\pi}{4}(r-1)i} D_{(r-1)/2}(i\sqrt{\lambda/2}\, s_b^2). \qquad (4.2.9)$$

It is of $O[(2\lambda)^{-(n+1)/4}]$. The asymptotic approximation to I can be approximated with $\tilde{I}_o + \tilde{I}_1 + \tilde{I}_2 + \tilde{I}_3$ so that the error is of $O(\lambda^{-5/4})$ when $\lambda \to \infty$ for all values of s_b. Hence

$$\tilde{I} \sim \tilde{I}_o + \tilde{I}_1 + \tilde{I}_2 + \tilde{I}_3. \qquad (4.2.10)$$

We shall next consider the case where the original path of integration C' ranges, from $s = -\infty$ to $s = -i\infty$ as shown in Fig. 4.2.2. C' can now be deformed to the steepest-descent paths that pass through the saddle-points at $s = 0$ and $s = s_b$. As a consequence, (4.2.3) can be broken into the sum of two integrals:

$$I = e^{-\lambda f(0)} \left[\int_{-\infty}^{\infty} G(s)\, e^{-\lambda \left(\frac{s^4}{4} - s_b^{\,2} \frac{s^2}{2} \right)}\, ds \right.$$

$$\left. - \int_{-i\infty}^{\infty} G(s)\, e^{-\lambda \left(\frac{s^4}{4} - s_b^{\,2} \frac{s^2}{2} \right)}\, ds \right] . \qquad (4.2.11)$$

The asymptotic expansion to the above can be obtained by Taylor series expanding $G(s)$ around $s = 0$ for the first integral and around $s = s_b$ for the second integral. Using the following identity [see Appendix, eq. (4A.1.13)],

$$\int_{-\infty}^{\infty} s^n\, e^{-\lambda \left(\frac{s^4}{4} - s_b^{\,2} \frac{s^2}{2} \right)}\, ds = [1 + (-1)^n] \left[2^{\frac{n-1}{2}} (2\lambda)^{-\left(\frac{n+1}{4} \right)} \right.$$

$$\left. \Gamma\left(\frac{n+1}{2} \right) \exp\left(\frac{\lambda s_b^{\,4}}{8} \right) D_{-(n+1)/2}\left(-\sqrt{\lambda/2}\, s_b^{\,2} \right) \right] \qquad (4.2.12)$$

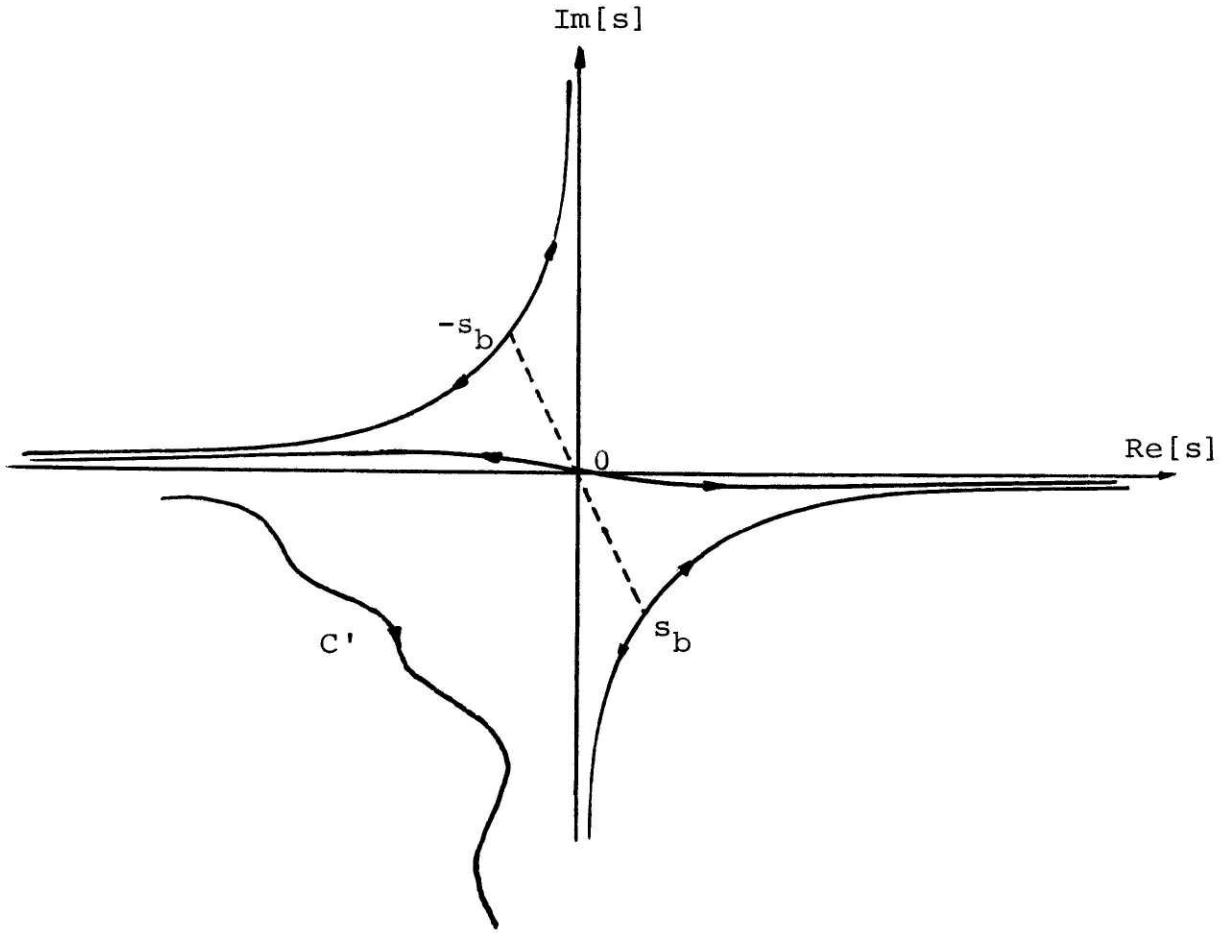

Fig. 4.2.2. The case where the original path of integration ranges from $s = -\infty$ to $s = -i\infty$.

and that for large λ,

$$I \sim e^{-\lambda f(0)} \sum_{n=0}^{\infty} \left[\frac{G^{(n)}(0)}{n!} \int_{-\infty}^{\infty} s^n \, e^{-\lambda \left(\frac{s^4}{4} - s_b^2 \frac{s^2}{2} \right)} \, ds \right.$$

$$\left. - \frac{G^{(n)}(s_b)}{n!} \int_{-i\infty}^{\infty} (s - s_b)^n \, e^{-\lambda \left(\frac{s^4}{4} - s_b^2 \frac{s^2}{2} \right)} \, ds \right] . \qquad (4.2.13)$$

the n-th term of this series is given by

$$\tilde{I}_n = e^{-\lambda f(0)} \left\{ \frac{G^{(n)}(0)}{n!} [1 + (-1)^n] \left[2^{\frac{n-1}{2}} (2\lambda)^{-\left(\frac{n+1}{4} \right)} \right. \right.$$

$$\left. \Gamma\left(\frac{n+1}{2} \right) \exp\left(\frac{\lambda s_b^4}{8} \right) D_{-(n+1)/2}(-\sqrt{\lambda/2}\, s_b^2) \right]$$

$$- \frac{G^{(n)}(s_b)}{n!} \sum_{r=0}^{n} {}_nC_r \, s_b^{n-r} \, 2^{\frac{r-1}{2}} (2\lambda)^{-\left(\frac{r+1}{4} \right)}$$

$$\left. e^{\lambda \frac{s_b^4}{8}} \sqrt{2\pi} \, e^{-\frac{\pi}{4}(r-1)i} D_{(r-1)/2}(i\sqrt{\lambda/2}\, s_b^2) \right\} . \qquad (4.2.14)$$

To obtain the leading order asymptotic approximation of I such that the error is of $O(\lambda^{-5/4})$ when $\lambda \to \infty$, we take the first four terms of the series as in (4.2.10).

The discussion above will suffice for the analysis of a dipole antenna interference field over layered media. In the analysis, we have chosen the Taylor-series approximation of $G(s)$ as opposed to a polynomial approximation so that we can associate different waves with different saddle-points. This will enhance our physical understanding of the wave behaviors.

4.3 Application to Evaluating Interference Fringes of Dipole Antennas

We have shown earlier that in geometrical-optics approximation, complication arises in the evaluation of the reflected-wave contribution, because of the proximity of a branch-point. A typical reflected-wave contribution from (1.3.3) is

$$T_R = \sum_{m=1}^{\infty} \int_{-\infty}^{\infty} \frac{k_\rho}{k_z} \hat{B}_m(k_\rho)\ e^{ik_{1z}2md}\ H_o^{(1)}(k_\rho\rho)\ dk_\rho \qquad (4.3.1)$$

where

$$\hat{B}_m(k_\rho) = X_{01}X_{10}\ R_{10}^{m-1}\ R_{12}^{m}\ e^{ik_z z}\ . \qquad (4.3.2)$$

The definition of X_{ij} and R_{ij} are given in (1.2.14). There is a branch-point at $k_\rho = k$ because $k_z = \sqrt{k^2 - k_\rho^2}$. Since this branch-point can be arbitrarily close to the saddle-point, a transformation of $k_\rho = k \sin\beta$ is used to remove it. After such transformation, the m-th reflected-wave term becomes

$$T_R^m = \int_\Gamma k \sin\beta\ B_m(\beta)\ \tilde{H}(\beta) \qquad (4.3.3)$$

$$e^{iR_m[\cos\alpha_m(k_1^2 - k^2\sin^2\beta)^{1/2} + k\sin\alpha_m \sin\beta]}\ d\beta.$$

In the above,

$$\alpha_m = \tan^{-1} \frac{\rho}{2md} ,$$

$$R_m = [\rho^2 + (2md)^2]^{1/2},$$

$$B_m(\beta) = \hat{B}_m(k \sin \beta),$$

$$\tilde{H}(\beta) = H_o^{(1)}(k\rho \sin \beta)\, e^{-ik\rho \sin \beta}$$

and Γ is the image of the original integration path on the β-plane. The contour Γ is shown in Fig. 4.3.1.

The transformation gives rise to three colinear saddle-points at

$$\beta_{m1} = \sin^{-1}\left(\frac{k_1}{k} \sin \alpha_m\right),$$

$$\beta_{m2} = \pi/2 \quad \text{and}$$

$$\beta_{m3} = \pi - \sin^{-1}\left(\frac{k_1}{k} \sin \alpha_m\right).$$

The steepest-descent paths that pass through these saddle-points

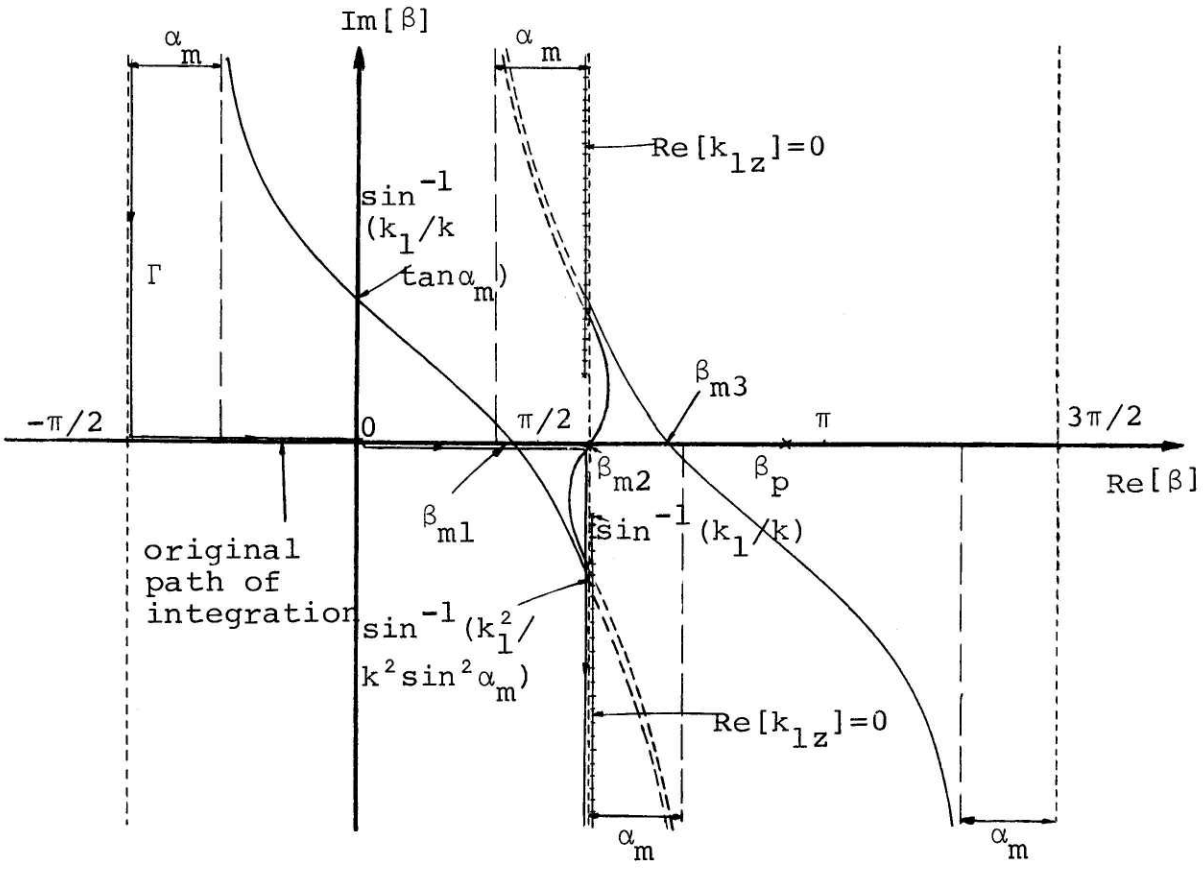

Fig. 4.3.1a. Steepest-descent paths on β-plane that pass through three colinear saddle-point when $\alpha_m < \theta_o$.

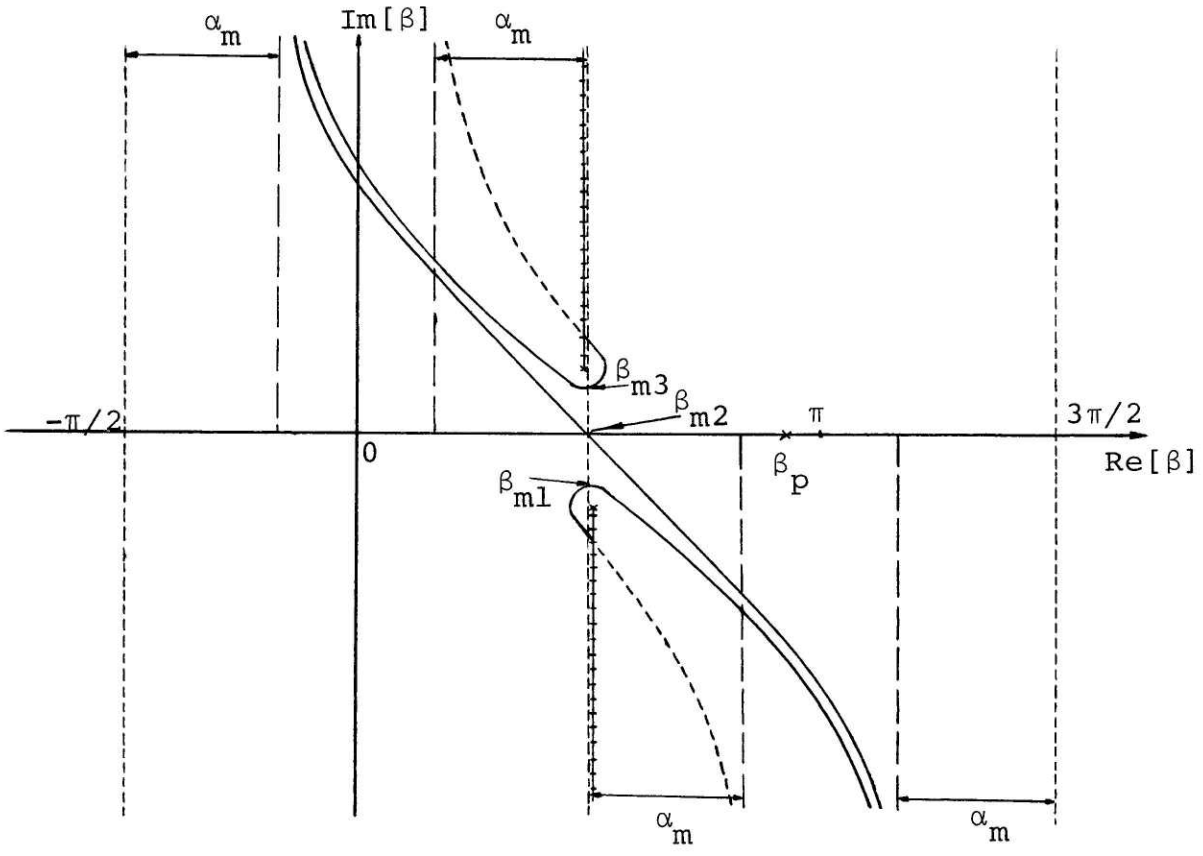

Fig. 4.3.1b. Same as (a) except that $\alpha_m > \theta_o$.

and the branch-cut for $\mathrm{Re}[k_{1z}] = 0$ are shown in Fig. 4.3.1 (see Appendix also). The three saddle-points can be arbitrarily close to each other and coalesce when $\sin \alpha_m = k/k_1$, i.e. $\beta_{m1} = \beta_{m2} = \beta_{m3} = \pi/2$. Hence, the method discussed in Section 4.2 can be used to derive the asymptotic approximation of T_R^m. With the following transformation,

$$t = \beta - \frac{\pi}{2}, \qquad \lambda = R_m, \qquad t_b = \beta_{m1} - \frac{\pi}{2} \tag{4.3.4}$$

$$g(t) = \tilde{H}(\beta)\, k \sin\beta\, B_m(\beta) \tag{4.3.5}$$

$$f(t) = -i[\cos\alpha_m (k_1^2 - k^2\sin^2\beta)^{1/2} + k \sin\alpha_m \sin\beta] \tag{4.3.6}$$

(4.3.3) becomes the form of (4.2.1). From (4.2.6),

$$s_b = 2^{3/4}\, e^{-i\,3\pi/8}\, k_1^{1/4}\, \sin^{1/2}\left[\pm\left(\frac{\theta_o - \alpha_m}{2}\right)\right] \tag{4.3.7}$$

where $\theta_o = \sin^{-1} k/k_1$. In the above, the + sign is chosen when $\alpha_m < \theta_o$ and the - sign is chosen for the converse. This ensures that the saddle-points at β_{m1} in Fig. 4.3.1a and Fig. 4.3.1b are both mapped into s_b such that s_b is always in the

fourth quadrant. This enables us to use the analysis of Section 4.2 directly to derive our approximations.

When $\alpha_m < \theta_o$, we infer from Fig. 4.3.1a that only the saddle-point at β_{m1} contributes, since the original path of integration can be deformed to pass through β_{m1}. This is similar to the first case in Section 4.2. Hence, from (4.2.9) and (4.2.10), the leading order approximation to T_R^m is given by

$$T_R^m \sim T_{Ro}^m + T_{R1}^m + T_{R2}^m + T_{R3}^m \tag{4.3.8}$$

where

$$T_{Rn}^m = e^{ik_1 R_m} \frac{G^{(n)}(s_b)}{n!} \sum_{r=0}^{n} {}^nC_r \, s_b^{n-r} \, 2^{\frac{r-1}{2}} \frac{1}{(2R_m)^{(r+1)/4}}$$

$$\sqrt{2\pi}\, e^{-\frac{\pi}{4}(r-1)i} \, e^{-ik_1 R_m \sin^2\left(\frac{\theta_o - \alpha_m}{2}\right)} D_{(r-1)/2}$$

$$\left[e^{-i\frac{\pi}{4}} 2(k_1 R_m)^{1/2} \sin\left(\frac{\theta_o - \alpha_m}{2}\right) \right] . \tag{4.3.9}$$

After replacing $\tilde{H}(\beta)$ with its approximation when $k\rho$ is large, $G(s_b)$ is given by

$$G(s_b) = \sqrt{2/\pi\rho}\; e^{-i\frac{\pi}{4}} \sqrt{k_1 \sin\alpha_m}\; B_m(\beta_m) \left.\frac{dt}{ds}\right|_{s = s_b} . \qquad (4.3.10)$$

In (4.3.9), the parabolic cylinder function has exponential dependence of $\exp\{ik_1 R_m \sin^2[(\theta_o - \alpha_m)/2]\}$. Therefore, T^m_{Rn} has $\exp(ik_1 R_m)$ dependence which is that of a spherical wave.

When $\alpha_m > \theta_o$, we infer from Fig. 4.3.1b that both saddle-points at β_{m1} and β_{m2} contribute to T_R^m. This is similar to the second case of Section 4.2 if we choose s_b to be in the fourth quadrant. Thus, the leading order approximations are given by (4.3.8) where T^m_{Rn}, from (4.2.14), is

$$T^m_{Rn} = e^{ik_1 R_m \cos(\alpha_m - \theta_o)} \frac{G^{(n)}(0)}{n!} [1 + (-1)^n]\, 2^{\frac{n-1}{2}}$$

$$\frac{1}{(2R_m)^{(n+1)/4}}\, \Gamma\left(\frac{n+1}{4}\right)\, e^{ik_1 R_m \sin^2\left(\frac{\theta_o - \alpha_m}{2}\right)}$$

$$D_{-(n+1)/2}\left[e^{i\frac{\pi}{4}}\, 2(k_1 R_m)^{1/2} \sin\left(\frac{\alpha_m - \theta_o}{2}\right)\right]$$

$$- e^{ik_1 R_m} \frac{G^{(n)}(s_b)}{n!} \sum_{r=0}^{n} {}_nC_r\, s_b^{n-r}\, 2^{\frac{r-1}{2}}\, \frac{1}{(2R_m)^{(r+1)/4}}$$

$$\sqrt{2\pi}\, e^{-\frac{\pi}{4}(r-1)i}\, e^{-ik_1 R_m \sin^2\left(\frac{\theta_o - \alpha_m}{2}\right)}$$

$$D_{(r-1)/2}\left[e^{-i\frac{\pi}{4}}\, 2(k_1 R_m)^{1/2} \sin\left(\frac{\alpha_m - \theta_o}{2}\right)\right] . \qquad (4.3.11)$$

In the above, the first term, which is the contribution from the saddle-point at $\pi/2$, is non-zero only for $n = 2$ since $G(0) = 0$. Its exponential dependence is $\exp[ik_1 R_m \cos(\alpha_m - \theta_o)]$ which is that of a conical wavefront. The second term is similar to (4.3.9), giving rise to a spherical wave. In fact the contribution due to the saddle-point at $\pi/2$ corresponds to the branch-point contribution discussed in Chapter 3, which gives rise to the lateral wave.

A remark is in order here on the sign of dt/ds. Since $\arg(dt/ds)$ mresures the angle of rotation of the mapping from the t-plane to the s-plane, the sign is chosen so that $\arg(dt/ds)$ gives the correct rotation. Since

$$\left.\frac{dt}{ds}\right|_{s = s_b} = \sqrt{\frac{2}{f''(t_b)}}\, s_b', \qquad (4.3.12)$$

for the correct rotation, we choose

$$[f''(t_b)]^{1/2} = \begin{cases} e^{i(\pi/4)}\, \sqrt{k_1}\, \dfrac{k_z}{k_{1z}}, & \alpha_m < \theta_o \\ -e^{i(\pi/4)}\, \sqrt{k_1}\, \dfrac{k_z}{k_{1z}}, & \alpha_m > \theta_o \end{cases} \qquad (4.3.13)$$

Also,

$$\left.\frac{dt}{ds}\right|_{s = 0} = e^{i\frac{\pi}{4}} \frac{s_b \cos^{1/2}\theta_o}{[k \sin(\alpha_m - \theta_o)]^{1/2}} \qquad \alpha_m > \theta_o. \tag{4.3.14}$$

(4.3.12) and (4.3.13) are imperative in deciding the right value of $G(s_b)$ in (4.3.10) and subsequently $G^{(n)}(s_b)$. (4.3.14) when applied to $G''(0)$ gives

$$G''(0) = g''(0) \frac{e^{i\frac{3\pi}{4}} s_b^3 \cos^{3/2}\theta_o}{[k \sin(\alpha_m - \theta_o)]^{3/2}} . \tag{4.3.15}$$

Having seen the application of the three-saddle-point analysis on deriving the asymptotic approximation of a typical reflected-wave integral, we can use it to derive the field components of a dipole antenna over stratified media. We make use of a similar concept exemplified by (3.4.17) and (3.4.18) of Chapter 3. In Fig. 4.3.2, three-saddle-point analysis was used to calculate the H_z component of an HED, and compared with the case of ordinary saddle-point and numerical integration. In Fig. 4.3.3a and b, E_ϕ component of an HED was calculated and compared with ordinary saddle-point analysis.

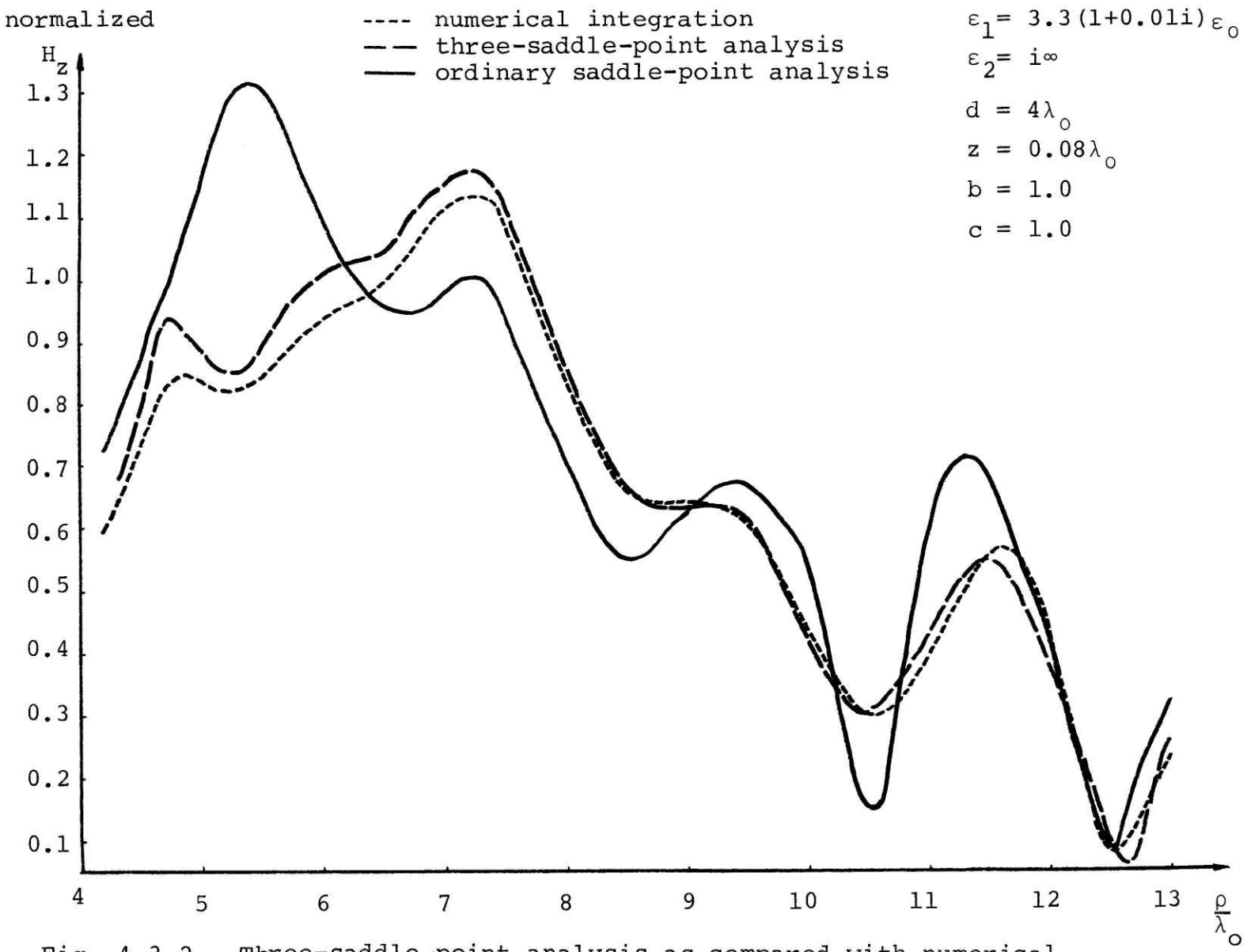

Fig. 4.3.2. Three-saddle-point analysis as compared with numerical integration and ordinary saddle-point analysis (λ_o is the free-space wavelength).

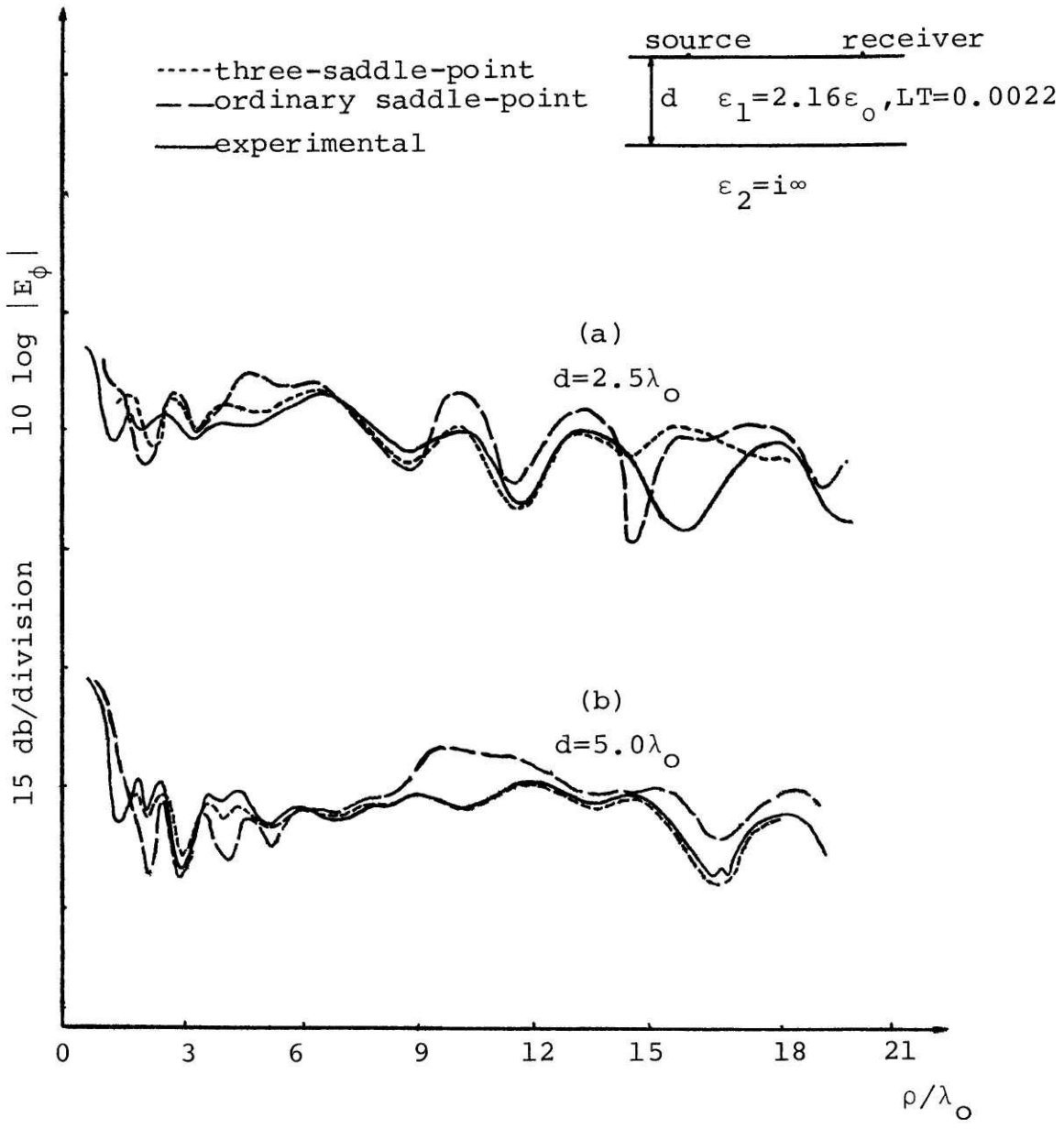

Fig. 4.3.3. E_ϕ component of an HED in its broadside direction using three-saddle-point analysis as compared with experimental result and ordinary saddle-point analysis.

The result shows marked improvement when the thickness of the first layer is 5 free-space wavelengths. When the thickness is 2.5 λ, there is improvement in the near field, but when ρ gets large, the result deteriorates. This is because that when ρ is large, the number of images that contribute to E_ϕ is large. The saddle-point analysis is unsatisfactory for large m since $\hat{B}_m(k_\rho)$ is a rapidly varying function then.

In the above, the dominant-wave contributions are TE waves. We saw excellent agreement between our analysis, expermental result and numerical integration. This is because the Sommerfeld pole is at infinity for TE waves propagating in non-magnetic material. The location of the Sommerfeld pole on β-plane is given by

$$\beta_p = \sin^{-1}\left[\frac{(k_1/k)^2 - b^2}{1 - b^2}\right]^{1/2} . \qquad (4.3.16)$$

Fig. 4.3.4 shows the locus of this pole for different values of b. When $b > k_1/k$, the pole can be near to the saddle-point at $\beta = \pi/2$, thus adversely affecting our analysis given above. For TM waves, $b = \varepsilon_1/\varepsilon_o > k_1/k$ for most media. Fig. 4.3.5 shows the failure of our analysis, when applied to calculate the E_z component of an HMD. Fig. 4.3.6a-c shows the effect of varying b, that is varying the location of the

Sommerfeld pole on the computed value of "E_z". It shows that when the pole is far away, the argreement with numerical integration improves. The only singularities that are near the saddle-points then are the branch-point singularities which are relatively "mild".

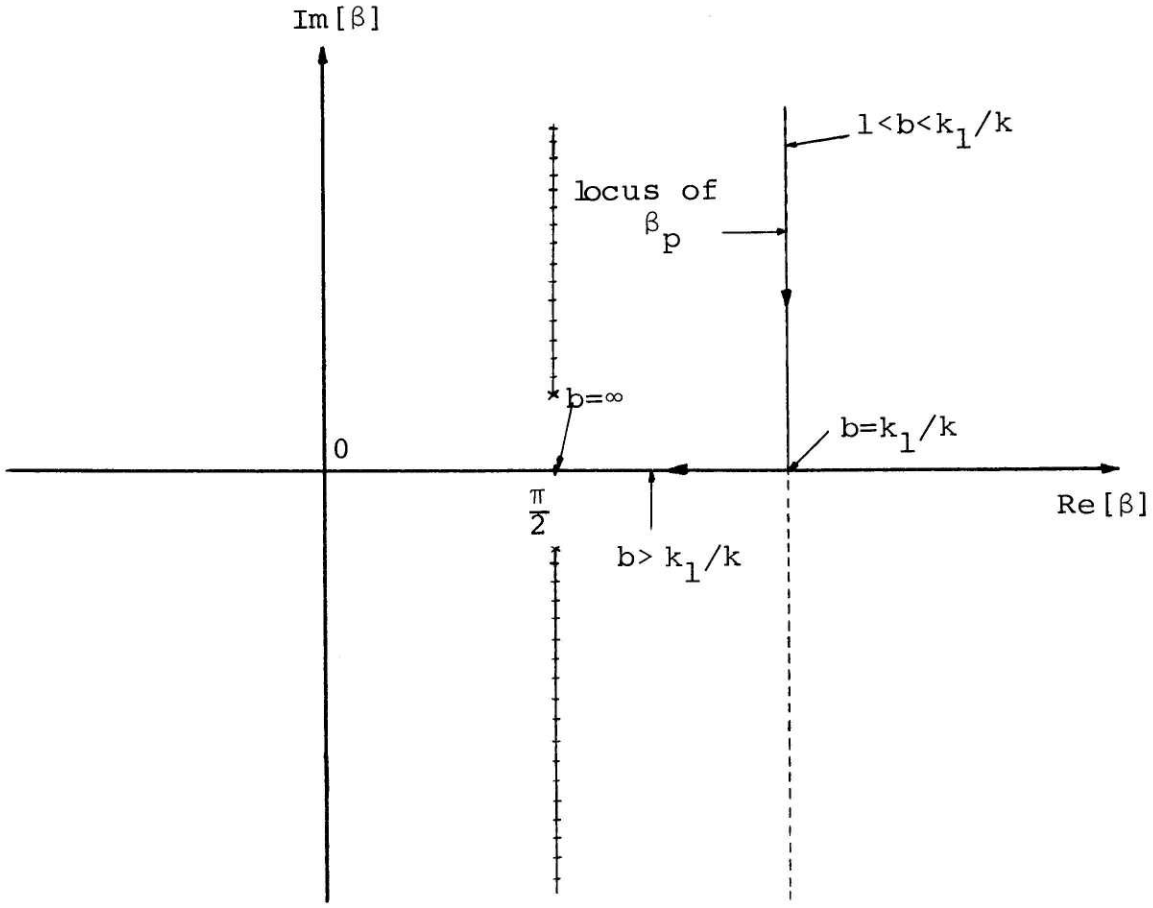

Fig. 4.3.4. Locus of β_p when b increases from 1 to ∞.

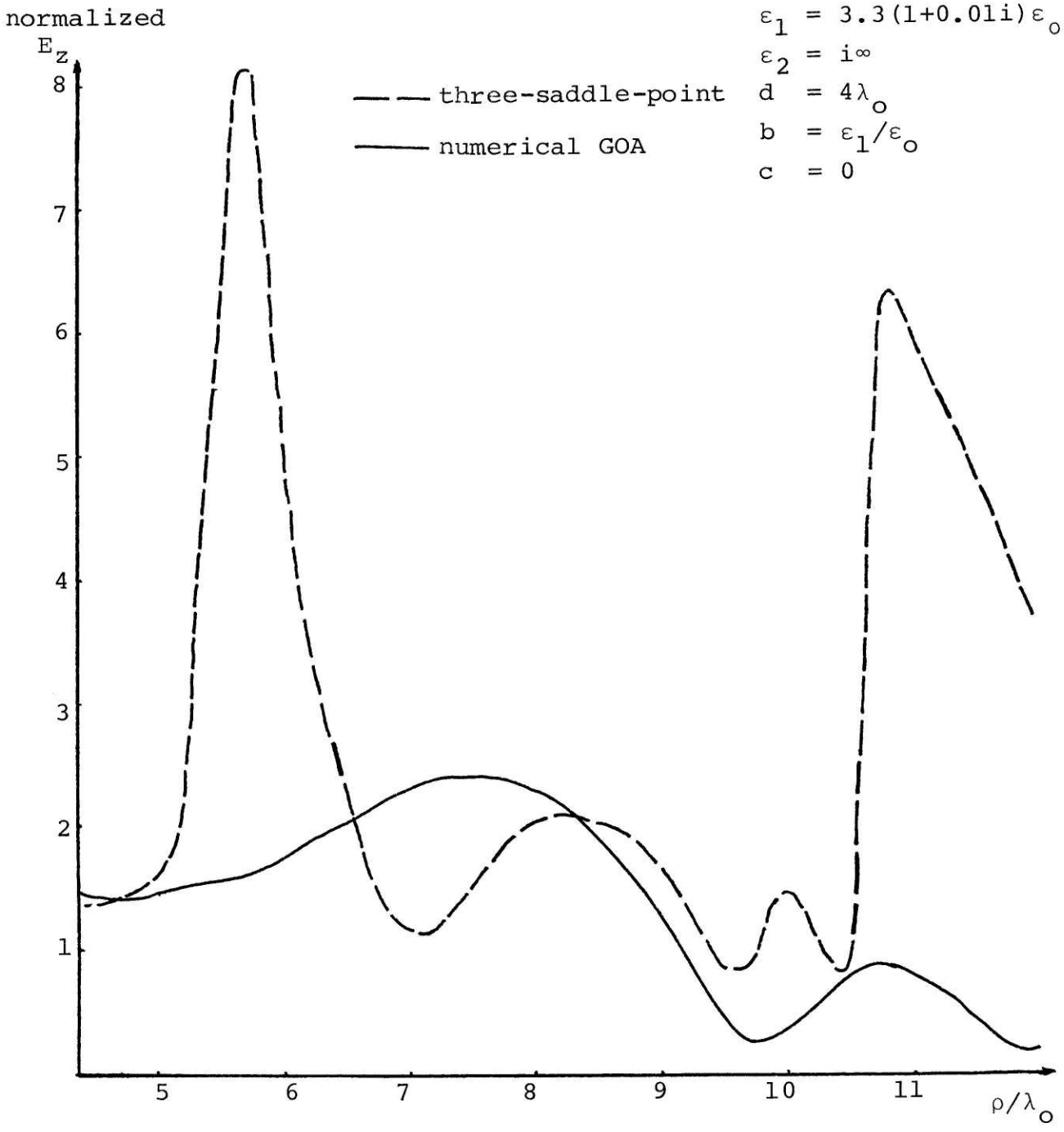

Fig. 4.3.5. Normalized E_z component of an HMD in its broadside direction using three-saddle-point analysis and numerical GOA. The failure of the analysis is due to the proximity of the Sommerfeld pole to the saddle-points.

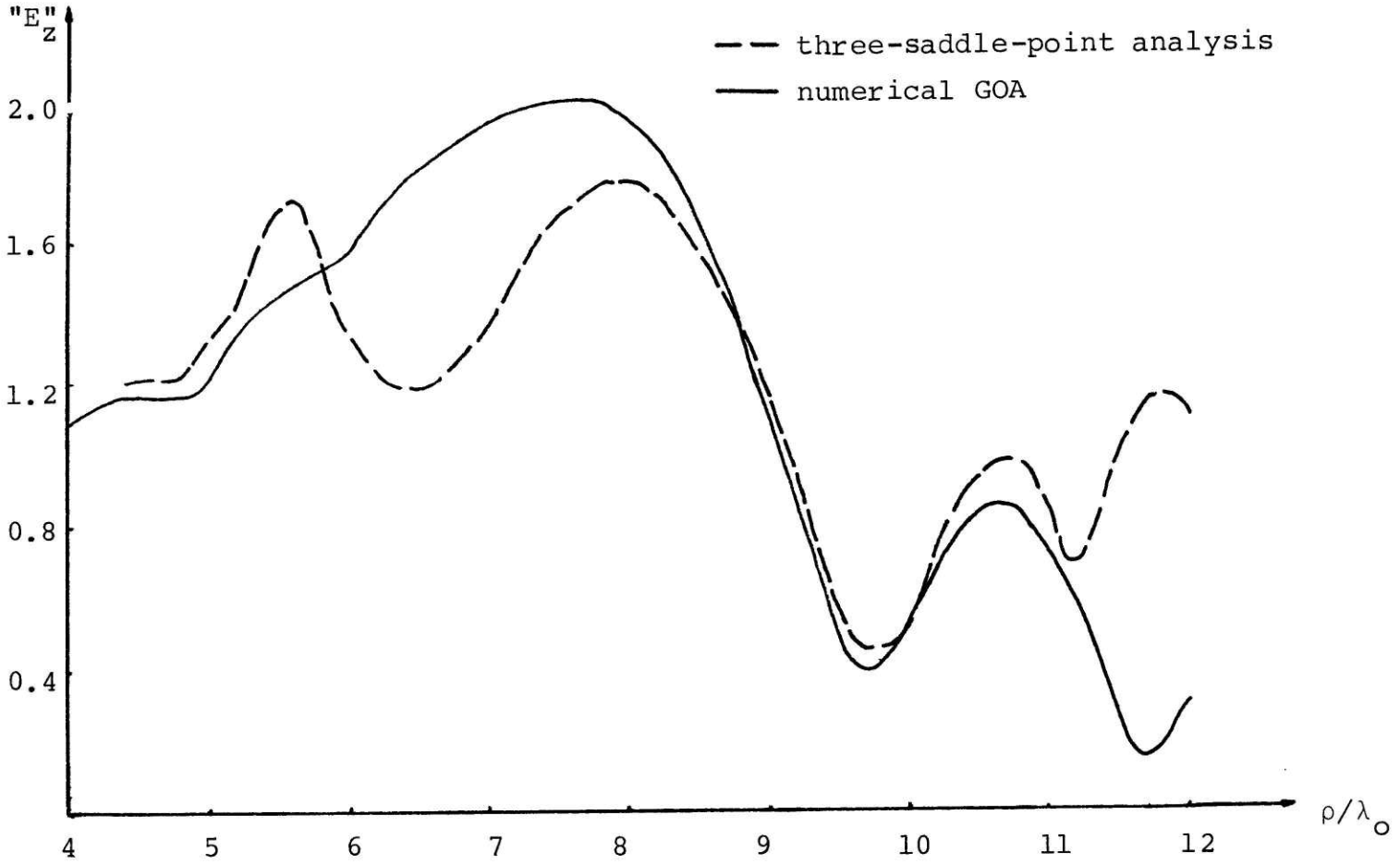

Fig. 4.3.6a. "E_z" with b k_1/k. Solution does not converge to correct value. All parameters are the same as Fig. 4.3.5 except that b = 2.

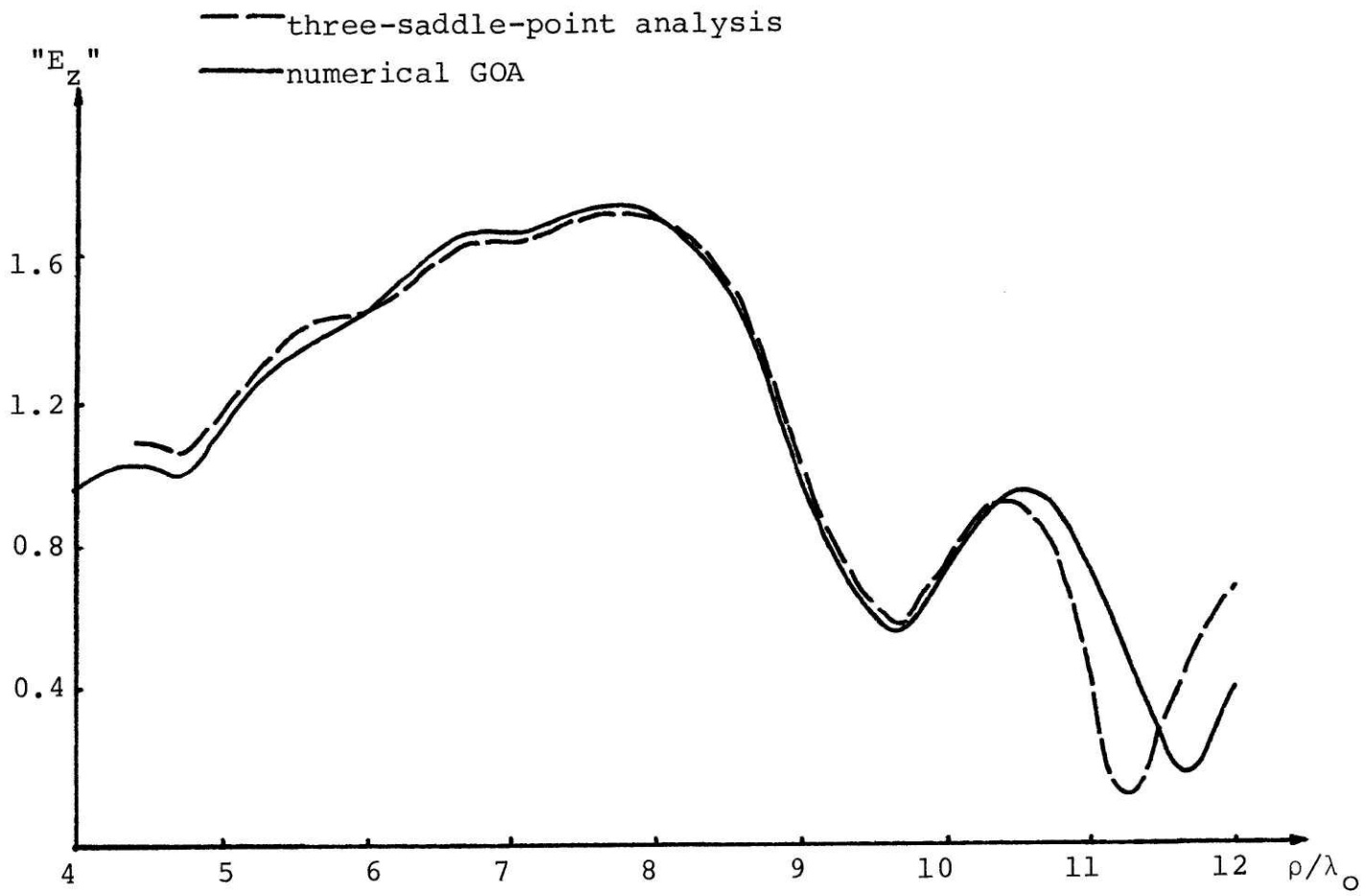

Fig. 4.3.6b. "E_z" component for b = 1.5. Solution does not converge well for large ρ because then, the dominant contribution comes from the second image source whose Sommerfeld pole is of order two.

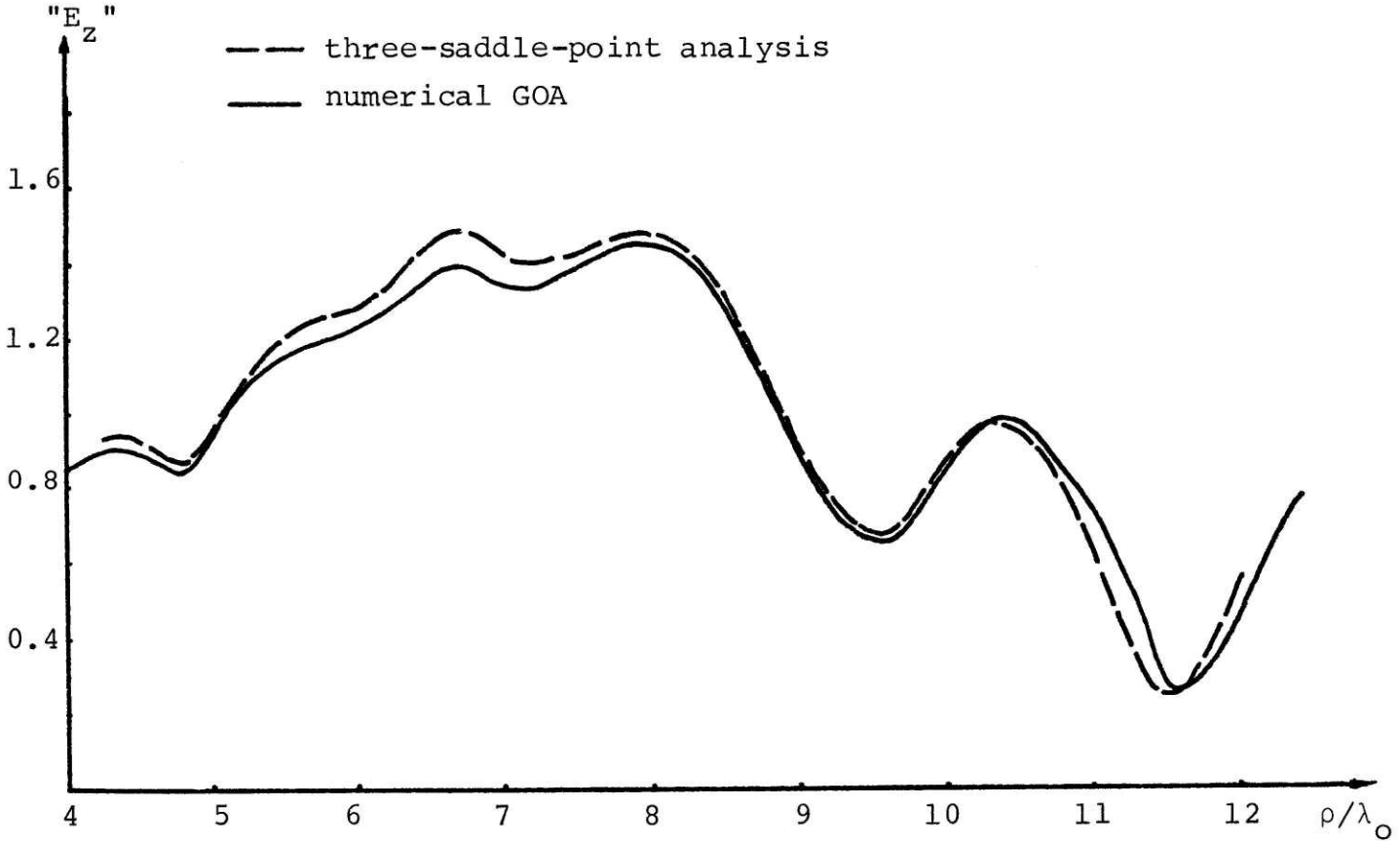

Fig. 4.3.6c. "E_z" component for b = 1.1. The solution agrees well with numerical GOA because the Sommerfeld pole is far away.

4.4 Conclusions

In Chapter 3, we saw that the use of modified saddle-point analysis, when applied to field evaluation, gave rise to poles on both Riemann Sheets. These poles can be arbitrarily close to or coalesce with the saddle point. This is undesirable for calculating interference fringes due to TM waves. In this Chapter, the use of a transformation results in the need for three-saddle-point analysis. In the three-saddle-point analysis, the pole does not coalesce with the saddle-points. Hence, for spacial cases, it can be used to analyze the field interference fringes due to TM waves.

However, the analysis left much to be desired as the approximation involves high derivatives of G(s). Therefore, the effect of a high-order pole is easily felt as exemplified by Fig. 4.3.6. We shall introduce the concept of generalized Weber's function in the next chapter to take into account the pole at β_p.

In this Chapter, we also saw the same behavior of waves generated by a spherical-wave source on top of a layered medium. The waves are sufficiently characterized by parabolic cylinder functions when they are TE waves. When $\alpha_m = \theta_o$, i.e. $s_b = 0$, and $G(0) = 0$, the largest term of T_R^m is given by

$$T_{Rl}^{m} = e^{ik_l R_m} G'(0)/(2R_m)^{1/2}.$$

Since $G'(0) \sim O(R_m^{-1/2})$, therefore $T_R^m \sim O(R_m^{-1})$ for large R_m. The first correction to the above is of $O(R_m^{-5/4})$. This is similar to that obtained by modified saddle-point analysis. However, the next correction term is of $O(R_m^{-6/4})$ which does not have a counterpart in the modified saddle-point analysis. When $\alpha_m \neq \theta_o$, the leading order approximation of T_R^m is of $O(R_m^{-1})$ for charge R_m, followed by correction terms of $O(R_m^{-2})$.

Appendix to Chapter 4

4A.1 Uniform Asymptotic Expansions of Integrals with an Algebraic Singularity of Any Fractional Order

An integral with an algebraic singularity of any fractional order can be represented by

$$I = \int_C g[(t - t_b)^{1/p}]\ e^{-\lambda f(t)}\ dt \qquad (4A.1.1)$$

where $p = 2, 3, 4, \ldots$, $g(z)$ is analytic in a region $|z| < R$ and the path of integration C extends to infinity. There is a branch-point singularity at $t = t_b$ where $|t_b| < R$. Assume further that $f'(0) = 0$ so that there is a simple saddle-point at $t = 0$. The branch-point at t_b can be removed with the following transformation

$$V^p = (t - t_b). \qquad (4A.1.2)$$

As such,

$$I = \int_{C'} g(V)\ pV^{p-1}\ e^{-\lambda f(V^p + t_b)}\ dV \qquad (4A.1.3)$$

where C' is the image of C on the V-plane. The saddle-points

occur at V where

$$f'(V^p + t_b)\ V^{p-1} = 0. \tag{4A.1.4}$$

Hence, there are simple saddle-points at locations where $V^p + t_b = 0$ and a saddle-point of order $p - 1$ at $V = 0$. Thus there are $p + 1$ saddle-points at $V = (-t_b)^{1/p}$ and at $V = 0$. To obtain an asymptotic expansion of I which is uniformly valid for all t_b, we seek the following transformation

$$f(V^p + t_b) - f(t_b) = \frac{s^{2p}}{2p} - \frac{(s_b s)^p}{p}\ . \tag{4A.1.5}$$

As a consequence,

$$I = e^{-\lambda f(t_b)} \int_{C''} s^{p-1}\ G(s)\ e^{-\lambda\left[\frac{s^{2p}}{2p} - \frac{(s_b s)^p}{p}\right]}\ ds \tag{4A.1.6}$$

where

$$G(s) = g(V)\ p(V/s)^{p-1}\ \frac{dV}{ds} \tag{4A.1.7}$$

and C'' is the image of C' on the s-plane. The transformation

(4A.1.5) maps all the saddle-points on the V-plane to the s-plane. From (4A.1.5)

$$s_b = \{2p[f(t_b) - f(0)]\}^{1/2p}. \tag{4A.1.8}$$

Furthermore,

$$\frac{dV}{ds} = \frac{s^{p-1}(s^p - s_b{}^p)}{f'(V^p + t_b)p\ V^{p-1}}\ . \tag{4A.1.9}$$

The location of the saddle-points on the s-plane is given by

$$s = 0 \quad \text{and} \quad s_b\, e^{i2\pi \frac{m}{p}}, \quad m = 0, \pm 1, \pm 2, \pm 3, \ldots \tag{4A.1.10}$$

where we have chosen the value of s_b in (4A.1.8) to have its principle value. Thus the saddle-points are as shown in Fig. 4A.1.1. Also the valleys of the exponential factor in (4A.1.6), i.e. the asymptotes extending to infinity where the exponential factor will vanish is given by

$$s = \alpha\, e^{ik\pi/p}, \quad k = 0, \pm 1, \pm 2, \ldots \tag{4A.1.11}$$

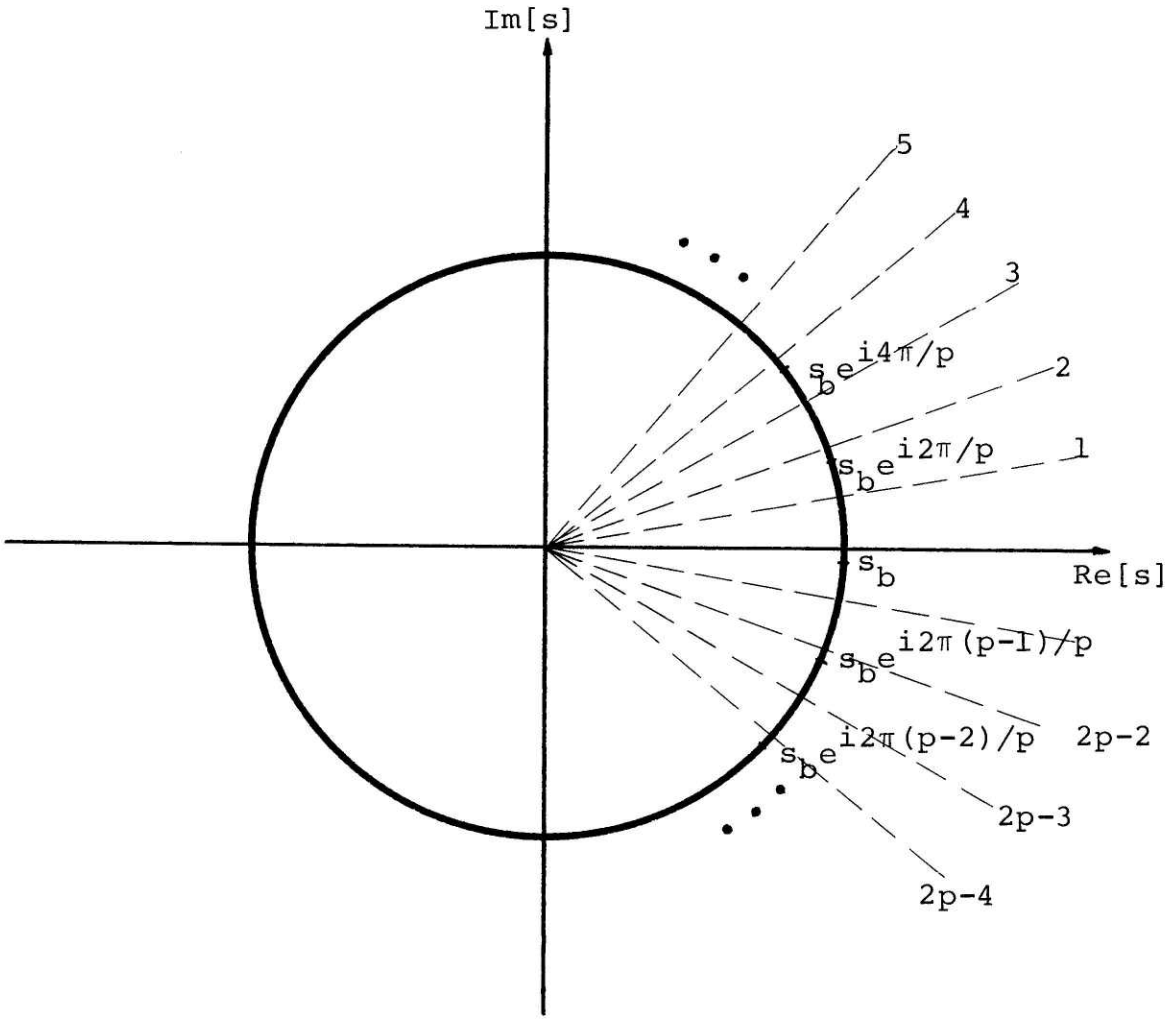

Fig. 4A.1.1. Location of saddle-points on the s-plane and the asymptotes to the valleys of the integrand.

where $\alpha \to \infty$ along the asymptotes. For the integral I to converge, the end-points of C" must at least be deformable to two of these valleys.

To obtain the leading order approximation of I, we shall approximate G(s) with a polynomial such that

$$G(s) = \sum_{n=0}^{2p-1} \gamma_n s^n + s^p(s^p - s_b{}^p)\, G_1(s). \qquad (4A.1.12)$$

Substituting (4A.1.12) into I, we obtain

$$I = e^{-\lambda f(t_b)} \left[\int_{C"} \sum_{n=0}^{2p-1} \gamma_n\, s^{n+p-1}\, e^{-\lambda\left[\frac{s^{2p}}{2p} - \frac{(s_b s)^p}{p}\right]}\, ds \right.$$

$$\left. + \int_{C"} s^{2p-1}(s^p - s_b{}^p)\, G_1(s)\, e^{-\lambda\left[\frac{s^{2p}}{2p} - \frac{(s_b s)^p}{p}\right]}\, ds \right] . \qquad (4A.1.13)$$

The order of magnitude of the latter integral can be estimated using integration by parts;

$$K = e^{-\lambda f(t_b)} \int_{C''} s^{2p-1}(s^p - s_b^p)\, G_1(s)\, e^{-\lambda\left[\frac{s^{2p}}{2p} - \frac{(s_b s)^p}{p}\right]} ds$$

$$= \frac{e^{-\lambda f(t_b)}}{\lambda} \int_{C''} s^{p-1}[pG_1(s) + sG_1'(s)]\, e^{-\lambda\left[\frac{s^{2p}}{2p} - \frac{(s_b s)^p}{p}\right]} ds.$$

(4A.1.14)

Since $G_1(s)$ in (4A.1.12) is an analytic function in a region around the origin, therefore K is of order $1/\lambda$ smaller than the original integral. Consequently, when $\lambda \to \infty$, the leading order approximation of I is

$$I \sim e^{-\lambda f(t_b)} \sum_{n=0}^{2p-1} \gamma_n \int_{C''} s^{n+p-1}\, e^{-\lambda\left[\frac{s^{2p}}{2p} - \frac{(s_b s)^p}{p}\right]} ds.$$

(4A.1.15)

We can obtain higher-order approximation to I by repeating the same procedure on K, thus obtaining an approximation to K with an error term that is of $1/\lambda^2$ smaller than I.

The integral in (4A.1.15) can be expressed in terms of parabolic cylinder function uniquely if we know the original

path of integration. Say C" can be deformed to two valleys given by (4A.1.11) where $k = k_1$ and k_2. Thus the integration path C" in I can be replaced by one which ranges from $s = \alpha\, e^{i(k_1\pi/p)}$ to the origin and from the origin to $s = \alpha\, e^{i(k_2\pi/p)}$ where α is real and $\alpha \to \infty$. We shall assume that no singularities are enclosed when C" is deformed to the above defined path as they only give rise to some additive terms. As such, we let

$$D(n + p - 1) = \int_{C"} s^{n + p - 1}\, e^{-\lambda\left[\frac{s^{2p}}{2p} - \frac{(s_b s)^p}{p}\right]}\, ds$$

$$= \lim_{\alpha\to\infty} \int_{\alpha\, e^{ik_1(\pi/p)}}^{\alpha\, e^{ik_2(\pi/p)}} s^{n + p - 1}\, e^{-\lambda\left[\frac{s^{2p}}{2p} - \frac{(s_b s)^p}{p}\right]}\, ds. \qquad (4A.1.16)$$

Fig. 4A.1.2 shows the paths of integration. To express D in terms of parabolic cylinder function (4A.1.16) can be divided into two integration one ranges from $e^{ik_1(\pi/p)}$ to 0 and the other one ranges from 0 to $e^{ik_2(\pi/p)}$ where $\alpha \to \infty$. Hence

$$D(n + p - 1) = \frac{1}{p}\,(\lambda/p)^{-\frac{n + p}{2p}}\, \Gamma\left(\frac{n + p}{p}\right) \exp\left(\frac{\lambda s_b^{2p}}{4p}\right)\left[e^{ik_2\frac{\pi}{p}(n + p)}\right.$$

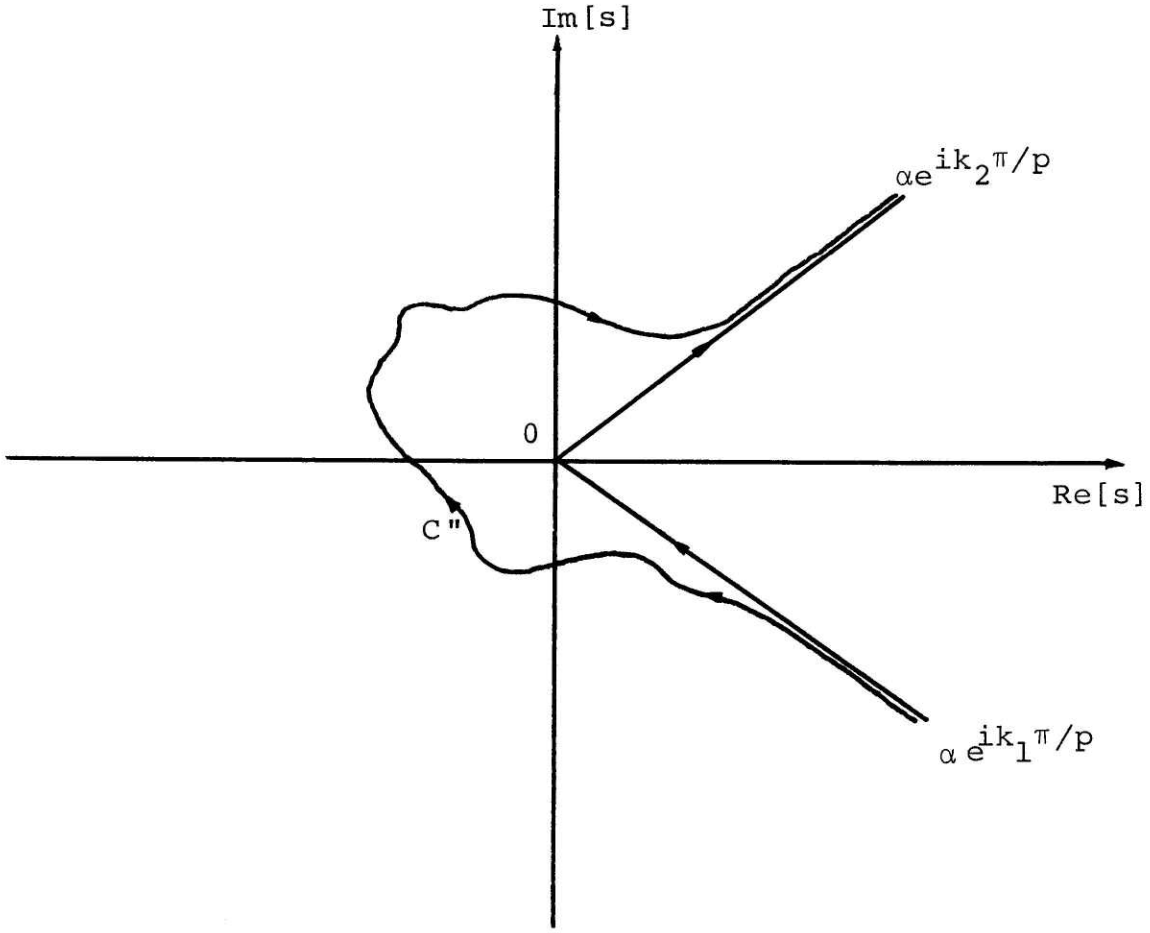

Fig. 4A.1.2. The original path of integration C" and the deformed path of integration.

$$D_{-(n + p)/2}(-\sqrt{\lambda/p}\, s_b^{\,p}\, e^{ik_2\pi})$$

$$- e^{ik_1 \frac{\pi}{p} (n + p)} D_{-(n + p)/2}(-\sqrt{\lambda/p}\, s_b^{\,p}\, e^{ik_1\pi})\Big] . \quad (4A.1.17)$$

If the original path of integration in (4A.1.1) is on the same or adjacent Riemann sheet or is deformable to it, then $|k_2 - k_1| = 2$ or 1. In evaluating $|k_2 - k_1|$, we have assumed the least possible value of $|k_2 - k_1|$ since adding $2\ell p$ (where ℓ is an integer) to k_1 and k_2 does not change the locations of the valleys they denote. If we let $\mu = \text{sgn}(k_2 - k_1)$, and C in (4A.1.1) is on the same Riemann sheet and $|k_2 - k_1| = 2$, then (4A.1.17) simplifies to

$$D(n + p - 1) = \frac{1}{p} (\lambda/p)^{-(n + p)/2p}\, \Gamma\left(\frac{n + p}{p}\right) \exp\left(\frac{\lambda\, s_b^{\,2p}}{4p}\right)$$

$$D_{-(n + p)/p}(-\sqrt{\lambda/p}\, s_b^{\,p}\, e^{ik_1\pi})$$

$$e^{ik_1 \frac{\pi}{p} (n + p)} \left[e^{i\mu \frac{2\pi}{p} (n + p)} - 1 \right] . \quad (4A.1.18)$$

When $|k_2 - k_1| = 1$, (4A.1.17) simplifies to

$$D(n + p - 1) = \frac{1}{p} (\lambda/p)^{-\frac{n + p}{2p}} \sqrt{2\pi} \exp\left(\frac{\lambda s_b^{2p}}{4p}\right) e^{\frac{ik_1 + k_2}{2p} \pi (n + p)}$$

$$e^{i\mu \frac{\pi}{2}} D_{n/p}(-i\sqrt{\lambda/2}\, s_b^p\, e^{ik_1 \pi}\, \mu). \qquad (4A.1.19)$$

The above identity has been arrived at using the linear relations of parabolic cylinder functions. Henceforth, we can write

$$I \sim e^{-\lambda f(t_b)} \sum_{n = 0}^{2p - 1} \gamma_n D(n + p - 1). \qquad (4A.1.20)$$

The values of γ_n can be solved from (4A.1.12). By noting that the first $p - 1$ derivatives of the latter term vanish at $s = 0$, we know that

$$\gamma_n = \frac{G^{(n)}(0)}{n!}, \qquad 0 \leq n \leq p - 1. \qquad (4A.1.21)$$

The values of γ_n for $p \leq n \leq 2p - 1$ can be obtained by noticing that the latter term in (4A.1.12) vanishes at p points given by $s = s_b\, e^{i(2m\pi/p)}$, $m = 0, 1, \ldots, p - 1$. Thus we can set up p linear equations and solve for γ_n for $n = p, p + 1, \ldots, 2p - 1$. Hence (4A.1.18) can be determined uniquely.

4A.2 The Steepest-Descent Paths That Pass Through the Saddle-Points

To show that the steepest-descent paths are asymptotic to the asymptotes as shown in Fig. 4.3.1 and Fig. 4A.2.1 when $\mathrm{Im}[\beta] \to \pm\infty$, and that they are on the correct Riemann sheets, it suffices to show that $\exp\{iR_m[\cos\alpha_m(k_1^2 - k^2\sin^2\beta)^{1/2} + k\sin\alpha_m\sin\beta]\}$ vanishes along such paths at ∞, and that its phases remain the same as that of the saddle-points along such asymptotes.

We can show that the asymptotes are in fact those shown in Fig. 4A.2.1. When $\mathrm{Im}[\beta] \to \pm\infty$, $|\sin\beta| \to \infty$, thus $k_{1z} = (k_1^2 - k^2\sin^2\beta)^{1/2} \simeq \pm ik\sin\beta$. Consequently, the exponential factor can be approximated by $\exp\{ikR_m\sin\beta[\sin\alpha_m \pm i\cos\alpha_m]\}$. The positive sign is chosen when we are on the Riemann sheet where $\mathrm{Im}[k_{1z}] > 0$ and conversely for the negative sign. Letting $\beta = \beta' + i\beta''$ where β' and β'' are real, the exponential factor can be written as

$$\exp\{ikR_m\cosh\beta''[\sin\alpha_m\sin\beta' \mp \cos\alpha_m\cos\beta'\tanh\beta'' + i(\tanh\beta''\cos\beta'\sin\alpha_m \pm \sin\beta'\cos\alpha_m)]\} \qquad \begin{matrix}\mathrm{Im}[k_{1z}] > 0 \\ \mathrm{Im}[k_{1z}] < 0\end{matrix} \qquad (4A.2.1)$$

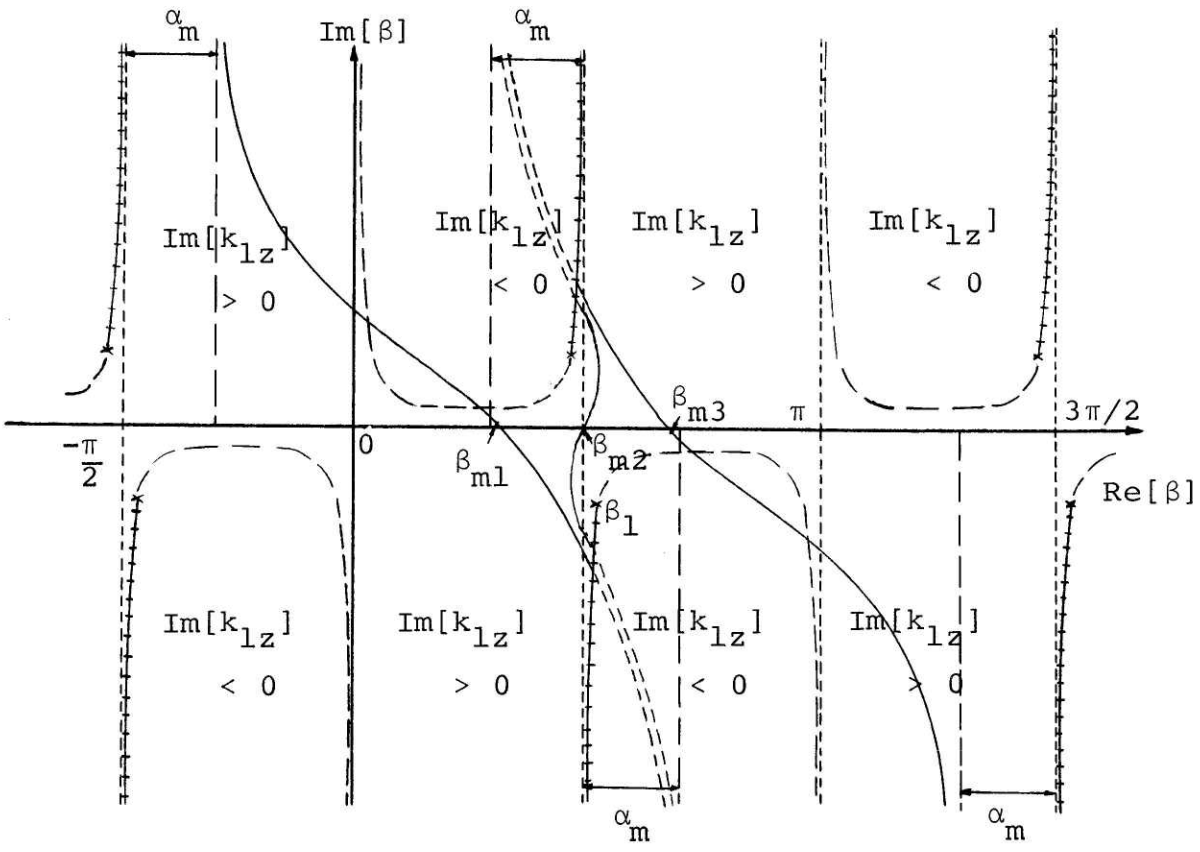

Fig. 4A.2.1. The steepest-descent paths that pass through the saddle-points and the regions where $\mathrm{Im}[k_{1z}] < 0$ and $\mathrm{Im}[k_{1z}] > 0$.

The notation means that the upper sign is chosen when $\mathrm{Im}[k_{1z}] > 0$ and the converse for $\mathrm{Im}[k_{1z}] < 0$. At the saddle-points β_{m1} and β_{m3}, the phase of the exponential factor is $\exp(ik_1 R_m)$ and at β_{m2}, it is $\exp[ik_1 R_m \cos(\alpha_m - \theta_o)]$. Thus for (4A.2.1) to have the same phase when $\beta'' \to \pm\infty$, the following must be true.

$$\lim_{|\beta''|\to\infty} \sin\alpha_m \sin\beta' \mp \cos\alpha_m \cos\beta' \tanh\beta'' = 0$$

$$\begin{matrix} \mathrm{Im}[k_{1z}] > 0 \\ \mathrm{Im}[k_{1z}] < 0. \end{matrix} \qquad (4A.2.2)$$

When $\beta'' \to +\infty$, $\tanh\beta'' \to 1$, as such,

$$\tan\beta' = \pm\cot\alpha_m, \qquad \begin{matrix} \mathrm{Im}[k_{1z}] > 0 \\ \mathrm{Im}[k_{1z}] < 0, \end{matrix} \qquad (4A.2.3)$$

or

$$\beta' = \begin{cases} \frac{\pi}{2} + n\pi - \alpha_m, & \mathrm{Im}[k_{1z}] > 0 \\ -\frac{\pi}{2} + n\pi + \alpha_m, & \mathrm{Im}[k_{1z}] < 0, \end{cases} \qquad (4A.2.4)$$

where $n = 0, \pm1, \pm2, \ldots$. Hence the asymptotes of interest

to us where (4A.2.1) would vanish when $\beta'' \to +\infty$ are at $\beta' = \pi/2 - \alpha_m$ and $\beta' = -\pi/2 + \alpha_m$. Along the first asymptote, the steepest-descent path has to be on the Riemann sheet where $\mathrm{Im}[k_{1z}] > 0$ and along the second asymptote, it has to be on the Riemann sheet where $\mathrm{Im}[k_{1z}] < 0$.

Similarly, when $\beta'' \to -\infty$, the asymptotes of interest to us are at $\beta' = \pi/2 + \alpha_m$ and $\beta' = 3\pi/2 - \alpha_m$. Along the first asymptote, the steepest-descent path has to be on the Riemann sheet where $\mathrm{Im}[k_{1z}] > 0$ and along the second asymptote, it has to be on the Riemann sheet where $\mathrm{Im}[k_{1z}] < 0$.

The choice of branch-cuts of $\mathrm{Re}[k_{1z}] = 0$ are shown in Fig. 4A.2.1. The loci of the points where $\mathrm{Im}[k_{1z}] = 0$ are shown as dashed lines joining the branch-cuts of $\mathrm{Re}[k_{1z}] = 0$. This is consistent with the observation that the locus of $\mathrm{Im}[k_{1z}] = 0$ on the k_ρ-plane is a hyperbolic curve that joins the $\mathrm{Re}[k_{1z}] = 0$ locus (see Fig. 3.3.1).

On the upper Riemann sheet, $\mathrm{Re}[k_{1z}] > 0$. To distinguish the signs of k_{1z} on the two sides of the branch-cut passing through β_1, we Taylor-series expand k_{1z} around β_1. Hence, for $|\beta - \beta_1| \ll 1$,

$$k_{1z} \simeq \pm\, e^{-i\frac{\pi}{4}} [2k_1(k_1^2 - k^2)^{1/2}(\beta - \beta_1)]^{1/2}. \qquad (4A.2.5)$$

Letting $\beta - \beta_1 = \varepsilon\, e^{i\sigma}$, the value of k_{1z} on the top Riemann

sheet is

$$k_{lz} \simeq e^{-i\frac{\pi}{4}} [2k_l(k_l^2 - k^2)^{1/2}\ \varepsilon]^{1/2} e^{i\frac{\sigma}{2}}, \quad -\pi/2 < \sigma < 3\pi/2. \tag{4A.2.6}$$

By setting $\sigma = -\pi/2$ and $3\pi/2$ successively, we see that $\mathrm{Im}[k_{lz}] < 0$ on the right side of the branch-cut and $\mathrm{Im}[k_{lz}] > 0$ on the left side of the branch-cut. As such, on the upper Riemann sheet, we can determine the region where $\mathrm{Im}[k_{lz}] > 0$. It is a simply-connected region. The region where $\mathrm{Im}[k_{lz}] < 0$ consists of disjoint regions. The boundaries between the two regions are the branch cuts and the locus of $\mathrm{Im}[k_{lz}] = 0$ (see Fig. 4A.2.1). This verifies the locations of the steepest-descent path when $\beta \to \pm\infty$ as shown in Fig. 4A.2.1. The shape of the steepest-descent paths in the neighborhood of the saddle-points can be determined by Taylor-series expanding the argument of the exponential function around them.

Chapter 5. GENERALIZED WEBER'S FUNCTION

5.1 Introduction

We have seen in the previous chapters that in finding the asymptotic expansion of an integral, we expand the integrals in terms of simpler integrals which can be expressed in terms of known functions. For ordinary saddle-point analysis, such functions are gamma functions. For modified saddle-point and three-saddle-point analyses, they are parabolic cylinder functions or Weber's functions.

However, when the number of saddle-points and singularities increases, it is impossible to express our simplified integrals in terms of known functions. The corresponding functions are dubbed generalized Weber's functions by Bleistein.[36] Uniform asymptotic expansion of an integral where there are many singularities in the neighborhood of many saddle-points can be represented in terms of such functions. In their applications to wave propagation, they characterize the behaviors of the waves just as Bessel functions characterize spherical and cylindrical waves. We shall see their applications in deriving the interference fringes of a dipole antenna over stratified media.

5.2 Asymptotic Expansions of Integrals with a Singularity Near Three Colinear Saddle-Points

An integral with a singularity in the neighborhood of three colinear saddle-points can be expressed as

$$I = \int_C (t - t_p)^r \, g(t) \, e^{-\lambda f(t)} \, dt \qquad (5.2.1)$$

where $f'(t) = 0$ at $t = 0$ and $\pm t_b$, r is fractional or a negative integer, $g(t)$ is analytic in a region around the origin and t_p is the location of the singularity. C is the path of integration extending to infinity such that I converges. If the above is obtained by a transformation to remove a branch-point singularity, it is generally true that $g(t)$ has a zero at $t = 0$. We shall make use of this fact in our analysis.

With a transformation of the following kind,

$$f(t) - f(0) = \frac{s^4}{4} - \frac{(s_b s)^2}{2} \qquad (5.2.2)$$

(5.2.1) becomes

$$I = e^{-\lambda f(0)} \int_{C'} (s - s_p)^r \, sG(s) \, e^{-\lambda [s^4/4 - (s_b s)^2/2]} \, ds \qquad (5.2.3)$$

where

$$G(s) = \left(\frac{t - t_p}{s - s_p}\right)^r \frac{g(t)}{s} \frac{dt}{ds} . \qquad (5.2.4)$$

$G(s)$ is analytic in a region around the origin. The steps for finding dt/ds, s_b and s_p resembles that described in Chapter 4. From (5.2.2)

$$\frac{dt}{ds} = \frac{s(s^2 - s_b^2)}{f'(t)} \qquad (5.2.5)$$

$$s_b = \sqrt{2}\ [f(0) - f(t_b)]^{1/4} \qquad (5.2.6a)$$

$$s_p = \sqrt{2}\ [f(0) - f(t_p)]^{1/4} \qquad (5.2.6b)$$

which means that the saddle-points and the singularity on the t-plane are mapped into their counterparts on the s-plane.

To obtain the asymptotic approximation of I for all s_p and s_b, we shall approximate $G(s)$ with a polynomial that interpolates the critical points; namely, the singularity and the saddle-points. As such, we can write $G(s)$ as

$$G(s) = \gamma_o + \gamma_1 s + \gamma_2 s^2 + \gamma_3 s^3 + s(s^2 - s_b^2)(s - s_p)\, G_1(s).$$

(5.2.7)

Solving the above for γ_n, we obtain

$$\gamma_o = G(0) \tag{5.2.8a}$$

$$\gamma_1 = \frac{2s_b^3[G(s_p) - \gamma_o - \gamma_2 s_p^2] - s_p^3[G(s_b) - G(-s_b)]}{2s_p s_b[s_b^2 - s_p^2]} \tag{5.2.8b}$$

$$\gamma_2 = \frac{G(-s_b) + G(s_b) - 2\gamma_o}{2s_b^2} \tag{5.2.8c}$$

$$\gamma_3 = \frac{2s_b[G(s_p) - \gamma_o - \gamma_2 s_p^2] - s_p[G(s_b) - G(-s_b)]}{2s_b s_p[s_p^2 - s_b^2]}\,. \tag{5.2.8d}$$

Substituting (5.2.7) into (5.2.3), we obtain

$$I = e^{-\lambda f(0)}\Big[\int_{C'} (s - s_p)^r\, s(\gamma_o + \gamma_1 s + \gamma_2 s^2 + \gamma_3 s^3)$$

$$e^{-\lambda[s^4/4 - (s_b s)^2/2]}\, ds + \int_{C'} (s - s_p)^{r+1}$$

$$s^2(s^2 - s_b^2)\, G_1(s)\, e^{-\lambda[s^4/4 - (s_b s)^2/2]}\, ds]. \qquad (5.2.9)$$

Using integration by parts, we can estimate the magnitude of the latter integral.

$$K = e^{-\lambda f(0)} \int_{C'} (s - s_p)^{r+1}\, s^2(s^2 - s_b^2)\, G_1(s)$$

$$e^{-\lambda[s^4/4 - (s_b s)^2/2]}\, ds$$

$$= \frac{e^{-\lambda f(0)}}{\lambda} \int_{C'} (s - s_p)^r\, L(s)\, e^{-\lambda[s^4/4 - (s_b s)^2/2]}\, ds$$

(5.2.10)

where

$$L(s) = (r + 1)s\, G_1(s) + (s - s_p)\, G_1(s) + (s - s_p)s\, G_1'(s).$$

(5.2.11)

We see that K is of order $1/\lambda$ smaller than I if

$g(t)$ does not vanish at $t = 0$. In the actual problem, $g(t)$ vanishes at $t = 0$, which means that the contribution of the saddle-point at $t = 0$ is of lesser importance. However, we shall see that the error in estimating I by the first integral in (5.2.9) is tolerable. Otherwise, to derive an approximation whose error is of order $1/\lambda$ smaller than I rigorously, we have to use a fourth order polynomial approximation. This will require finding derivative of $G(s)$ which is a formidable task if $G(s)$ is a very complicated function. Thus when λ is large,

$$I \sim e^{-\lambda f(0)} \int_{C'} (s - s_p)^r s \sum_{n=0}^{3} \gamma_n s^n e^{-\lambda[s^4/4 - (s_b s)^2/2]} ds. \tag{5.2.12}$$

If C' is as shown in Fig. 5.2.1, we can deform C' so that it extends from $-i\infty$ to 0 and then from 0 to ∞. We assume, for this case, that s_p is in the second quadrant so that the pole is not enclosed in the course of deforming the path of integration. Letting $s = u/\lambda^{1/4}$, (5.2.12) becomes

$$I \sim \frac{e^{-\lambda f(0)}}{\lambda^{(r+2)/4}} \int_{-i\infty}^{\infty} u(u - \lambda^{1/4} s_p)^r \sum_{n=0}^{3} \frac{\gamma_n u^n}{\lambda^{n/4}} e^{-[u^4/4 - \sqrt{\lambda}\,(s_b u)^2/2]}$$

$$du. \tag{5.2.13}$$

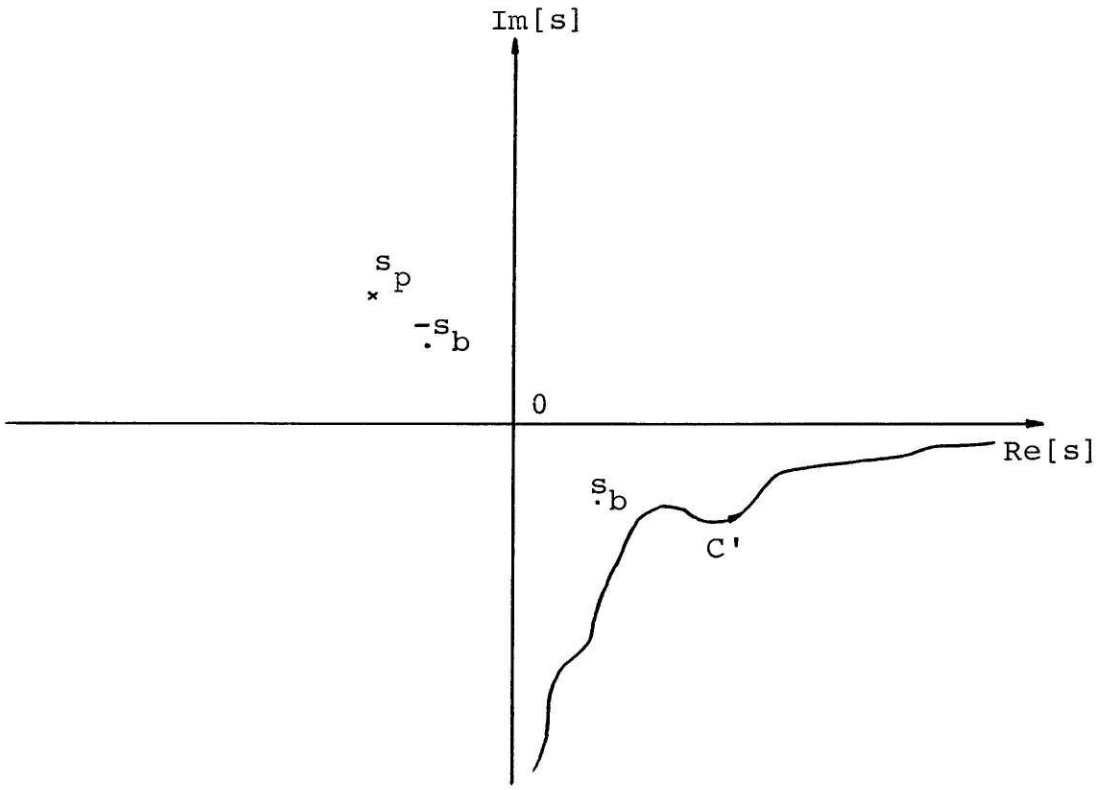

Fig. 5.2.1. The original path of integration with respect to saddle-points and pole on the s-plane.

If we define

$$W_g(\sigma, \delta; n, r) = \int_{-i\infty}^{\infty} (u - \delta)^r u^n e^{-\left(\frac{u^4}{4} - \sigma \frac{u^2}{2}\right)} du, \qquad (5.2.14)$$

which we shall call generalized Weber's function, then

$$I \sim \frac{e^{-\lambda f(0)}}{\lambda^{(r+2)/4}} \sum_{n=0}^{3} W_g(\sqrt{\lambda}\, s_b^2, \lambda^{1/4} s_p; n + 1, r) \frac{\gamma_n}{\lambda^{n/4}} \qquad (5.2.15)$$

when $\lambda \to \infty$.

A subtle point need to be emphasized here. When the branch of s_b and s_p in (5.2.5) is chosen such that C' extends from $-i\infty$ to $+\infty$, the same branch has to be chosen for all t_b so that C' remains unchanged; that is it still extends from $-i\infty$ to $+\infty$ on the s-plane. This will cause the generalized Weber's function to exhibit Stoke's phenomenon in its asymptotic approximation similar to the parabolic cylinder function when s_b varies.

5.3 Application to Evaluating Interference Fringes of Dipole Antennas

An integral which has a singularity in the neighborhood of three colinear saddle-points in the evaluation of interference fringes is given by (4.3.3). It is the integral representation of the reflected wave for a dipole antenna over two layer media. Reproduced here, it is

$$T_R^m = \int_\Gamma k \sin\beta \, B_m(\beta) \, \tilde{H}(\beta) \, e^{iR_m[\cos\alpha_m (k_1^2 - k^2\sin^2\beta)^{1/2} + k \sin\alpha_m \sin\beta]} \, d\beta \qquad (5.3.1a)$$

where

$$\alpha_m = \tan^{-1}\frac{\rho}{2md}, \qquad R_m = [\rho^2 + (2md)^2]^{1/2} \qquad (5.3.1b)$$

$$B_m(\beta) = X_{01}X_{10} \, R_{10}^{m-1} \, R_{12}^m \, e^{ik_z z}\Big|_{k_\rho = k\sin\beta} \qquad (5.3.1c)$$

$$\tilde{H}(\beta) = H_o^{(1)}(k\rho \sin\beta) \, e^{-ik\rho\sin\beta}. \qquad (5.3.1d)$$

After some algebraic manipulation, we can write $B_m(\beta)$ as

$$B_m(\beta) = \frac{4b\, k_z k_{1z} (k_{1z} - bk_z)^{2m} R_{12}^m}{(b^2 - 1)^{m+1} (k_\rho - k_{\rho_p})^{m+1} (k_\rho + k_{\rho_p})^{m+1}} \left. e^{ik_z z} \right|_{k_\rho = k \sin\beta} \tag{5.3.2}$$

where

$$k_{\rho_p} = \left[\frac{b^2 k^2 - k_1^2}{b^2 - 1} \right]^{1/2} .$$

There is a pole of order $m + 1$ at

$$\beta_p = \sin^{-1} \left[\frac{b^2 - (k_1/k)^2}{b^2 - 1} \right]^{1/2}$$

which can be near to the saddle-points at β_{m1}, β_{m2} and β_{m3} as shown in Fig. 4.3.1. With the following transformation,

$$t = \beta - \frac{\pi}{2}, \qquad \lambda = R_m, \qquad t_b = \beta_{m1} - \frac{\pi}{2}, \qquad t_p = \beta_p - \frac{\pi}{2} \tag{5.3.3a}$$

$$(t - t_p)^{-(m+1)} \, g(t) = B_m(\beta) \tag{5.3.3b}$$

$$f(t) = -i[\cos \alpha_m (k_1^2 - k^2 \sin^2 \beta)^{1/2} + k \sin \alpha_m \sin \beta]. \qquad (5.3.3c)$$

(5.3.1a) becomes the form of (5.2.1) where $r = -(m + 1)$. We obtain from (5.2.5) and (5.2.6) that

$$s_b = 2^{3/4} e^{-i \frac{3\pi}{8}} k_1^{1/4} \sin^{1/2} \left(\frac{\theta_o - \alpha_m}{2} \right) \qquad (5.3.4)$$

$$s_p = 2^{3/4} e^{i \frac{5\pi}{8}} k_1^{1/4} \left[\sin \left(\frac{\theta_o - \alpha_m}{2} \right) - \sin \left(\frac{\theta_p - \alpha_m}{2} \right) \right]^{1/2} \qquad (5.3.5)$$

where

$$\theta_p = \sin^{-1} \left(\frac{k}{k_1} \sin \beta_p \right), \qquad \theta_o = \sin^{-1} \frac{k}{k_1}.$$

In the above, we have chosen the branch for s_b such that it is in the fourth quadrant when $\theta_o > \alpha_m$. This will cause the image of Γ on the s-plane to extend from $-i\infty$ to $+\infty$. To leave the image of Γ unchanged on the s-plane when $\theta_o < \alpha_m$, we choose the branch for s_b such that

$$s_b = 2^{3/4} e^{i \frac{\pi}{8}} k_1^{1/4} \sin^{1/2} \left(\frac{\alpha_m - \theta_o}{2} \right) \qquad (5.3.6)$$

This also causes β_{m1} to correspond to s_b and β_{m3} to correspond to $-s_b$ always.

Note that the above choice of branch for s_b is different from that of (4.3.7). For clarification, Fig. 5.3.1 shows the locus of s_b for real k_1 when α_m increases from 0 to $\pi/2$. C_W is the path of integration for the generalized Weber's function. It is immaterial to know the exact location of the original path of integration on the s-plane as long as we can deform it to C_W without enclosing s_p. This is true for the integral T_R^m which enables us to make use of (5.2.15).

Making use of (5.2.4) and the large ρ approximation for $\tilde{H}(\beta)$, we obtain

$$G(0) = -(-s_p)^{m+1}\sqrt{2k/\pi\rho}\, e^{i\frac{\pi}{4}} \left.\frac{s_b^2 \cos\theta_o}{\sin(\alpha_m - \theta_o)} \frac{B_m(\beta)}{k\cos\beta}\right|_{\beta=\pi/2} \tag{5.3.7a}$$

$$G(s_b) = (s_b - s_p)^{m+1} e^{-i\frac{\pi}{2}} 2\sqrt{\frac{k_1 \sin\alpha_m}{\pi k_1\rho}}\, B_m(\beta_{m1}) \frac{k_1\cos\alpha_m}{k\cos\beta_{m1}} \tag{5.3.7b}$$

$$G(-s_b) = (-s_b - s_p)^{m+1} e^{-i\frac{\pi}{2}} 2\sqrt{\frac{k_1 \sin\alpha_m}{\pi k_1\rho}}\, B_m(\beta_{m3}) \frac{k_1\cos\alpha_m}{k\cos\beta_{m3}} \tag{5.3.7c}$$

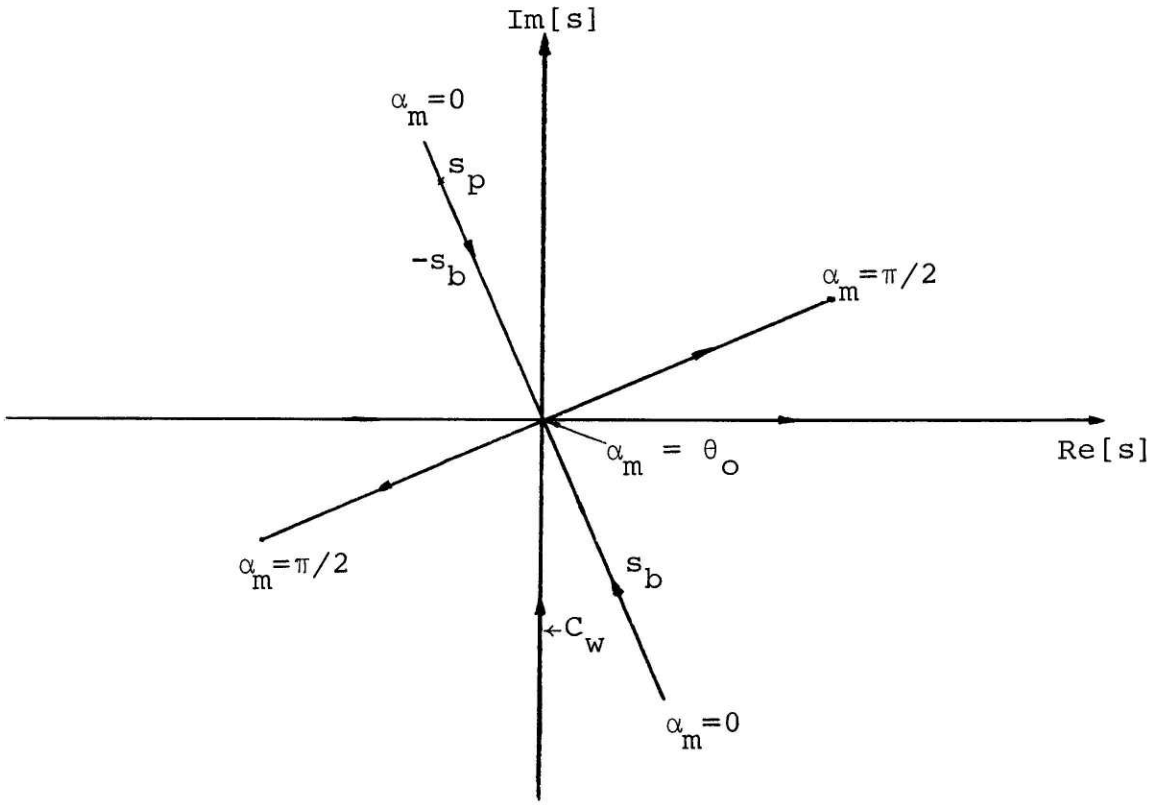

Fig. 5.3.1. The locus of s_b and $-s_b$ when α_m increases from 0 to $\pi/2$. C_w is the path of integration for the generalized Weber's function.

$$G(s_p) = (k \cos \beta_p)^{-(m+1)} \left[\frac{ik_1 \dfrac{k \cos \beta_p}{k_1 \cos \theta_p} \sin(\theta_p - \alpha_m)}{s_p(s_p^2 - s_b^2)} \right]^m \sqrt{2/\pi\rho}$$

$$e^{-i\frac{\pi}{4}} \sqrt{k_{\rho p}} \frac{B_m(\beta_p)(k_1 \sin \theta_p - k_{\rho p})^{m+1}}{s_p} . \qquad (5.3.7d)$$

Using the above, we can obtain γ_n from (5.2.8), and thus the uniform asymptotic approximation from (5.2.15). The approximation will be valid for all values of s_b and s_p. Similarly, we can obtain the asymptotic approximation of all field components, regardless of the fact that they arise from either TE or TM waves. The value of generalized Weber's function can be obtained by numerical integration.

Figure 5.3.2a shows the use of the above analysis to compute the E_z component of an HMD. The improvement is remarkable compared with Fig. 4.3.5. Fig. 5.3.2b is similar except that the subsurface reflector is metallic. Fig. 5.3.3 and Fig. 5.3.4 shows the effect of the location of the Sommerfeld pole on the approximation. There is no noticeable effects as in Fig. 4.3.6a and b. Note that the vertical scale for the latter two diagrams are exaggerated; thus the larger discrepancies with numerical GOA are artificial.

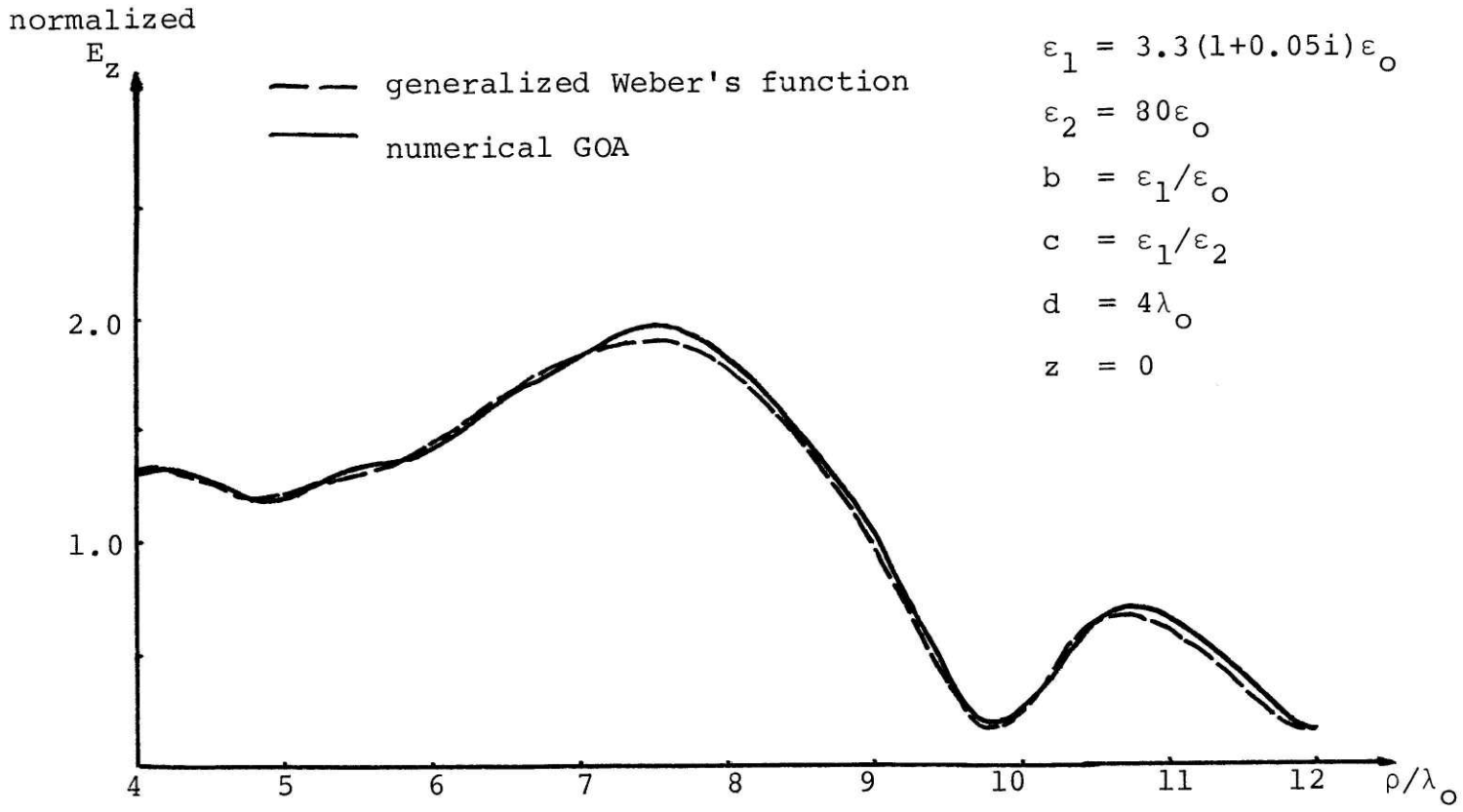

Fig. 5.3.2(a). E_z component of an HMD using generalized Weber's functions in the asymptotic expansion of the integral representation.

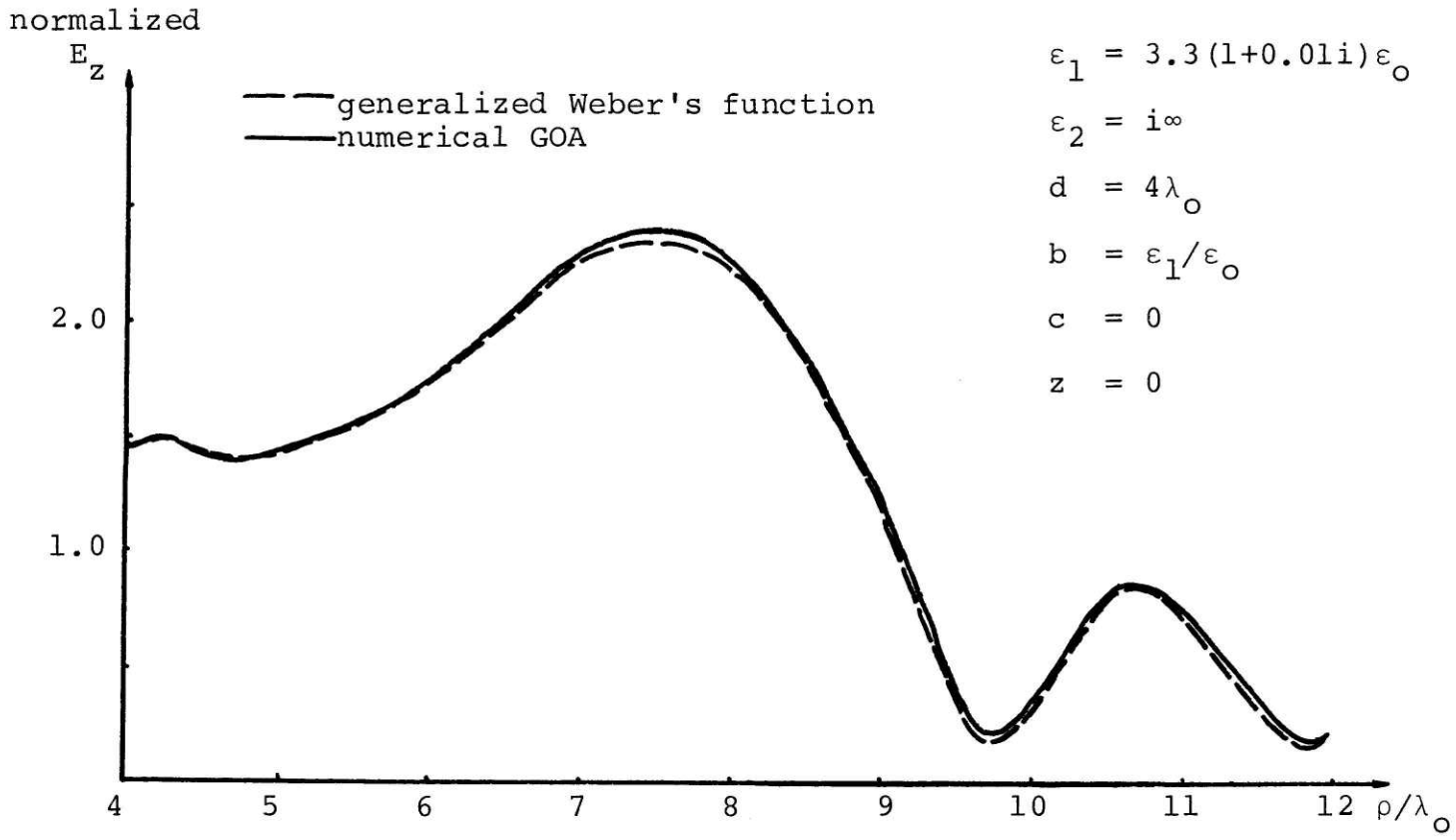

Fig. 5.3.2(b). Same as (a) except that the subsurface reflector is now metallic.

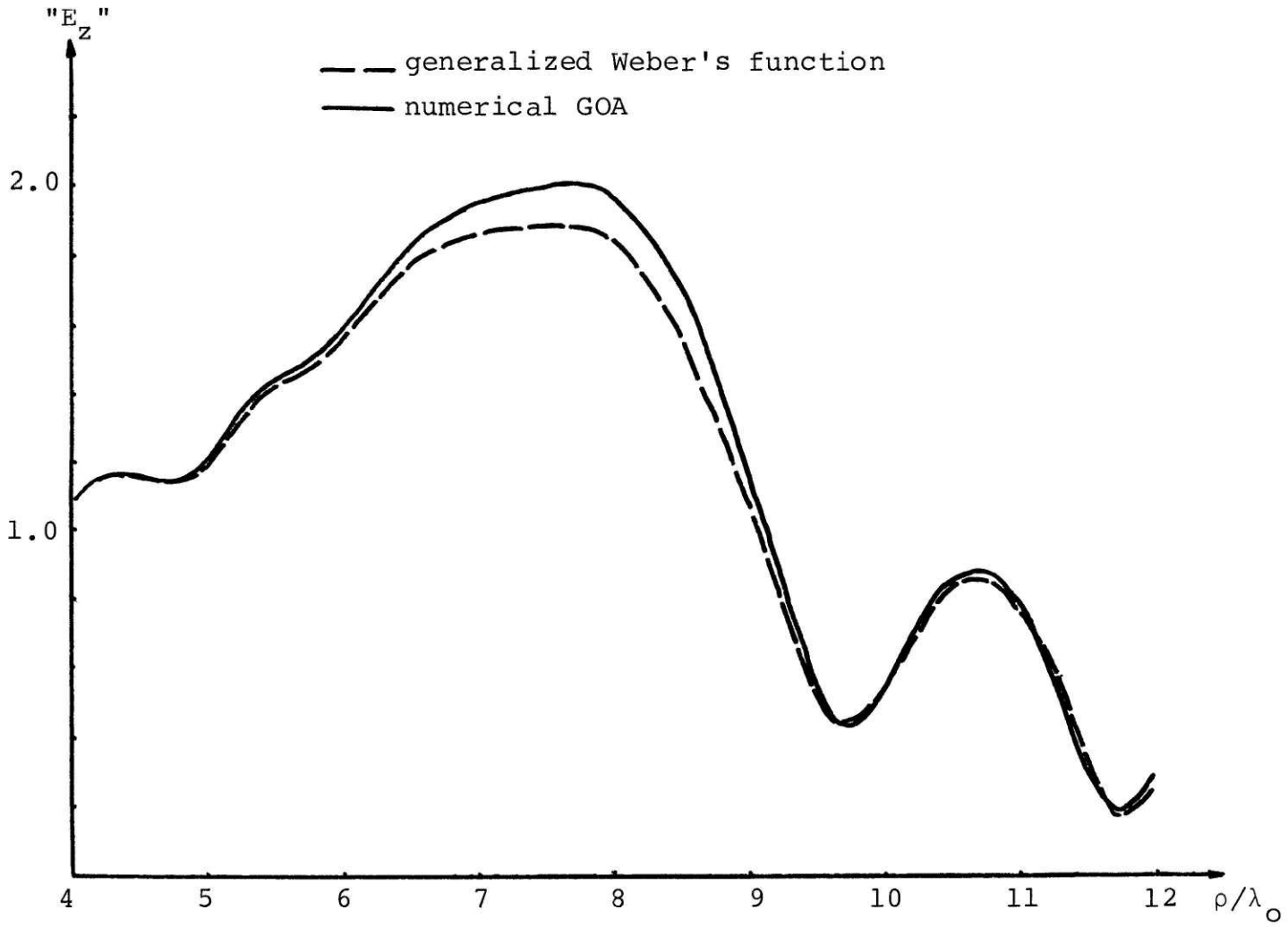

Fig. 5.3.3. Same as Fig. 5.3.2(b) except that b = 2.0

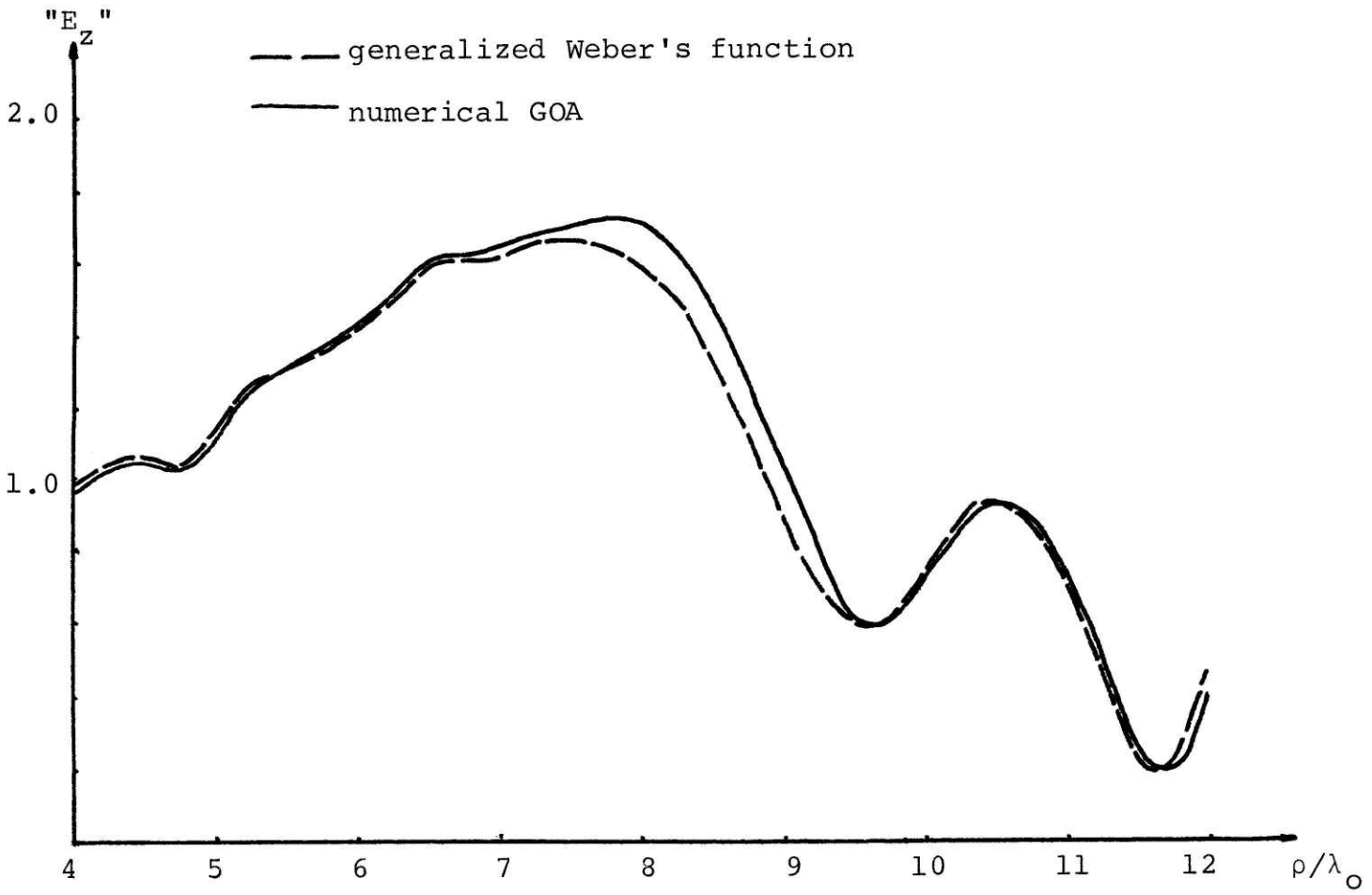

Fig. 5.3.4. Same as Fig. 5.3.2(b) except that b = 1.5.

5.4 Conclusions

We see in this chapter the analysis of the interference fringes of an HMD. In previous chapters, we have pretended to ignore the effect of the Sommerfeld pole on TM waves generated by an HMD. This is only true for cases when the Sommerfeld pole is far away from the saddle-points of our interest, i.e. when generalized Weber's function can be approximated by parabolic cylinder function. For most cases, the effect of the Sommerfeld pole cannot be neglected, and it affects the angular dependence of the wave observed. However, the effect of the Sommerfeld pole is peripheral, i.e. if we are to carry out the saddle-point analysis similar to that of Chapter 4, the pole is never enclosed when we deform the original path of integration to the steepest-descent path passing through the saddle-points. In other words, we cannot associate any characteristic wave with the Sommerfeld pole. Moreover, generalized Weber's function can be approximated by parabolic cylinder function always when $\lambda \to \infty$. Thus, the effect of the pole is not noticeable in the far-field.

The generalized Weber's functions, like parabolic cylinder functions also exhibit Stoke's phenomenon. Thus there is the existence of the lateral wave and the spherical wave as before. This is more apparent if we were to follow the analysis in the line of Chapter 4. We also see that the use of polynomial ap-

proximation for G(s) circumvents the difficulties of differentiating G(s), which in our problem, is relatively complicated and formidable.

Though we have shown that the field of a dipole source over stratified media can be approximated by special functions, one must be aware that this is not the same as the mode-expansion method. Our approximation by a series is only true in the asymptotic sense. This is because G(s) (the notation of which we have used throughout our analysis) in general has other singularities on the finite complex plane which are distant from the saddle-points. Thus the approximation of G(s) by polynomials or Taylor series is only valid over a finite region. We have previously emphasized that such an approximation of G(s) for an integral whose range of integration extends to infinity results in an asymptotic approximation. This also means that all the singularities of the integrand on the complex plane have some effects on our approximation. Some of these are of lesser effect than the others. Thus, in our approximation, we have taken into account only the singularities of immediate significance. We can imagine that if we have taken into account all the effects of the singularities, our series representation would be exact.

We have seen in the above that the value of the integral I is only determined by the values of the integrand at some

critical points; namely, the saddle-points and singularities. This is similar to the concept of singularity expansion. Our original integral in our problem is complicated to the extent of being intractable if we seek to derive from it physical feelings for the behaviour of the wave. We see that by expanding our original integral in terms of its critical point contribution, we have gained physical insight in the behaviour of the wave. This justifies our representation of the integral in terms of a series of special or little-known functions.

References

1. El-Said, M. A. H., "Geophysical prospection of underground water in the desert by means of electromagnetic interference fringes," Proc. IRE, 44, p. 24-30 and 940, 1956.

2. Simmons, G., et al, "The surface electrical properties experiment," Geochim. Cosmochin. Acta, 36, Suppl. 3, p. 258-270, 1972.

3. Rossiter, J. R., et al, "Radio interferometry depth sounding: Part II-- Experimental results," Geophysics, 38, no. 3, p. 581-599, June 1973.

4. Rossiter, J. R., et al, "Detection of thin layer by radio interferometry," Geophysics, 40, no. 2, p. 299-308, April 1975.

5. Strangway, D. W., et al, "Radio frequency interferometry-- a new technique for studying glacier," J. Glaciol., 1972.

6. Baños, Jr., A., Dipole Radiation in the Presence of a Conducting Half-Space, Pergamon, New York, 1966.

7. Brekhovskikh, L. M., Waves in Layered Media, Academic Press, New York, 1960.

8. Ott, H., "Reflexion und brechung von Kugelwellen: effekle Q. ordrung," Ann. Physik, 41, p. 443-466, 1941.

9. Sommerfeld, A., Partial Differential Equations, Academic Press, New York, 1949.

10. Wait, J. R., Electromagnetic Waves in Stratified Media, Pergammon Press, New York, 1970.

11. Wait, J. R. (Ed), Electromagnetic Probing in Geophysics, Golem Press, Boulder, Colo., 1971.

12. Wait, J. R., "The magnetic dipole over the horizontal stratified earth," Can. J. Phys., 29, p. 577-592, 1951.

13. Kong, J. A., "Electromagnetic fields due to dipole antennas over stratified anisotropic media," Geophysics, Dec. 1972.

14. Kong, J. A., Theory of Electromagnetic Waves, John Wiley and Sons, New York, 1975.

15. Kong, J. A., L. Tsang and G. Simmons, "Geophysical subsurface probing with radio-frequency interferometry, IEEE Trans. on Antennas and Propagation, AP-22, no. 4, July 1974, p. 616.

16. Tsang, L., R. Brown, J. A. Kong and G. Simmons, "Numerical

evaluation of electromagnetic field due to dipole antennas in the presence of stratified media," J. Geophys. Res., 79, p. 2077-2081, 1974.

17. Tsang, L., and J. A. Kong, "Interference patterns of a horizontal electric dipole over layered dielectric media," J. Geophys. Res., 78, no. 17, June 1973.

18. Tsang, L., "Detection of subsurface electromagnetic properties with a horizontal electric dipole," Master's Thesis, Massachusetts Institute of Technology, MA, 1972.

19. Tsang, L., "Theoretical models for subsurface geophysical probing with electromagnetic waves," Doctor's Thesis, Massachusetts Institute of Technology, MA, 1975.

20. Sinha, A. R., "Electromagnetic fields of an oscillating magnetic dipole over an anisotropic earth," Geophysics, 33, no. 2, p. 346-353, 1968.

21. Annan, A. P., "Radio interferometry depth sounding, Part I-- Theoretical discussion," Geophysics, 38, no. 3, p. 557-580, June 1973.

22. Annan, A. P., et al, "The electromagnetic response of a low-loss, 2-layer dielectric earth for horizontal electric dipole excitation," Geophysics, 40, no. 2, p. 285-298, April 1975.

23. Boukamp, C. J., "On Sommerfeld's surface wave," Phys. Rev., 80, p. 294(L), 1950.

24. Epstein, P. S., "Radio-wave propagation and electromagnetic surface waves," Proc. Nat. Acad. Sci., 33, p. 195-199, 1947.

25. Kahan, T., and G. Eckart, "On the existence of a surface wave in dipole radiation over a plane earth," Proc. IRE, 38, p. 807-812, 1950.

26. Chan, W. M., et al, "Geophysical subsurface probing with a horizontal magnetic dipole," IEEE Trans. on Antennas and Propagation, Nov. 1976.

27. Kong, J. A., L. C. Shen, and L. Tsang, "Field of an antenna submerged in dissipative dielectric medium," IEEE Trans. on Antennas and Propagation, p. 887-889, 1977.

28. King, R. W. P., and B. Sandler, "Subsurface communication between dipoles in general media," IEEE Trans. on Antennas and Propagation, to be published.

29. Dahlquist, G., and Å. Björck, Numerical Methods, Prentice-Hall, Inc., Englewood Cliffs, New Jersey, 1974.

30. Abramowitz, M., and I. A. Stegun, Handbook of Mathematical Functions, Dover Publications, Inc., New York, 1972.

31. "MACSYMA Reference Manual," Massachusetts Institute of Technology, Cambridge, Massachusetts, 02139

32. Olver, F. W. J., Introduction to Asymptotic and Special Functions, Academic Press, New York, 1974.

33. Gradshteyn, I. S. and I. M. Rhyzik, Tables of Integrals, Series, and Products, Academic Press, New York, 1965.

34. Whittaker, E. T., and G. N. Watson, A Course in Modern Analysis, University Press, Cambridge, 1958.

35. Bleistein, N., "Uniform asymptotic expansion of integrals with staionary point and a nearby algebraic singularity," Comm. Pure Appl. Math., 19, p. 253, 1966.

36. Bleistein, N., "Uniform asymptotic expansions of integrals with many nearby stationary points and algebraic singularities," J. Math. and Mech., 17, no. 6, p. 533-559, 1967.